POLYMER INCLUSION MEMBRANES FOR SUSTAINABLE SEPARATION AND RECOVERY OF CRITICAL BATTERY METAL IONS

A Dissertation Presented for the

Doctor of Philosophy

Degree

The University of Tennessee, Knoxville

Babafemi O. Adigun

May 2026

Copyright © 2026 by Babafemi Oyedapo Adigun.

All rights reserved.

ACKNOWLEDGEMENTS

This dissertation represents not only years of scientific inquiry, but also the collective support, mentorship, encouragement, and faith of many individuals who have shaped my journey. I would like to begin by expressing my profound gratitude to the Almighty God for providing the strength, guidance, and perseverance required to complete this journey. Without His grace, none of this would have been possible.

First and foremost, I dedicate this work to the memory of my late parents and my sister, Doyin. Their love, guidance, and sacrifices laid the foundation for who I am today. Though they are not here to witness this milestone, their values, discipline, and unwavering belief in education continue to guide my decisions and strengthen my resolve. Everything I have achieved rests upon the foundation they built, though they are not here to see this moment, I carry their legacy and love in every page of this dissertation.

I extend my deepest gratitude to my advisor, Dr. Sheng Dai. Thank you for your unwavering support, patience, and belief in my potential. You provided not only scientific direction but also the space and trust necessary for growth. Under your mentorship, I evolved from a young Ph.D. student into an independent research scientist. Your guidance has shaped my scientific thinking and will continue to influence my career.

I sincerely thank Dr. Bishnu Thapaliya, Dr. Tao Wang, Dr. Huimin Luo, and all members of our research group for their collaboration, intellectual exchange, and generous support throughout my graduate studies. The discussions, troubleshooting sessions, shared insights, and teamwork significantly enriched this work. Their resourcefulness and willingness to engage deeply

with scientific challenges strengthened both the quality of this research and my development as a scientist.

I am deeply grateful to my undergraduate course advisor, Dr. Temilola Oluseyi, whose mentorship during my formative academic years profoundly influenced my path. Thank you for equipping me with the essential foundations of chemistry and for the guidance during my early academic years that set me on this path.

To my friends Shola, Tope, Badmus and Taofeek and the friends I met along this journey Yvonne, Ope, Amarachi, Akin, Lee, Amber and many others whose names may not be written here but whose presence are deeply felt thank you for your emotional encouragement, laughter, and companionship. Graduate school is as much an emotional journey as it is an intellectual one, and your support has made the difficult days manageable and the successes meaningful.

PREFACE

This dissertation, titled "Polymer Inclusion Membranes for Sustainable Separation and Recovery of Critical Battery Metal Ions," represents a comprehensive body of research conducted at the University of Tennessee, Knoxville, in collaboration with the Institute of Advanced Materials & Manufacturing. This work is born out of the urgent global necessity to establish a circular economy for lithium-ion battery (LIB) materials, addressing the dual challenges of environmental sustainability and resource security.

The core of this research focuses on the design, characterization, and application of Polymer Inclusion Membranes (PIMs). Unlike traditional hydrometallurgical processes, which are often chemical-intensive and operationally complex, the membrane systems developed herein offer a modular, energy-efficient, and low-waste alternative. The scientific narrative progresses from fundamental transport mechanisms to the execution of a sequential separation framework capable of isolating Lithium, Cobalt, Nickel, and Manganese from complex leachates.

This body of work is comprised of original research published in peer-reviewed journals. It transitions from a critical review of ionic liquid-based PIMs to experimental chapters detailing a complexation-driven "proton pumping" strategy and a multi-stage separation system for NMC 622 battery waste.

This dissertation serves as a bridge between fundamental membrane science and practical environmental engineering. It is my hope that the findings presented here will contribute significantly to the field of sustainable separations and provide a scalable blueprint for future battery recycling technologies.

ABSTRACT

The rapid expansion of lithium-ion battery (LIB) technologies has intensified demand for critical metals including lithium (Li), cobalt (Co), nickel (Ni), and manganese (Mn), necessitating sustainable separation and recycling strategies. Conventional hydrometallurgical recovery relies on multistage solvent extraction systems characterized by high solvent consumption, complex phase management, and limited selectivity in multi-metal leachates. This dissertation investigates polymer inclusion membranes (PIMs) as a mechanistically tunable, solvent-minimized system for selective recovery of critical battery metal ions.

PIMs based on poly(vinylidene fluoride-co-hexafluoropropylene) (PVDF-co-HFP) were fabricated with organophosphorus extractants (Cyanex 301, HDEHP), phosphonium carriers ($P_{66614}Cl$), and imidazolium ionic liquids to selectively separate critical battery metal ions. Ion separation was governed by carrier-mediated diffusion coupled to thermodynamic complexation equilibria. A complexation-driven ion-exchange PIM enabled proton-coupled counter-transport of Co^{2+} and Ni^{2+} while suppressing Li^{+} transport, demonstrating selectivity arising from differential stability constants and interfacial extraction kinetics. Sequential membrane systems integrating cation-exchange and chloride-mediated anion-exchange mechanisms achieved staged separation of Li^{+}, Co^{2+}, Ni^{2+}, and Mn^{2+} from mixed systems and simulated NMC 622 leachates.

Transport kinetics, membrane thickness effects, and compositional dependencies were quantitatively evaluated to establish diffusion-controlled flux behavior. Membrane stability was addressed via Layer-by-Layer (LbL) polyelectrolyte reinforcement to mitigate extractant and ionic liquid leaching. Although LbL deposition improved mechanical robustness and reduced carrier loss, transport flux decreased due to increased diffusional resistance, revealing a structure–

mobility tradeoff. These findings provide mechanistic insight into carrier-mediated ion transport in PIMs and establish their potential as modular, environmentally sustainable alternatives for critical battery metal recovery within a circular materials economy.

TABLE OF CONTENTS

Background and Motivation 1

Chapter One Introduction 5

1.1 Critical Battery Metals: Demand, Environmental Challenges, and Sustainable Recovery 6

1.2 Challenges in Metal Separation Recovery 9

1.3 Membrane-Based Separation Technologies 10

1.3.1 Bulk Liquid Membranes 12

1.3.2 Supported Liquid Membranes 12

1.3.3 Emulsion Liquid Membranes 14

1.4 Evolution Toward More Stable Liquid Membrane 15

1.5 Research Objective 15

1.6 Organization of the Dissertation 17

1.7 References 19

Chapter Two Literature Review: Polymer Inclusion Membranes for Metal Ion Separation 24

2.1 Polymer Inclusion Membranes 25

2.2 Components of Polymer Inclusion Membranes 26

2.2.1 Polymer Matrix 27

2.2.2 Carrier and Extractants 31

2.2.3 Plasticizers 35

2.3 Transport Mechanism in Polymer Inclusion Membranes 38

2.3.1 Carrier Mediated Transport Mechanism 38

2.3.2 Diffusion and Flux of Transport of Ions 41

2.3.2 Kinetic Modelling of Transport in Polymer Inclusion Membranes 43
2.4 References 46
Chapter Three Materials and Methods 52
3.1 Methods 53
3.1.1 Preparation of Polymer Inclusion Membrane 53
3.1.2 Layer-by-Layer Membrane Reinforcement 54
3.1.3 Metal Ion Transport Experiments 54
3.1.4 Inductively Coupled Plasma Optical Emission Spectroscopy 55
3.2 Material Characterization 55
3.2.1 Scanning Electron Microscopy 55
3.2.2 Fourier Transform Infrared Spectroscopy 56
3.2.3 Nuclear Magnetic Resonance Spectroscopy 56
3.2.4 Thermogravimetric Analysis 56
3.2.5 UV–Visible Spectroscopy 57
3.2.6 Dynamic Mechanical Analysis 57
3.2.7 X-ray Diffraction 57
Chapter Four Complexation-Driven Ion-Exchange Polymer Inclusion Membranes for Separation of Cobalt and Nickel ions from Lithium-Ion Via Proton Pumping 58
4.1 Abstract 59
4.2 Introduction 60
4.3 Materials and Methods 62
4.3.1 Materials 62

4.3.2 Membrane Preparation 63
4.3.3 Extraction and Stripping Experiments 64
4.3.4 Mass Loss of IEPIM 65
4.3.5 Transport Experiments 65
4.4 Results and Discussion 66
4.4.1 Membrane Characterization 66
4.4.2 Extraction and stripping studies with cobalt (II) and nickel (II) 70
4.4.3 Membrane Transport of Co(II) and Ni(II) and separation from Li(I) 72
4.4.4 Effect of Membrane Thickness on Transport of ions 76
4.4.5 Membrane Stability 77
4.4.6 Transport Mechanism 79
4.5 Conclusion 80
4.6 References 82
Chapter Five Total Separation of Lithium, Cobalt, Manganese and Nickel across Polymer Inclusion Membranes 86
5.1 Abstract 87
5.2 Introduction 87
5.3 Materials and Methods 90
5.3.1 Materials 90
5.3.2 Preparation of Polymer Inclusion Membranes 90
5.3.3 PIM Extraction and Stripping Experiments 91
5.3.4 PIM Transport Experiments 92

5.4 Results and Discussion 93
5.4.1 Effect of Chloride Ion Concentration on Selective Extraction of Cobalt . 95
5.4.2 Selective Membrane Separation of Co^{2+} from Ni^{2+} 98
5.4.3 Sequential Membrane Separation of Co^{2+}, Ni^{2+} and Li^{+} 99
5.4.4 Optimization of the Sequential Separation of Co, Ni, and Li 102
5.4.5 Sequential transport from NMC 622 leachate 105
5.4.6 Membrane Stability 107
5.4.7 Membrane Characterization 110
5.5 Layer-by-Layer Reinforcement of Polymer Inclusion Membranes 111
5.5.1 LbL Deposition Procedure 113
5.5.2 Characterization 113
5.5.2 Evaluation of Polymer Inclusion Membrane Leaching 115
5.5.3 Impact of Layer-by-Layer Reinforcement on Ion Transport 117
5.6 Conclusion 118
5.6 References 120
Chapter Six Ionic Liquid-Enhanced Recycling of Lithium-Ion Battery Black Mass via Heavy Liquid Centrifugal Separation 129
6.1 Abstract 130
6.2 Introduction 131
6.3 Materials and Methods 136
6.3.1 Materials 136
6.3.2 Methods 136

6.3.3 Characterization 137
6.4 Results and Discussion 137
6.4.1 Separation of cathode/anode mixture 137
6.4.2 Separation of Black Mass 142
6.5 Conclusions 145
6.6 References 146
Chapter Seven Conclusions and Recommendations 150
7.1 Conclusion 150
7.2 Recommendations and Future Work 152
7.2.1 Mitigation of Membrane Component Leaching 152
7.2.2 Toward Scalable and Integrated Membrane Systems 152
7.3 Final Perspective 152
Appendix 154
Vita 160

LIST OF TABLES

Table 1.1. Comparison of traditional metal separation methods including solvent extraction, precipitation, adsorption, and ion exchange. 10

Table 2.1 Common polymer matrix used in PIMs. 28

Table 4.1 Co^{2+} and Ni^{2+} rate constant (k), permeability coefficient (P), and initial fluxes (J_0) for transport across IEPIM with varying weight compositions. 75

Table 4.2 Co^{2+} and Ni^{2+} rate constant (*k*), permeability coefficient (*P*), and initial fluxes (J_0) for transport across IEPIM. 76

Table 4.3 Co^{2+} and Ni^{2+} rate constant (k), permeability coefficient (P), and initial fluxes (J_0) for transport across IEPIM for the three cycles. 79

Table 5.1 The rate constant (*k*), permeability coefficient (*P*), and initial fluxes (J_0) for the transport of Co^{2+} across PIM 99

Table 5.2 Comparison of kinetic parameters (rate constant, permeability, initial flux, and recovery percentage) for the separation of Co^{2+} across different studies 99

Table 5.3 First transport sequence for the separation of Co and Ni from Li 102

Table 5.4. Mechanical properties of pristine PIM and LbL PIM 115

Table 6.1. Quick comparison table of ILs for separation and purification. 133

Table S.1 Phosphorous concentrations in the immersed solution. 155

Table S.2 Metal composition of black mass determined by ICP-OES. 158

Table S.3 Yield and composition of separated electrode active materials from black mass. 158

LIST OF FIGURES

Figure 1.1 Schematic diagram of lithium-ion battery.[8] 7

Figure 1.2 Schematic representation of bulk supported and emulsion liquid membrane transport showing feed phase, liquid membrane phase, and receiving phase.[35] 13

Figure 2.1 Transport mechanism of metal ions across membranes (a) co-transport mechanism (b) counter transport mechanism.[58] 40

Figure 4.1 Chemical structures (a) [C_8mim][NTf_2], (b) PVDF-HFP, (c). Cyanex 301 63

Figure 4.2 Top view SEM image of (a) pure PVDF-HFP membrane and (b) IEPIM, (c) Thermogravimetric analysis of Pure PVDF-HFP, Cyanex 301, IEPIM before, and after transport experiments. FTIR Spectra of pure PVDF-HFP membrane, Cyanex 301 [C_8mim][NTf_2] and IEPIM before and after use showing distinct peaks for (d) PVDF-HFP (e) Cyanex 301, and (f) [C_8mim][NTf_2]. 67

Figure 4.3 (a) Extraction of Co^{2+} and Ni^{2+} into IEPIM in the feed solutions. (b) Stripping of Co^{2+} and Ni^{2+} from IEPIM in the stripping solutions. Three cycles of (c) extraction of Co^{2+} and Ni^{2+} into IEPIM and (d) stripping Co^{2+} and Ni^{2+} from IEPIM 69

Figure 4.4 (a) Mass changes of IEPIM for three cycles (b) UV-Vis spectra showing imidazolium peaks (c) phosphorus concentration in the solution after immersion in deionized water. 71

Figure 4.5 Kinetic plots of the (a) Transport of Co^{2+}, (b) Transport of Ni^{2+}, and (c) Initial flux at varying weight composition of the extractant across IEPIM in the feed solution. 73

Figure 4.6 Transport of Co^{2+} and Ni^{2+} across an IEPIM in the feed and stripping solutions over time (b) Plot of pH in the feed solution over time (c) Kinetic plots of the transport of Co^{2+} and Ni^{2+} across the IEPIM in the feed solution. 74

Figure 4.7 (a) Initial flux of Co^{2+} and Ni^{2+} (b) Transport efficiency of Co^{2+} (c) Transport efficiency of Ni^{2+} at different membrane thicknesses across IEPIM. 77

Figure 4.8 Transport efficiency of 3 transport cycles. Feed solution: 100 mL of 0.1 mM Li^{+}, Co^{2+}, and Ni^{2+}. Receiving Solution: 2M HCl. Membrane composition 50% wt. PVDF-co-HFP and 30% wt. Cyanex 301 and 20% wt. $[C_8mim][NTf_2]$. 78

Figure 4.9 Plausible mechanism for transporting Co^{2+} and Ni^{2+} across IEPIM in this study..... 80

Figure 5.1 Chemical structures of polymer host and carriers. 91

Figure 5.2 (a) Extraction percentage of Co^{2+} at different HCl concentration in the feed solution (b) Extraction and Stripping percentage of Co^{2+} and Ni^{2+} in 9M HCl. 94

Figure 5.3 UV-Vis spectra of (a) cobalt-chloride complexes in concentrated chloride solution (b) cobalt, manganese and nickel chloride complexes in aqueous and 9 M HCl solution. 95

Figure 5.4 (a) Transport of Co^{2+} and Ni^{2+} across an PIM in the feed and receiving solutions over time (b) Kinetic plots of the transport of Co^{2+} PIM in the feed solution. 97

Figure 5.5 (a) First transport sequence of Co^{2+} and Ni^{2+} (b) Second transport sequence of Co^{2+} across a PIM in the feed and receiving solutions over time. Kinetic plots of (c) First transport sequence (d) Second transport sequence. 101

Figure 5.6 (a) 1st transport sequence separation of Co^{2+} and Ni^{2+} from Li^{+} (b) 2nd transport sequence of Co^{2+} from Ni^{2+} 103

Figure 5.7 Picture of the 3- jacketed glass compartment for the optimized transport experiment. 103

Figure 5.8 (a)1st transport sequence separation of Co^{2+} and Ni^{2+} from Li^{+} and Mn^{2+} (b) Transport efficiency of the first transport sequence (c) 2nd transport sequence of Co^{2+} from

Ni^{2+} (d) Transport efficiency of the second transport sequence. (e) 3rd transport sequence of Co^{2+} from Ni^{2+} (f) Transport efficiency of the third transport sequence. (g) Separation percentage of the metal ions. 104

Figure 5.9 Stability of membrane after (a) 1st transport sequence (b) 2nd transport sequence. 107

Figure 5.10 Thermogravimetric analysis of PVDF-HFP, HDEHP PIM, Cyanex 301 PIM and $P_{66614}Cl$ PIM. 109

Figure 5.11 SEM images of (a) $P_{66614}Cl$ PIM (b) Cyanex 301 PIM (c) HDEHP PIM. 109

Figure 5.12 DMA Analysis of Pristine PIM and LbL PIM 114

Figure 5.13 UV–Vis spectra of leached components from Pristine PIM and 50 LbL PIM..... 116

Figure 6.1. (a) TGA curves of the separated bottom and upper layers. (b) Photo of graphite/NMC mixtures after centrifugal separation. 138

Figure 6.2 (a) Illustration of NMC/Graphite separation in HL. (b) Photos of NMC and Graphite in HL. 138

Figure 6.3 (a) TGA curves of bottom and upper layer products from black mass. (b) XRD patterns of black mass and bottom/upper layer products. 141

Figure 6.4 (a) XRD patterns of anode layer from black mass after treatment with ionic liquids. (b) TGA curves of black mass and anode layer products from black mass after treatment with ionic liquids. (c) The first charge/discharge curves of graphite|Li 143

Figure S.1 FTIR Spectra of Cyanex 301 showing the peak corresponding to S—H stretching bonds. 154

Figure S.2 Transport of Co^{2+}, Ni^{2+} and Li^{+} after 24 hours across IEPIM for three cycles: (a) 1st cycle, (b) 2nd cycle, (c) 3rd cycle..... 154

Figure S.3 Mass changes of the PIMs after immersion in 9 M HCl and deionized water for 4 days with constant shaking. 155

Figure S.4 SEM images of (a) $P_{66614}Cl$ PIM (b) Cyanex 301 PIM (c) HDEHP PIM after transport experiments. 156

Figure S.5 FTIR analysis of (a) Cyanex 301, $P_{66614}Cl$, HDEHP (b) Pure PVDF-co-HFP, $P_{66614}Cl$ PIM, HDEHP PIM and Cyanex 301 PIM. 157

Figure S.6 TGA curves of the separated bottom and upper layers, XRD peaks of (b) pristine graphite (c) pristine NMC (d) anode layer and (e) cathode layer after separation. 159

Figure S.7 XRD pattern for different additives added to bromoform (a) NMP (b) Ionic Liquid (c) NMP/Ionic Liquid of the anode layer (d) NMP (e) Ionic Liquid (f) NMP/Ionic Liquid of the cathode layer. 160

LIST OF ABBREVIATIONS

BLM	Bulk Liquid Membrane
CTA	Cellulose Triacetate
D2EHAG:	N-[N,N-di(2-ethylhexyl)aminocarbonylmethyl]glycine
DMA	Dynamic Mechanical Analysis
FTIR	Fourier Transform Infrared Spectroscopy
HLCS	Heavy Liquid Centrifugal Separation
ICP-OES	Inductively Coupled Plasma Optical Emission Spectroscopy
IEPIM	Ion-Exchange Polymer Inclusion Membrane
IL	Ionic Liquid
IR	Infrared Spectroscopy
J_0	Initial Flux
k	Rate Constant
LbL	Layer-by-Layer
LIB	Lithium-Ion Battery
NMC	Nickel Manganese Cobalt
NMC 622	$LiNi_{0.6}Mn_{0.2}Co_{0.2}O_2$
P	Permeability Coefficient
PIM	Polymer Inclusion Membrane
[PR4][TS]	trihexyl(tetradecyl)phosphoniu

PVC	Poly(vinyl chloride)
PVDF	Poly(vinylidene fluoride)
PVDF-HFP	Poly(vinylidene fluoride-co-hexafluoropropylene)
SEM	Scanning Electron Microscopy
SLM	Supported Liquid Membrane
SX	Solvent Extraction
TGA	Thermogravimetric Analysis
TIOA	triisooctylamine,
UV–Vis	Ultraviolet–Visible Spectroscopy
wt%	Weight Percent
XRD	X-ray Diffraction

BACKGROUND AND MOTIVATION

The global demand for energy, advanced technologies, and electronic devices has increased dramatically over the past several decades. Modern society depends heavily on materials that enable the production of energy storage systems, electronic devices, and transportation technologies. Among these materials, metals such as lithium, cobalt, nickel, and manganese have become critically important due to their role in the development of lithium-ion batteries (LIBs). These batteries power a wide range of modern technologies, including portable electronics, electric vehicles, and large-scale energy storage systems that support renewable energy infrastructure. As nations pursue strategies to reduce carbon emissions and transition toward sustainable energy systems, the demand for lithium-ion batteries and the metals used in their construction is expected to grow substantially.

Although these metals are essential for enabling modern energy technologies, their extraction and production present significant environmental and geopolitical challenges. Conventional mining and refining operations are often associated with substantial environmental impacts, including land degradation, water contamination, and greenhouse gas emissions. Mining activities can disrupt ecosystems, generate hazardous waste streams, and consume large amounts of energy and water resources. As global demand for battery materials continues to rise, the environmental footprint associated with primary metal extraction is expected to increase if alternative strategies for resource management are not developed.

In addition to environmental concerns, the supply of critical battery metals is influenced by geopolitical factors and global supply chain dynamics. Many of the metals used in lithium-ion batteries are geographically concentrated in a limited number of regions. For example, a significant

portion of the world's cobalt production originates from a small number of countries, creating potential supply vulnerabilities and market instability. Fluctuations in metal prices, trade policies, and geopolitical tensions can therefore influence the availability and cost of materials required for battery manufacturing. These challenges highlight the need for sustainable and resilient strategies to secure critical metal resources while reducing dependence on environmentally intensive mining practices.

One promising approach for addressing these challenges is the recovery and recycling of metals from secondary sources such as industrial waste streams and end-of-life batteries. Recycling technologies have the potential to recover valuable metals that would otherwise be lost during disposal while reducing the environmental burden associated with primary resource extraction. By recovering metals from used batteries and other waste materials, it becomes possible to establish a circular materials economy in which critical resources are reused rather than continuously extracted from the earth. However, the efficient recovery of metals from complex mixtures remains a significant technical challenge due to the chemical similarities among many metal ions and the presence of multiple elements within battery materials.

To address these challenges, several separation and recovery strategies have been developed to extract valuable metals from primary and secondary resources. Common approaches include hydrometallurgical techniques such as solvent extraction, precipitation, adsorption, and ion exchange processes. These methods have been widely implemented in industrial metal recovery due to their effectiveness in dissolving and separating metals from complex mixtures. However, despite their widespread use, many of these technologies suffer from inherent limitations such as waste generation and selectivity. As the demand for sustainable resource recovery continues to

grow, there is increasing interest in developing alternative separation technologies that can reduce waste generation while improving efficiency and selectivity.

Polymer inclusion membranes (PIMs) have emerged as particularly promising candidates for metal ion separation and recovery. Polymer inclusion membranes are composite materials that incorporate a polymer matrix together with carrier molecules capable of selectively interacting with target metal ions. The membrane acts as a selective barrier that facilitates the transport of specific ions from a feed solution to a receiving phase. Compared with earlier liquid membrane systems, polymer inclusion membranes offer improved structural stability and reduced loss of membrane components during operation. PIMs provide several advantages that make them attractive for metal separation applications such as selectivity, ease of operation, low solvent use, easy to fabricate and adaptable to a wide range of separation conditions. Because of these advantages, polymer inclusion membranes have attracted growing research interest for applications in metal recovery, environmental remediation, and resource recycling. In particular, their ability to selectively transport metal ions across a membrane phase offers a promising strategy for separating critical battery metals from complex aqueous mixtures.

Motivated by these considerations, the research presented in this dissertation explores the development and optimization of polymer inclusion membranes for the sustainable separation and recovery of critical battery metal ions. The primary goal of this work is to investigate membrane compositions and carrier systems capable of selectively separating lithium, cobalt, nickel, and manganese from complex mixtures representative of lithium-ion battery materials.

Through the integration of membrane chemistry, ionic liquid design, and mechanistic analysis, this research aims to advance polymer inclusion membrane technology as a sustainable platform for critical metal recovery. The findings presented in this dissertation contribute to the broader goal

of developing environmentally friendly separation technologies capable of supporting the circular economy of lithium-ion battery materials.

CHAPTER ONE

INTRODUCTION

1.1 Critical Battery Metals: Demand, Environmental Challenges, and Sustainable Recovery

The modern world relies heavily on metals for a wide range of applications including infrastructure, electronics, transportation, and renewable energy systems. As technological development accelerates, the demand for metals essential to advanced technologies continues to rise. [1-3] In particular, critical battery metals such as lithium (Li), cobalt (Co), nickel (Ni), and manganese (Mn) have become increasingly important due to their central role in lithium-ion batteries (LIBs), which power portable electronics, electric vehicles, and grid-scale energy storage systems. Lithium-ion batteries have emerged as the dominant energy storage technology due to their high energy density, long cycle life, and relatively low self-discharge. These characteristics have enabled their widespread use across multiple sectors, ranging from consumer electronics to electric transportation. The rapid growth of electric vehicle markets and renewable energy infrastructure has led to unprecedented demand for lithium-ion batteries. Production capacity has increased dramatically over the past decade and is projected to continue expanding as governments and industries pursue decarbonization strategies and the electrification of transportation. [4-6]

The performance of lithium-ion batteries depends strongly on the availability and composition of key transition metals used in cathode materials. Lithium serves as the primary charge carrier within the electrochemical cell, enabling efficient ionic transport during charge and discharge processes. Cobalt contributes to structural stability and improves the thermal safety of cathode materials, while nickel enhances energy density by increasing the amount of reversible lithium intercalation. Manganese contributes to

structural stability and improves safety by stabilizing cathode crystal structures.[7-11] Advanced cathode chemistries such as lithium nickel manganese cobalt oxide (NMC) combine these metals

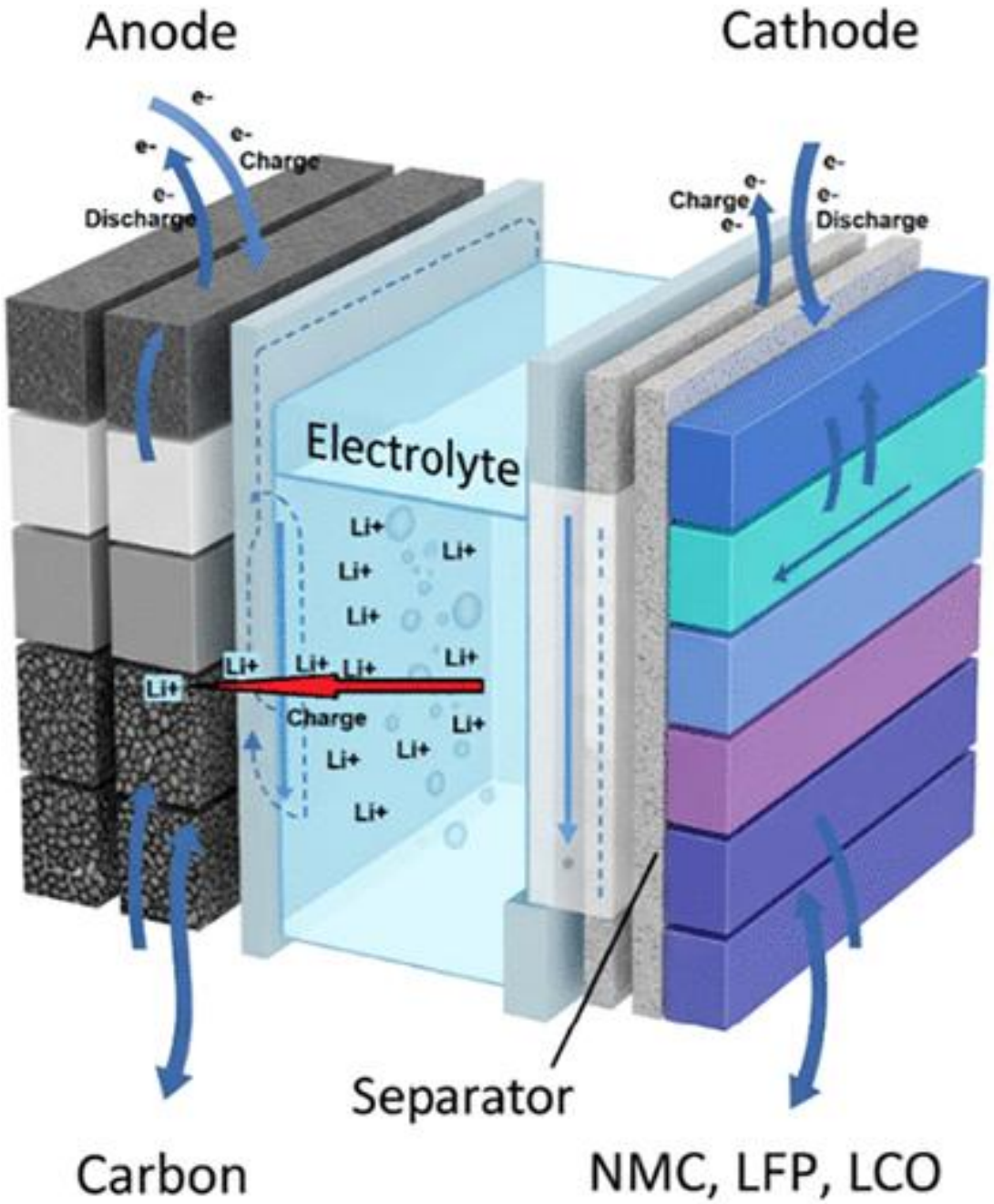

Figure 1.1 Schematic diagram of lithium-ion battery.[8]

to achieve optimal electrochemical performance. However, the increasing reliance on these elements presents significant challenges related to supply chain security, environmental sustainability, and resource availability.

While critical battery metals are essential for the development of energy storage technologies, their extraction and processing pose significant environmental and geopolitical challenges. Metals used in battery manufacturing are typically obtained through mining operations that involve extensive land disturbance, high energy consumption, and the generation of substantial quantities of waste. Mining and refining processes can lead to soil degradation, water contamination, and the release of harmful pollutants into surrounding ecosystems. In addition to environmental concerns, the geographic distribution of many critical metals is uneven, creating vulnerabilities in global supply chains. For example, a large portion of the world's cobalt production originates from a limited number of countries, increasing the risk of supply disruptions and price volatility.[12-16] As global demand for lithium-ion batteries continues to rise, ensuring reliable access to these materials has become an important strategic issue for many nations.

The environmental and geopolitical challenges associated with primary metal extraction highlight the need for sustainable resource management strategies. One promising solution involves the recovery of valuable metals from secondary resources such as industrial waste streams and spent lithium-ion batteries. Recycling of battery materials provides an opportunity to recover critical metals while reducing the environmental impact associated with mining activities. Recycling also contributes to the development of a circular economy for battery materials, in which metals are recovered and reused rather than discarded after a single life cycle. This approach reduces dependence on primary resource extraction while ensuring a more stable supply of materials for future battery production.[17-25]

1.2 Challenges in Metal Separation Recovery

To recover valuable metals from ores and recycled materials, several separation technologies have been developed and widely implemented in industrial processes. Conventional metal separation methods include solvent extraction, precipitation, adsorption, and ion exchange techniques. These approaches are commonly used in hydrometallurgical processes for the extraction and purification of metals from aqueous solutions. Solvent extraction remains one of the most widely used industrial separation techniques due to its ability to selectively extract certain metal ions from aqueous solutions using organic extractants. However, solvent extraction processes often require large volumes of organic solvents and multiple extraction stages to achieve effective separation of metal ions with similar chemical properties. [26-28] This can increase process complexity and lead to environmental concerns related to solvent disposal and chemical waste generation. Precipitation methods provide a relatively simple approach for separating metals by converting dissolved ions into insoluble compounds. Although precipitation is effective for separating metals present at high concentrations, it often produces large volumes of sludge and may result in co-precipitation of unwanted species, reducing product purity.[29] Ion exchange and adsorption processes provide alternative strategies for metal separation using solid sorbent materials. These methods can be effective for removing metal ions from dilute solutions; however, their performance may be limited by sorbent capacity, regeneration requirements, and reduced selectivity when separating chemically similar ions.[27-28] **Table 1.1** summarizes the advantages and limitations of commonly used metal separation techniques.

Table 1.1. Comparison of traditional metal separation methods including solvent extraction, precipitation, adsorption, and ion exchange.

Methods	Advantages	Disadvantages
• Solvent Extraction	• High efficiency for specific extractions. • Widely used in industrial processes.	• Less flexible; may require multiple extraction steps for mixed ions. • Large volumes of extractant needed. • Environmental concerns, solvent disposal issues.
• Ion Exchange	• Well established and simple process for metal separation. • Regeneration of resins.	• Matrix degradation over time. • Resin fouling and saturation can limit continuous operation.
• Adsorption	• Tunable with different adsorbents. • Effective and simple process.	• Lower selectivity, variability in performance. • Disposal of spent adsorbents can pose environmental concerns.
• Precipitation	• Simple and easy process. • Effective for separating metal ions at high concentration	• Sludge generation • Impurities may co-precipitate with the desired product
• Membrane-based separation	• High selectivity due to tunable IL properties. • Lower environmental footprint.	• Stability of membrane. • Scalability to industrial process.

Overall, while conventional separation methods remain important for industrial metal recovery, many of these processes suffer from limitations related to waste generation, high chemical consumption, and insufficient selectivity when separating complex mixtures of metal ions.

1.3 Membrane-Based Separation Technologies

In response to the environmental and operational limitations associated with traditional metal separation processes, membrane-based technologies have emerged as promising alternatives for sustainable resource recovery. Membrane separation processes offer several advantages compared to conventional hydrometallurgical techniques, including lower energy consumption, reduced chemical usage, and the ability to achieve highly selective separations under relatively mild

operating conditions. These features make membrane systems particularly attractive for applications in environmental remediation, wastewater treatment, and the recovery of valuable metals from industrial waste streams and end-of-life products.

Membrane technologies operate by selectively transporting chemical species across a barrier that separates two phases. This barrier regulates the movement of ions or molecules based on differences in physicochemical properties such as size, charge, solubility, and chemical affinity. As a result, membrane-based separations can be engineered to selectively recover specific metal ions from complex aqueous mixtures. Compared with traditional solvent extraction processes, which typically require multiple extraction and stripping stages, membrane systems can integrate separation processes into a single step, improving process efficiency and reducing waste generation.

Among membrane-based approaches, liquid membrane systems represent an important class of separation technologies that combine the principles of liquid–liquid extraction with membrane transport processes. Liquid membranes utilize an immiscible liquid phase that acts as a selective barrier between two aqueous solutions, commonly referred to as the feed phase and the receiving (or stripping) phase. During operation, solute species are extracted from the feed phase into the liquid membrane, diffuse through the membrane phase, and are subsequently released into the receiving phase. This process enables continuous extraction and stripping of target species within a single separation system. Over the past several decades, several configurations of liquid membrane systems have been developed to improve separation efficiency and operational performance. The most widely studied configurations include bulk liquid membranes (BLMs), supported liquid membranes (SLMs), and emulsion liquid membranes (ELMs). Each configuration

possesses unique structural characteristics and operational advantages, although each also presents specific challenges related to stability and scalability.

1.3.1 Bulk Liquid Membranes

Bulk liquid membranes represent one of the earliest forms of liquid membrane technology. In this configuration, two aqueous solutions, the feed and receiving phases, are separated by an intermediate organic liquid layer that serves as the membrane phase. The organic liquid is typically immiscible with water and contains an extractant or carrier molecule capable of selectively binding target solutes. During operation, metal ions from the feed phase are extracted into the organic membrane phase, transported across the membrane, and subsequently stripped into the receiving phase. Bulk liquid membrane systems have been widely investigated in laboratory studies because of their relatively simple configuration and their ability to demonstrate fundamental transport mechanisms. However, despite their conceptual simplicity, bulk liquid membranes often suffer from low mass transfer efficiency and limited scalability. These systems typically require large volumes of organic solvents, and the stability of the membrane layer can be difficult to maintain during prolonged operation. Consequently, although BLM systems have been valuable for studying transport mechanisms, their practical application in large-scale industrial separations remains limited.[30-32]

1.3.2 Supported Liquid Membranes

Supported liquid membranes were developed to address some of the limitations associated with bulk liquid membrane systems. In SLM systems, the liquid membrane phase is immobilized within the pores of a microporous solid support material. The porous support provides structural stability and prevents direct mixing between the feed and receiving phases while allowing the liquid membrane to function as the selective transport medium. Supported liquid membranes offer

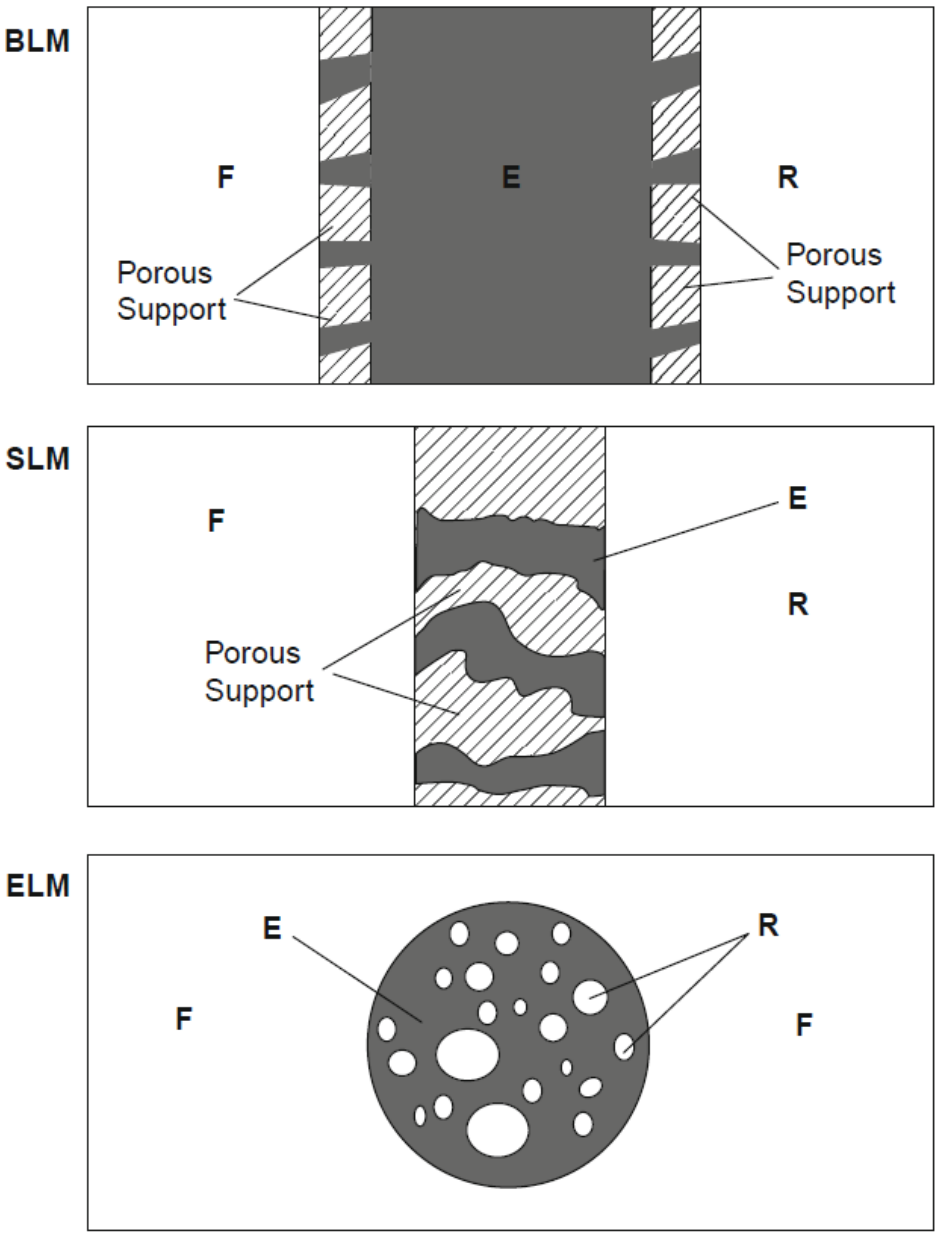

Figure 1.2 Schematic representation of bulk supported and emulsion liquid membrane transport showing feed phase, liquid membrane phase, and receiving phase.[35]

several advantages compared to bulk liquid membranes, including reduced solvent consumption, improved membrane stability, and higher surface area-to-volume ratios when implemented in configurations such as hollow-fiber or spiral-wound modules. These structural improvements

enable more efficient mass transfer and improved process performance. Despite these advantages, supported liquid membranes also face several challenges that have limited their widespread industrial adoption. One of the primary limitations is membrane instability, which may arise from the gradual loss of the liquid membrane phase from the pores of the support material. Factors such as pressure fluctuations, carrier degradation, and solvent dissolution into the aqueous phases can lead to membrane deterioration over time. Because of these stability concerns, significant research efforts have focused on developing improved membrane architectures capable of retaining the liquid phase more effectively while maintaining high separation performance.[33-36]

1.3.3 Emulsion Liquid Membranes

Another important configuration of liquid membrane systems is the emulsion liquid membrane (ELM). In this approach, the receiving phase is emulsified within an immiscible liquid membrane phase to form water-in-oil droplets. These droplets are then dispersed in the feed solution, allowing solutes to transfer from the feed phase through the membrane phase into the internal receiving phase contained within the emulsion droplets. Emulsion liquid membranes offer extremely high mass transfer rates due to the large interfacial area between phases. As a result, ELM systems have demonstrated strong potential for applications in metal recovery, wastewater treatment, and chemical separations. However, ELM systems also present significant operational challenges. Maintaining the stability of the emulsion while simultaneously enabling efficient recovery of the internal receiving phase requires careful control of surfactants and operating conditions. Instability in the emulsion structure can lead to membrane rupture, loss of separation efficiency, and difficulties in downstream processing. Additionally, osmotic pressure differences between phases can cause swelling or rupture of emulsion droplets, further complicating system stability.[35-36]

1.4 Evolution Toward More Stable Liquid Membrane

Although bulk, supported, and emulsion liquid membrane systems demonstrated the feasibility of carrier-mediated transport for metal separations, their long-term stability has remained a persistent challenge. In many early systems, the liquid membrane phase was susceptible to loss through dissolution, evaporation, or mechanical instability. Carrier degradation and solvent leakage often resulted in declining transport efficiency during extended operation.

To address these challenges, researchers began developing modified liquid membrane systems designed to improve mechanical integrity and carrier retention. Among these developments, PIMs have attracted considerable attention because they combine the selectivity of liquid membrane systems with the structural stability of polymeric materials. Recent studies have shown that PIM systems can achieve highly selective metal ion transport while requiring significantly lower solvent volumes and generating less chemical waste compared to conventional solvent extraction processes. Furthermore, PIMs enable simultaneous extraction and stripping within a single membrane system, simplifying the overall separation process.[37-39] The ability of PIMs to perform selective separations while reducing chemical waste and energy consumption aligns closely with the principles of green chemistry and sustainable materials processing. Consequently, polymer inclusion membranes represent a promising platform for advancing next-generation separation technologies aimed at supporting the transition toward a circular economy for critical battery materials.

1.5 Research Objective

Despite the significant progress made in metal recovery technologies, the efficient separation of critical battery metals from complex aqueous mixtures remains a major scientific and

technological challenge. Lithium, cobalt, nickel, and manganese often coexist in battery leachates and industrial waste streams in similar chemical environments, making their selective separation difficult using conventional methods. Many current hydrometallurgical processes rely on multi-stage solvent extraction and precipitation techniques that require large volumes of chemicals, generate significant secondary waste streams, and often involve complex operational steps. These limitations highlight the need for alternative separation technologies that are more sustainable, selective, and energy efficient. The objectives of this dissertation are therefore centered on addressing these scientific and technological challenges through the design, development, and evaluation of polymer inclusion membrane systems for sustainable metal ion separation. Specifically, this research seeks to advance the understanding of membrane composition, transport mechanisms, and structural stability to improve the performance of PIM-based separation systems for lithium-ion battery metals.

The research presented in this dissertation focuses on the development and optimization of polymer inclusion membranes for the selective separation and recovery of critical battery metals. The primary objectives of this work include:

1. Investigating PIMs systems for selective recovery of lithium-ion battery metals.
2. Understanding the influence of membrane composition onion transport behavior.
3. Evaluating strategies to improve PIMs stability and durability.
4. Developing optimized membrane systems capable of separating lithium, cobalt, nickel, and manganese from complex mixtures.

Through these investigations, this dissertation seeks to advance the development of sustainable separation technologies that can support the growing demand for critical battery metals while reducing the environmental impacts associated with conventional mining and refining processes.

By improving the efficiency and selectivity of PIMs systems, this work contributes to the broader goal of enabling circular resource management for lithium-ion battery materials and supporting the transition toward more sustainable energy technologies.

1.6 Organization of the Dissertation

The remainder of this dissertation is organized as follows. Chapter one provides a comprehensive overview of the global demand for critical battery metals, the challenges associated with their separation and recovery. The chapter also introduces polymer inclusion membranes as promising alternatives for sustainable metal separation and establishes the research objectives of this dissertation.

Chapter two presents a detailed review of polymer inclusion membrane technology, including the evolution of membrane design, the role of carrier molecules and ionic liquids, and the fundamental mechanisms governing ion transport through these membranes.

Chapter three describes the materials, experimental procedures, and characterization techniques used throughout this work. This chapter includes membrane fabrication methods, analytical techniques used to characterize membrane structure and stability, and experimental setups used for ion transport studies.

Chapter four focuses on the separation of lithium-ion battery metals using polymer inclusion membranes. The effects of membrane composition, carrier type, and experimental conditions on the transport and selectivity of cobalt, nickel, manganese, and lithium are systematically investigated.

Chapter five examines the stability and structural optimization of polymer inclusion membranes, including the implementation of a layer-by-layer deposition strategy aimed at improving membrane mechanical strength and operational durability.

Finally, chapter six summarizes the key findings of this dissertation and discusses future research directions for advancing polymer inclusion membrane technology for sustainable critical metal recovery.

References

(1) Di Lecce, D.; Verrelli, R.; Hassoun, J. Lithium-ion batteries for sustainable energy storage: recent advances towards new cell configurations. *Green Chemistry* 2017, *19* (15), 3442-3467.

(2) Khan, F. N. U.; Rasul, M. G.; Sayem, A.; Mandal, N. K. Design and optimization of lithium-ion battery as an efficient energy storage device for electric vehicles: A comprehensive review. *Journal of Energy Storage* 2023, *71*, 108033.

(3) Gao, Y.; Pan, Z.; Sun, J.; Liu, Z.; Wang, J. High-energy batteries: beyond lithium-ion and their long road to commercialisation. *Nano-micro letters* 2022, *14* (1), 94.

(4) Frith, J. T.; Lacey, M. J.; Ulissi, U. A non-academic perspective on the future of lithium-based batteries. *Nature Communications* 2023, *14* (1), 420.

(5) McKerracher, C.; Izadi-Najafabadi, A.; O'Donovan, A.; Albanese, N.; Soulopolous, N.; Doherty, D.; Boers, M.; Fisher, R.; Cantor, C.; Frith, J. Electric vehicle outlook 2020. *Bloomberg New Energy Finance* 2020, (July).

(6) Li, Z. A Review of the Current Status of Global Electric Vehicle Charging Infrastructure Development. *International Journal of Global Economics and Management* 2024, *3* (3), 123-134.

(7) Chu, B.; Guo, Y.-J.; Shi, J.-L.; Yin, Y.-X.; Huang, T.; Su, H.; Yu, A.; Guo, Y.-G.; Li, Y. Cobalt in high-energy-density layered cathode materials for lithium ion batteries. *Journal of Power Sources* 2022, *544*, 231873.

(8) Kilavuz, E. Sustainable Lithium-Ion Battery Recycling: Challenges, Innovations, and Pathways to a Circular Economy. *ACS Sustainable Resource Management* **2025**, *2* (10), 1838-1858.

(9) Zheng, X.; Cai, Z.; Sun, J.; He, J.; Rao, W.; Wang, J.; Zhang, Y.; Gao, Q.; Han, B.; Xia, K. Nickel-rich layered oxide cathodes for lithium-ion batteries: Failure mechanisms and modification strategies. *Journal of Energy Storage* 2023, *58*, 106405.

(10) Zeng, X.; Zhan, C.; Lu, J.; Amine, K. Stabilization of a high-capacity and high-power nickel-based cathode for Li-ion batteries. *Chem* 2018, *4* (4), 690-704.

(11) Wei, H.-x.; Tang, L.-b.; Yan, C.; He, Z.-j.; Mao, J.; Dai, K.; Wu, X.-w.; Jiang, J.-b.; Zheng, J.-c. Lithium-rich manganese-based cathode materials with highly stable lattice and surface enabled by perovskite-type phase-compatible layer. *Nano Energy* 2021, *88*, 106288.

(12) Li, P.; Luo, S.; Zhang, L.; Liu, Q.; Wang, Y.; Lin, Y.; Xu, C.; Guo, J.; Cheali, P.; Xia, X. Progress, challenges, and prospects of spent lithium-ion batteries recycling: a review. *Journal of Energy Chemistry* 2024, *89*, 144-171.

(13) Lv, W.; Wang, Z.; Cao, H.; Sun, Y.; Zhang, Y.; Sun, Z. A critical review and analysis on the recycling of spent lithium-ion batteries. *ACS Sustainable Chemistry & Engineering* 2018, *6* (2), 1504-1521.

(14) Lehtimäki, H.; Karhu, M.; Kotilainen, J. M.; Sairinen, R.; Jokilaakso, A.; Lassi, U.; Huttunen-Saarivirta, E. Sustainability of the use of critical raw materials in electric vehicle batteries: A transdisciplinary review. *Environmental Challenges* 2024, *16*, 100966.

(15) Niri, A. J.; Poelzer, G. A.; Zhang, S. E.; Rosenkranz, J.; Pettersson, M.; Ghorbani, Y. Sustainability challenges throughout the electric vehicle battery value chain. *Renewable and Sustainable Energy Reviews* 2024, *191*, 114176.

(16) Yang, Y.; Okonkwo, E. G.; Huang, G.; Xu, S.; Sun, W.; He, Y. On the sustainability of lithium ion battery industry–A review and perspective. *Energy Storage Materials* 2021, *36*, 186-212.

(17) Hantanasirisakul, K.; Sawangphruk, M. Sustainable reuse and recycling of spent Li-ion batteries from electric vehicles: chemical, environmental, and economical perspectives. *Global Challenges* 2023, *7* (4), 2200212.

(18) Roy, J. J.; Cao, B.; Madhavi, S. A review on the recycling of spent lithium-ion batteries (LIBs) by the bioleaching approach. *Chemosphere* 2021, *282*, 130944.

(19) Ordoñez, J.; Gago, E. J.; Girard, A. Processes and technologies for the recycling and recovery of spent lithium-ion batteries. *Renewable and Sustainable Energy Reviews* 2016, *60*, 195-205.

(20) Okonkwo, E. G.; Wheatley, G.; He, Y. The role of organic compounds in the recovery of valuable metals from primary and secondary sources: a mini-review. *Resources, Conservation and Recycling* 2021, *174*, 105813.

(21) Garole, D. J.; Hossain, R.; Garole, V. J.; Sahajwalla, V.; Nerkar, J.; Dubal, D. P. Recycle, recover and repurpose strategy of Spent Li-ion Batteries and catalysts: current status and future opportunities. *ChemSusChem* 2020, *13* (12), 3079-3100.

(22) R. M. Izatt, S. R. Izatt, R. L. Bruening, N. E. Izatt and B. A. Moyer, Chemical Society Reviews, 2014, 43, 2451-2475.

(23) S. H. Ali, D. Giurco, N. Arndt, E. Nickless, G. Brown, A. Demetriades, R. Durrheim, M. A. Enriquez, J. Kinnaird, A. Littleboy, L. D. Meinert, R. Oberhänsli, J. Salem, R. Schodde, G. Schneider, O. Vidal and N. Yakovleva, Nature, 2017, 543, 367-372.

(24) B. K. Reck and T. E. Graedel, Science, 2012, 337, 690-695.

(25) R. U. Ayres, Resources, conservation and recycling, 1997, 21, 145-173.

(26) X. Q. Sun, H. M. Luo and S. Dai, *Talanta*, 2012, **90**, 132-137.

(27) S. Hussaini and A. M. Tita, in *Recycling Technologies for Secondary Zn-Pb Resources*, Springer, 2023, pp. 403-459.

(28) S. Gupta and B. Babu, *Chemical Engineering Journal*, 2009, **150**, 352-365.

(29) A. B. Botelho Junior, D. B. Dreisinger and D. C. Espinosa, *Mining, Metallurgy & Exploration*, 2019, **36**, 199-213.

(30) A. Yılmaz, A. Kaya, H. Alpoguz, M. Ersoz and M. Yilmaz, *Sep Purif Technol*, 2008, **59**, 1-8.

(31) H. Ma, K. E. Waters and H. Wang, *Mining, Metallurgy & Exploration*, 2023, **40**, 13-39.

(32) A. Kumar, A. Thakur and P. S. Panesar, *Reviews in Environmental Science and Bio/Technology*, 2019, **18**, 153-182.

(33) N. Kocherginsky, Q. Yang and L. Seelam, *Separation and Purification technology*, 2007, **53**, 171-177.

(34) M. Amini, A. Rahbar-Kelishami, M. Alipour and O. Vahidi, *Journal of Membrane Science and Research*, 2018, **4**, 121-135.

(35) Kislik, V. S. *Liquid membranes: principles and applications in chemical separations and wastewater treatment*; Elsevier, 2009.

(36) Scott, R. Encyclopedia of analytical science. *Reference Reviews, 2nd ed.; Elsevier: Amsterdam, The Netherlands* **2005**, *19*, 554-561.

(37) Nghiem, L.; Mornane, P.; Potter, I.; Perera, J.; Cattrall, R.; Kolev, S. Extraction and transport of metal ions and small organic compounds using polymer inclusion membranes (PIMs). *Journal of Membrane Science* **2006**, *281* (1-2), 7-41. DOI: 10.1016/j.memsci.2006.03.035.

(38) Almeida, M. I. G. S.; Cattrall, R. W.; Kolev, S. D. Recent trends in extraction and transport of metal ions using polymer inclusion membranes (PIMs). *Journal of Membrane Science* **2012**, *415-416*, 9-23. DOI: 10.1016/j.memsci.2012.06.006.

(39) Yoshida, W.; Baba, Y.; Kubota, F.; Kolev, S. D.; Goto, M. Selective transport of scandium(III) across polymer inclusion membranes with improved stability which contain an amic acid carrier. *Journal of Membrane Science* **2019**, *572*, 291-299. DOI: 10.1016/j.memsci.2018.11.021.

CHAPTER TWO

LITERATURE REVIEW: POLYMER INCLUSION MEMBRANES FOR METAL ION SEPARATION

2.1 Polymer Inclusion Membranes

Polymer inclusion membranes (PIMs) represent an important class of membrane-based separation materials that have gained considerable attention for the selective transport and recovery of metal ions. These membranes combine the advantages of liquid membrane systems and solid polymer membranes, enabling highly selective separations while maintaining improved mechanical stability and operational durability. Over the past several decades, PIMs have emerged as promising alternatives to traditional metal separation technologies due to their tunable composition, low solvent consumption, and potential for environmentally sustainable operation. Membrane separation technologies in general provide a selective barrier that allows the transport of specific chemical species while preventing the passage of others. Compared with conventional separation methods such as solvent extraction, precipitation, or ion exchange, membrane processes can often operate with lower energy requirements and reduced chemical usage. These characteristics make membrane-based technologies attractive for applications involving the separation and recovery of valuable metals from complex mixtures.[1-5]

The growing interest in PIM technology is reflected in the increasing number of research studies focusing on the development of new membrane compositions and improved transport mechanisms. Recent studies have highlighted the increasing importance of membrane technologies in sensing, wastewater treatment, and resource recovery.[4-10] PIMs evolved from earlier liquid membrane systems that were developed to combine solvent extraction and membrane separation into a single process. PIMs were developed as a more stable alternative to traditional liquid membranes. In PIMs, the liquid phase containing the carrier and plasticizer is immobilized within a solid polymer matrix, creating a quasi-solid membrane structure that retains the advantages of carrier-mediated transport while significantly improving membrane stability. The immobilization of the liquid

phase within the polymer network prevents the loss of membrane components and enhances the mechanical robustness of the membrane during operation.

One of the defining characteristics of PIMs is their ability to perform extraction and stripping processes simultaneously. In conventional solvent extraction processes, metal ions are first extracted into an organic phase and subsequently stripped into a receiving phase through multiple process steps. In contrast, PIMs allow the extraction of metal ions from a feed solution and their release into a receiving solution within a single membrane system. This integrated transport process can significantly reduce chemical consumption and simplify separation operations. Another important advantage of PIMs is their tunability. The chemical composition of the membrane can be adjusted by modifying the polymer matrix, carrier, plasticizer, or additional additives. These modifications allow researchers to design membranes with tailored selectivity for specific metal ions. As a result, PIMs have been widely investigated for the separation of various metal ions including transition metals, rare earth elements, and heavy metals from industrial and environmental systems.

2.2 Components of Polymer Inclusion Membranes

The performance of PIMs is governed primarily by their composition and the interactions between the membrane components. A typical PIM consists of a polymer matrix, a carrier or extractant, and a plasticizer. The careful selection and optimization of these components are essential for achieving efficient and selective transport of metal ions across the membrane. Each component in the membrane performs a specific function that contributes to the overall separation process. Understanding the role of each component is critical for designing PIM systems capable of efficiently separating metal ions from complex mixtures.

2.2.1 Polymer Matrix

The polymer matrix forms the structural backbone of polymer inclusion membranes (PIMs) and plays a fundamental role in determining the physical stability and transport properties of the membrane. While the carrier facilitates selective ion transport and the plasticizer enhances membrane flexibility, the polymer matrix provides mechanical integrity and immobilizes the membrane components within a stable framework. The polymer matrix therefore serves as the platform that supports carrier mediated ion transport while maintaining the overall stability of the membrane system. In PIMs, the polymer matrix performs several important functions. First, it provides mechanical strength and structural support that prevents the leakage of the carrier and plasticizer from the membrane phase. Second, it immobilizes the active membrane components within a solid network, allowing the membrane to maintain its shape and integrity during operation. Third, the polymer matrix influences the microstructure and free volume within the membrane, which can affect the diffusion of carrier–metal complexes and ultimately control ion transport rates.[11-14]

The choice of polymer matrix is therefore a critical factor in the design of PIM systems. An ideal polymer for PIM fabrication should possess several key characteristics. These include good film forming ability, mechanical strength, chemical stability, compatibility

with carriers and plasticizers, and resistance to degradation in aqueous environments. In addition, the polymer should allow homogeneous dispersion of the carrier and plasticizer to ensure uniform transport properties throughout the membrane. The chemical structure and morphology of the polymer matrix significantly influence the internal microenvironment of the membrane. Within PIMs, the polymer network forms a semi rigid structure that surrounds the carrier and plasticizer molecules. This environment determines the mobility of membrane components and the diffusion

Table 2.1 Common polymer matrix used in PIMs.

Polymer matrix	Structure
PVC	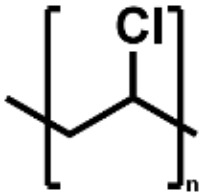
CTA	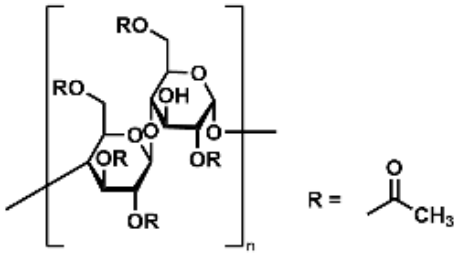
PVDF	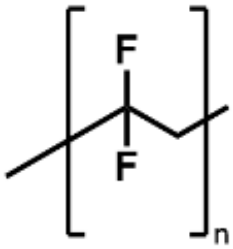
PVDF-HFP	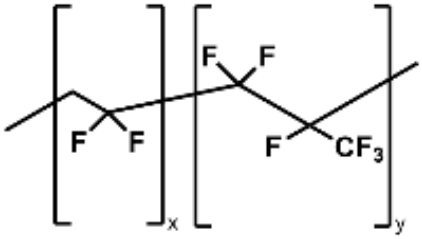

pathways available for metal–carrier complexes. Polymers with higher free volume generally allow greater mobility of carrier molecules and metal complexes, which can enhance ion transport across the membrane. Conversely, highly rigid polymer matrices may restrict molecular diffusion and reduce transport rates.[15-18] However, polymers with excessive flexibility may compromise

membrane mechanical stability and lead to structural deformation during operation. Therefore, a balance between rigidity and flexibility is required for optimal membrane performance. The polarity of the polymer matrix can also influence membrane behavior. Polar polymers may interact more strongly with carriers or metal complexes through dipole interactions or hydrogen bonding.[19-20] These interactions can affect both the distribution of carriers within the membrane and the diffusion of metal complexes. Several polymers have been widely investigated for the preparation of PIMs. Among these, polyvinyl chloride (PVC) and cellulose triacetate (CTA) are the most frequently used polymer matrices in membrane-based metal separation studies. Other polymers such as polyvinylidene fluoride (PVDF) and its copolymers have also been explored in recent years due to their excellent chemical resistance and mechanical stability.

Cellulose Triacetate (CTA)

Cellulose triacetate is another widely used polymer matrix for PIM systems. CTA is derived from cellulose and contains acetyl functional groups that impart moderate polarity to the polymer structure. This polarity can improve compatibility with certain carriers and plasticizers. CTA based membranes are often transparent and flexible, making them convenient for experimental studies involving membrane transport. The polymer also exhibits good resistance to aqueous environments and maintains stable membrane structures during long term operation. One advantage of CTA is its ability to form relatively homogeneous membranes with well distributed carrier molecules. This property can improve the reproducibility of membrane performance in experimental studies. CTA has therefore been widely used in research focused on metal ion transport across PIMs.[19-22]

Polyvinyl Chloride (PVC)

Polyvinyl chloride is one of the most commonly used polymers in PIM fabrication. PVC is widely available, relatively inexpensive, and exhibits excellent film forming properties. It can easily dissolve in common organic solvents such as tetrahydrofuran, which facilitates membrane preparation through solution casting methods. PVC based PIMs often exhibit good mechanical stability and durability under various operating conditions. The hydrophobic nature of PVC also helps retain the carrier and plasticizer within the membrane matrix, reducing the likelihood of component leaching during operation. Because of these properties, PVC has been widely used as a polymer matrix for PIMs designed for metal ion separation. However, PVC membranes may exhibit relatively limited flexibility without the addition of plasticizers. As a result, the incorporation of suitable plasticizers is typically required to enhance membrane elasticity and improve diffusion of carrier–metal complexes.[23-25]

Polyvinylidene Fluoride (PVDF)

Polyvinylidene fluoride and its copolymers have attracted attention in membrane research due to their excellent chemical resistance and thermal stability. PVDF contains strong carbon fluorine bonds that provide high resistance to chemical degradation and oxidative environments. PVDF based membranes often exhibit superior mechanical strength compared with many other polymer matrices. These properties make PVDF attractive for applications involving harsh chemical conditions or long-term operation. In addition, PVDF can form porous or semi crystalline structures that may influence membrane transport behavior.[25-28] Although PVDF is less commonly used than PVC or CTA in traditional PIM systems, it has gained interest in advanced membrane systems designed for improved durability and performance.

2.2.2 Carrier and Extractants

Carriers, also referred to as extractants, represent the most critical functional component of polymer inclusion membranes (PIMs). While the polymer matrix provides structural stability, the carrier is responsible for the selective transport of metal ions across the membrane. The efficiency, selectivity, and transport kinetics of PIM systems are therefore largely governed by the chemical properties and concentration of the carrier incorporated within the membrane.[29-30] In PIM systems, carriers function by reversibly interacting with target metal ions at the membrane interface. The carrier forms a metal–carrier complex that is soluble within the membrane phase. This complex then diffuses across the membrane under the influence of a concentration gradient or chemical potential difference between the feed and receiving solutions. At the receiving interface, the metal ion is released from the carrier through a stripping reaction, allowing the carrier molecule to diffuse back through the membrane and participate in another transport cycle. This mechanism enables continuous and selective ion transport through the membrane.[31-35] Carriers used in PIMs are often derived from extractants commonly employed in solvent extraction processes. Many of these compounds have been extensively studied in hydrometallurgical applications and exhibit strong affinities for specific metal ions. By immobilizing these extractants within a polymer matrix, it is possible to combine the selectivity of solvent extraction with the operational simplicity of membrane separation. Several factors influence the performance of carriers in PIM systems. These include the strength of the metal–carrier interaction, the solubility of the carrier in the membrane phase, the diffusion coefficient of the carrier–metal complex, and the stability of the carrier under operating conditions. An effective carrier must exhibit sufficient affinity for the target metal ion to enable selective complex formation, while also allowing rapid dissociation of the complex in the receiving phase to complete the transport cycle. Carriers used in polymer inclusion membranes

(PIMs) can be broadly classified into three main categories according to their extraction mechanisms. These categories include acidic carriers, neutral carriers, and basic carriers. Each classes of carrier interacts with metal ions through distinct chemical mechanisms and therefore exhibits different selectivity patterns and transport behaviors. The classification of carriers according to their extraction chemistry is widely adopted in solvent extraction and membrane separation studies because it provides a framework for understanding metal complexation and transport mechanisms.[35-37]

The choice of carrier type is one of the most important design considerations when developing PIM systems for metal separation. The chemical structure of the carrier determines the strength of metal–carrier interactions, the stability of the resulting complexes, and the overall selectivity of the membrane toward different metal ions. Understanding the fundamental behavior of acidic, neutral, and basic carriers is therefore essential for designing membranes capable of separating complex mixtures of metal ions.

Basic Carriers

Basic carriers are typically composed of extractants that interact with metal ions through anion exchange or ion pair formation mechanisms. In acidic solutions, many metal ions form negatively charged complexes with anions such as chloride or sulfate. Basic carriers can extract these negatively charged complexes by forming ion pairs that are soluble in the membrane phase. These carriers often contain nitrogen and phosphorus atoms, including quaternary amines, phosphonium compounds, tertiary amines, and pyridine derivatives. These compounds usually contain nitrogen or phosphorus atoms with lone electron pairs that can interact with anionic metal complexes. In many cases, the extraction mechanism involves protonation of the amine followed by ion pair

formation with the metal complex. A simplified reaction for extraction of a metal chloride complex can be expressed as

$$R_3N + H^+ + MCl_4^- \rightleftharpoons (R_3NH^+)(MCl_4^-)$$

where R_3N represents the amine carrier and $(R_3NH^+)(MCl_4^-)$ represents the ion pair extracted into the membrane phase.

In PIM systems, basic carriers can facilitate the transport of metal complexes across the membrane through reversible ion pairing interactions. After the metal complex diffuses across the membrane, it can be released in the receiving phase by altering the chemical conditions such as pH or anion concentration. One limitation of basic carriers is that the presence of competing anions in the feed solution may interfere with metal extraction. Additionally, strong interactions between the carrier and the metal complex may reduce the rate of metal release in the receiving phase. These factors must be carefully considered when designing PIM systems using basic carriers.[39-44]

Acidic Carriers

Acidic carriers are among the most widely studied extractants for metal separation processes and are commonly incorporated into PIM systems. These carriers contain acidic functional groups capable of exchanging protons with metal ions during complex formation. The extraction mechanism typically involves a proton exchange reaction in which the carrier releases one or more protons while simultaneously forming a complex with the metal ion. Acidic carriers generally contain functional groups such as phosphoric acids, phosphinic acids, phosphonic acids, or carboxylic acids. These functional groups possess oxygen donor atoms that coordinate with metal ions to form stable metal–carrier complexes. The extraction reaction for a divalent metal ion can be represented in simplified form as

$$M_{(aq)}^{2+} + 2(HR)_{(org)} \rightleftharpoons MR_{2(org)} + 2H_{(aq)}^{+}$$

where HR represents the acidic carrier molecule and MR_2 represents the metal–carrier complex formed within the membrane phase.

Organophosphorus extractants represent an important class of acidic carriers widely used in metal separation processes. Examples include di-(2-ethylhexyl) phosphoric acid (D2EHPA), Cyanex 272, and Cyanex 301. The extraction efficiency of acidic carriers is strongly influenced by solution pH because proton exchange is an integral part of the complexation mechanism. At lower pH values, high proton concentrations suppress metal extraction by shifting the equilibrium toward the protonated carrier form. As the pH increases, proton concentration decreases and metal extraction becomes more favorable. This pH dependent behavior allows acidic carriers to selectively separate metals based on their extraction equilibria.[45-51]

Neutral Carriers

Neutral carriers extract metal ions through coordination mechanisms rather than proton exchange reactions. These carriers typically contain donor atoms such as oxygen, nitrogen, or sulfur that can coordinate directly with metal ions. Because neutral carriers do not release protons during complex formation, the extraction process is generally less dependent on solution pH compared with acidic carriers. Neutral carriers commonly contain phosphoryl or carbonyl functional groups that exhibit strong coordination ability toward metal ions. Typical examples include tri-n-butyl phosphate (TBP), trioctylphosphine oxide (TOPO), and dibutyl butyl phosphonate. These compounds have been widely used in solvent extraction processes for the separation of actinides, lanthanides, and various transition metals. The extraction mechanism for neutral carriers often involves solvation of the metal ion or metal complex. In acidic solutions, metal ions frequently exist as coordination complexes with anions such as chloride, nitrate, or sulfate. Neutral carriers can stabilize these

complexes through coordination interactions with donor atoms. A simplified representation of this process can be expressed as

$$M^{n+} + nA^{-} + xL \rightleftharpoons ML_xA_n$$

where L represents the neutral carrier ligand and ML_xA_n represents the resulting solvated metal complex.[52-55] Because neutral carriers interact directly with metal ions through coordination bonds, the selectivity of these carriers is often influenced by the electronic properties and coordination preferences of the metal ion. One advantage of neutral carriers is that they often exhibit high chemical stability and reduced sensitivity to pH changes compared with acidic carriers. In addition, the absence of proton exchange reactions can simplify the transport mechanism in some membrane systems. However, the strength of coordination interactions must be carefully balanced. If the metal–carrier complex is too stable, release of the metal ion in the receiving phase may become difficult, which can reduce overall transport efficiency. Therefore, optimal carrier design requires balancing complex stability with efficient stripping of the metal ion.

2.2.3 Plasticizers

Plasticizers represent an essential component of PIMs and play a critical role in determining membrane flexibility, microstructure, and ion transport behavior. While the polymer matrix provides structural integrity and the carrier enables selective metal complexation, plasticizers modify the physical properties of the membrane by increasing polymer chain mobility and facilitating the diffusion of carrier–metal complexes. The incorporation of suitable plasticizers therefore enables efficient ion transport while maintaining sufficient mechanical stability of the membrane. In many polymer matrices used for PIM fabrication, the polymer chains are relatively rigid and tightly packed. This rigidity can restrict the mobility of carrier molecules and limit the diffusion of metal–carrier complexes through the membrane phase. Plasticizers reduce

intermolecular forces between polymer chains, increasing the free volume within the polymer matrix. The resulting increase in polymer chain mobility creates diffusion pathways that facilitate the movement of carrier molecules and metal complexes across the membrane.[11-12]

Plasticizers influence the internal microstructure of PIMs by modifying the arrangement of polymer chains. When plasticizers are incorporated into the membrane matrix, they insert themselves between polymer chains and weaken intermolecular interactions such as van der Waals forces or dipole interactions. This process increases the spacing between polymer chains and produces a more flexible membrane structure. The increase in free volume within the membrane enhances the mobility of both the carrier molecules and the carrier–metal complexes. As a result, the diffusion coefficient of the transporting species increases, which can significantly improve membrane permeability and metal ion flux.

In addition to increasing free volume, plasticizers can improve the compatibility between the polymer matrix and the carrier. Many carriers used in PIM systems are hydrophobic organic molecules that must be uniformly dispersed within the polymer network. Plasticizers often act as intermediate phases that enhance miscibility between the polymer and the carrier, thereby preventing phase separation and ensuring uniform membrane composition.

A wide variety of plasticizers have been used in the preparation of PIMs. The most used plasticizers are hydrophobic organic compounds that exhibit high boiling points, good compatibility with both the polymer matrix and the carrier, and suitable viscosity for membrane formation. One of the most widely used plasticizers in PIM systems is 2-nitrophenyl octyl ether (2-NPOE).[11-12] This compound possesses high dielectric constant and low volatility, which makes it highly effective for dissolving carrier molecules and facilitating metal transport. 2-NPOE is frequently used in membranes designed for the transport of transition metals because it enhances

the solubility of metal–carrier complexes within the membrane phase. Another commonly used plasticizer is 2-nitrophenyl pentyl ether (2-NPPE).[13,57] Similar to 2-NPOE, this compound improves membrane flexibility and enhances ion diffusion within the membrane matrix. The shorter alkyl chain of 2-NPPE may influence membrane viscosity and transport properties compared with longer chain plasticizers. Dioctyl phthalate (DOP) and related phthalate esters have also been used as plasticizers in PIM formulations. These compounds exhibit good compatibility with many polymer matrices and can improve membrane elasticity. However, environmental concerns associated with certain phthalate compounds have motivated the exploration of alternative plasticizers in recent years. Other plasticizers that have been investigated including ionic liquids. In some cases, ionic liquids can act simultaneously as carriers and plasticizers due to their liquid nature and strong interaction with metal ions.

Plasticizers influence metal ion transport in PIM systems through several mechanisms. First, by increasing polymer chain mobility, plasticizers reduce resistance to diffusion of the carrier–metal complex within the membrane phase. This effect can significantly increase membrane permeability. Second, plasticizers often increase the solubility of the carrier and the metal–carrier complex within the membrane matrix. Enhanced solubility facilitates the formation of mobile complexes that can diffuse more easily across the membrane. Third, plasticizers may influence the thermodynamic stability of the metal–carrier complex within the membrane phase. The polarity and dielectric properties of the plasticizer can alter the interaction between the carrier and the metal ion, thereby affecting complex formation and dissociation during transport.[29,34]

The combined influence of these factors ultimately determines the overall flux of metal ions through the membrane. In many PIM systems, the diffusion of the carrier–metal complex within

the membrane phase represents the rate limiting step of the transport process. Plasticizers therefore play a key role in controlling the kinetics of metal ion transport.

2.3 Transport Mechanism in Polymer Inclusion Membranes

The transport of metal ions across polymer inclusion membranes (PIMs) occurs through carrier mediated mechanisms that involve reversible complexation between metal ions and carrier molecules embedded within the membrane phase. Unlike conventional diffusion through porous membranes, transport in PIM systems is facilitated by chemical interactions between the carrier and the target ion. This mechanism enables selective separation of metal ions even when they possess similar ionic radii or chemical properties. The overall transport process generally consists of several sequential steps occurring at the feed membrane interface, within the membrane phase, and at the membrane receiving interface. These steps include metal ion complexation at the membrane surface, diffusion of the carrier–metal complex through the membrane matrix, and dissociation of the complex in the receiving phase. The continuous cycling of the carrier between these steps enables sustained transport of metal ions across the membrane. Understanding the mechanisms governing ion transport is essential for optimizing membrane composition and improving separation performance.

2.3.1 Carrier Mediated Transport Mechanism

Carrier mediated transport is the fundamental mechanism responsible for metal ion movement across PIM systems. In this process, carrier molecules within the membrane selectively bind metal ions present in the feed solution. The resulting metal–carrier complex is soluble within the membrane phase and can diffuse through the polymer matrix toward the receiving phase. The transport process can be described through the following sequence of steps:

- Complexation at the feed–membrane interface

Metal ions present in the feed solution interact with carrier molecules located at the membrane surface. A reversible complex is formed between the metal ion and the carrier. The formation of this complex depends on the affinity of the carrier for the metal ion as well as the chemical conditions of the aqueous phase, including pH and the presence of competing ions.

- Diffusion through the membrane phase

Once the metal–carrier complex is formed, it diffuses through the membrane phase driven by the concentration gradient between the feed and receiving phases. The rate of diffusion depends on factors such as membrane viscosity, plasticizer concentration, and the diffusion coefficient of the complex within the membrane matrix.

- Decomplexation at the membrane–receiving interface

At the membrane–receiving interface, the metal ion is released from the carrier due to the presence of a stripping agent or changes in chemical conditions within the receiving solution. These conditions are typically designed to destabilize the metal–carrier complex and promote dissociation of the metal ion.

- Carrier regeneration and return diffusion

After releasing the metal ion, the free carrier molecule diffuses back toward the feed interface. The regenerated carrier can then participate in another transport cycle, allowing continuous movement of metal ions across the membrane.

This cyclic transport process allows sustained movement of metal ions across the membrane while the carrier remains immobilized within the membrane phase.

metal complex through the membrane, and release of the metal ion at the receiving interface.[12,57-58]

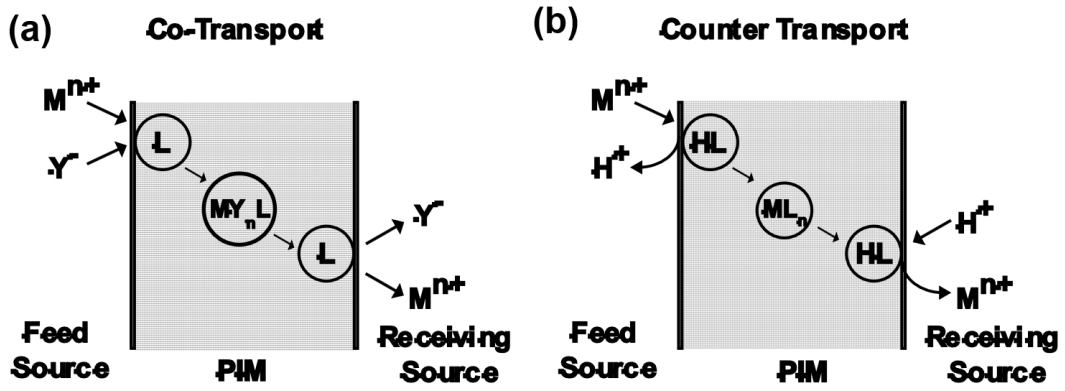

Figure 2.1 Transport mechanism of metal ions across membranes (a) co-transport mechanism (b) counter transport mechanism.[58]

The transport of metal ions through PIM systems can occur through two ways: co-transport and counter-transport. These mechanisms describe how ions and their associated species move across the membrane during carrier mediated transport. In the co-transport mechanism, metal ions and their associated anions form complexes with neutral carriers. In this process, both the metal ion and the accompanying anion are transported together through the membrane as a neutral complex. The neutral carrier coordinates with the metal ion and its counter anions to form a stable complex that diffuses through the membrane phase. This process can be represented by

$$M^{n+} + nY^- + L \rightleftharpoons (MY_nL)_{membrane}$$

where M^{n+} represents the metal ion, Y^- represents the associated anions, and L represents the neutral carrier. The complex MY_nL diffuses through the membrane and subsequently releases the metal ion in the receiving phase. Co-transport mechanisms are commonly observed in systems where neutral carriers such as phosphine oxides or organophosphates are used.

In contrast, counter-transport involves the exchange of ions between the membrane phase and the aqueous solution. In this mechanism, metal ions form complexes with organic carriers and diffuse through the membrane while exchanging cations or anions with the carrier. One common example

involves acidic carriers in which protons are exchanged with metal ions during complex formation. This process can be described by

$$M^{n+} + nHL \rightleftharpoons (MLn)_{membrane} + nH^{+}$$

where HL represents the protonated acidic carrier. During this reaction, the metal ion replaces protons bound to the carrier, forming a metal–carrier complex that diffuses through the membrane. The released protons are transported in the opposite direction, creating a counter-transport process. Counter-transport mechanisms are frequently observed in systems using acidic extractants such as organophosphorus compounds. The transport process is often influenced by the pH gradient between the feed and receiving phases. The receiving phase typically contains conditions that promote proton release and metal stripping, thereby sustaining continuous transport across the membrane.

2.3.2 Diffusion and Flux of Transport of Ions

Once the metal–carrier complex is formed at the feed–membrane interface, its diffusion through the membrane phase becomes a critical step controlling the overall transport process. In polymer inclusion membranes, the polymer matrix acts as a dense medium through which the carrier–metal complex migrates via molecular diffusion. The rate of diffusion is strongly influenced by the physicochemical properties of the membrane, including polymer chain mobility, the free volume within the polymer network, and the presence of plasticizers that reduce membrane rigidity and enhance molecular mobility.

Plasticizers play a particularly important role in facilitating diffusion by increasing the flexibility of the polymer chains and generating micro-voids within the membrane structure. These micro-voids provide pathways that allow carrier–metal complexes to move through the membrane phase. The transport of metal ions through PIMs is commonly described using diffusion models based on

Fick's laws. According to Fick's first law, the steady state flux of a species across a membrane is proportional to the concentration gradient across the membrane thickness. The flux (J) can be expressed as

$$J = -D\frac{dC}{dx}$$

where D represents the diffusion coefficient of the metal–carrier complex within the membrane phase and $\frac{dC}{dx}$ represents the concentration gradient across the membrane thickness.[12,60-61]

This formulation highlights the importance of both diffusion within the membrane and the ability of the carrier to extract the metal ion from the aqueous phase. Efficient transport requires both strong complexation between the metal ion and the carrier and rapid diffusion of the resulting complex through the membrane matrix. The diffusion coefficient itself is influenced by several membrane properties. Increased polymer chain mobility typically enhances diffusion rates because the carrier–metal complex encounters less resistance as it migrates through the membrane phase. Similarly, membranes with larger free volume or higher plasticizer content generally exhibit higher diffusion coefficients. Conversely, highly rigid polymer matrices or membranes with low plasticizer content can restrict molecular motion and reduce transport rates. Membrane thickness is another important parameter affecting transport flux. Thicker membranes increase the diffusion path length, thereby reducing the overall transport rate. For this reason, many PIM systems are fabricated as thin films to minimize diffusion resistance while maintaining mechanical stability. In many PIM systems, diffusion of the carrier–metal complex through the membrane phase represents the rate limiting step in the overall transport process. Even when complexation at the feed interface occurs rapidly, slow diffusion through the membrane matrix can limit the overall

flux of metal ions. Consequently, membrane composition, thickness, carrier concentration, and plasticizer content strongly influence transport kinetics and overall separation performance.

2.3.2 Kinetic Modelling of Transport in Polymer Inclusion Membranes

Kinetic modeling plays an important role in understanding the transport behavior of metal ions across polymer inclusion membranes. While thermodynamic considerations determine whether metal extraction and complexation are favorable, kinetic models describe the rate at which metal ions are transported across the membrane. These models allow researchers to quantify membrane performance, identify rate limiting steps, and evaluate how membrane composition influences transport efficiency. In many PIM systems, metal ion transport is described using first order kinetic models that relate the decrease in metal ion concentration in the feed phase to transport across the membrane. Because the receiving phase typically contains conditions that rapidly strip the metal ion from the carrier complex, the concentration of the metal ion in the receiving phase remains relatively low during the early stages of transport. Under these conditions, the concentration gradient across the membrane is primarily controlled by the feed solution.[60-61]

The rate of metal ion transport from the feed phase can therefore be expressed as

$$ln\frac{(C_{f,t})}{(C_{f,0})} = -kt$$

where:

$C_{f,0}$ = initial concentration of the metal ion (mol L^{-1}) in the feed solution.

$C_{f,t}$ = concentration of the metal ion in the feed solution at time (t).

k = rate constant

This relationship indicates that the natural logarithm of the concentration ratio decreases linearly with time. Experimental transport studies therefore often involve plotting $\ln\left(\frac{C_{f,t}}{C_{f,0}}\right)$ versus time to

determine the rate constant (k) from the slope of the resulting linear relationship. The apparent rate constant is related to the permeability coefficient of the membrane, which describes the overall ability of the membrane to transport the metal ion. The permeability coefficient P can be calculated using the following relationship:

$$P = \frac{V}{A}k$$

where:

V = the volume of the feed solution and

$A =$ the effective membrane surface area.

The permeability coefficient is a key parameter used to compare transport performance among different membrane systems. Higher permeability values indicate faster transport of metal ions across the membrane. Another useful parameter used to describe membrane transport is the initial flux J_0, which represents the rate of metal ion transfer at the beginning of the transport process. The initial flux can be expressed as

$$J_0 = PC_{f,0}$$

This parameter provides insight into the efficiency of the membrane during the early stages of transport when the concentration gradient is at its maximum.

Several factors can influence the kinetic parameters of ion transport in PIM systems. Carrier concentration plays a critical role because higher carrier loading generally increases the availability of binding sites for metal ions. However, excessive carrier content can sometimes increase membrane viscosity and reduce diffusion rates. Plasticizer concentration also affects transport kinetics by modifying membrane flexibility and diffusion pathways. Increased plasticizer content generally enhances the mobility of carrier–metal complexes and therefore increases

permeability. Membrane thickness is another important parameter affecting transport kinetics. Thicker membranes increase diffusion distance, which reduces the permeability coefficient and slows overall transport rates. For this reason, many PIM systems are fabricated as thin films to minimize diffusion resistance while maintaining sufficient mechanical stability.

Kinetic modeling therefore provides valuable information about how membrane composition and operating conditions influence ion transport. By analyzing transport kinetics and permeability parameters, researchers can optimize membrane formulations to achieve improved selectivity and faster transport rates for target metal ions.

References

1. Nghiem, L.; Mornane, P.; Potter, I.; Perera, J.; Cattrall, R.; Kolev, S. Extraction and transport of metal ions and small organic compounds using polymer inclusion membranes (PIMs). *Journal of Membrane Science* **2006**, *281* (1-2), 7-41. DOI: 10.1016/j.memsci.2006.03.035.

2. Almeida, M. I. G. S.; Cattrall, R. W.; Kolev, S. D. Recent trends in extraction and transport of metal ions using polymer inclusion membranes (PIMs). *Journal of Membrane Science* **2012**, *415-416*, 9-23. DOI: 10.1016/j.memsci.2012.06.006.

3. Yoshida, W.; Baba, Y.; Kubota, F.; Kolev, S. D.; Goto, M. Selective transport of scandium(III) across polymer inclusion membranes with improved stability which contain an amic acid carrier. *Journal of Membrane Science* **2019**, *572*, 291-299. DOI: 10.1016/j.memsci.2018.11.021.

4. Cattrall, R.W. (1997). *Chemical Sensors*. Oxford: Oxford University Press.

5. Pechenkina, I. and Mikhelson, K. (2015). Materials for the ionophore-based membranes for ion-selective electrodes: problems and achievements (review paper). *Russ. J.Electrochem.* 51 (2): 93–102.

6. Bakker, E. (2014). Enhancing ion-selective polymeric membrane electrodes by instrumental control. *TrAC Trends Anal. Chem.* 53: 98–105.

7. Morf, W.E., Seiler, K., Rusterholz, B., and Simon, W. (1990). Design of a calcium selective optode membrance based on neutral ionophores. *Anal. Chem.* 62 (7):738–742.

8. Kavanagh, A., Byrne, R., Diamond, D., and Radu, A. (2011). A two-component polymeric optode membrane based on a multifunctional ionic liquid. *Analyst* 136 (2): 348–353.

9. A. J. Schow, R. T. Peterson and J. D. Lamb, *Journal of membrane science*, 1996, **111**, 291-295.

10. J. Aguilar, M. Sanchez-Castellanos, E. R. de San Miguel and J. De Gyves, *Journal of Membrane Science*, 2001, **190**, 107-118.

11. M. I. G. Almeida, R. W. Cattrall and S. D. Kolev, *Journal of Membrane Science*, 2012, **415**, 9-23.

12. L. D. Nghiem, P. Mornane, I. D. Potter, J. M. Perera, R. W. Cattrall and S. D. Kolev, *Journal of Membrane Science*, 2006, **281**, 7-41.

13. Y. Yıldız, A. Manzak and O. Tutkun, *Desalination and Water Treatment*, 2016, **57**, 4616-4623.

14. K. Annane, A. Sahmoune, P. Montels and S. Tingry, *Chemical engineering research and design*, 2015, **94**, 605-610.

15. C. Specht, R. W. Cattrall, T. G. Spassov, M. I. Spassova and S. D. Kolev, *Reactive and Functional Polymers*, 2018, **130**, 81-89.

16. N. S. Abdul-Halim, P. G. Whitten and L. D. Nghiem, *Separation Science and Technology*, 2016, **51**, 1515-1522.

17. Y. Sun, Z. Wang, Y. Wang, M. Liu, S. Li, L. Tang, S. Wang, X. Yang and S. Ji, *Chemical Engineering Research and Design*, 2020, **153**, 136-145.

19. Z. Wang, Y. Sun, N. Tang, C. Miao, Y. Wang, L. Tang, S. Wang and X. Yang, *Separation and Purification Technology*, 2019, **222**, 136-144.

20. Z. H. Qin, Y. Z. Wang, L. Sun, Y. X. Gu, Y. Zhao, L. Xia, Y. Liu, B. Van der Bruggen and Y. Zhang, *Journal of Hazardous Materials*, 2022, **436**, 129315.

21. F. Sellami, O. Kebiche-Senhadji, S. Marais, L. Colasse and K. Fatyeyeva, *Separation and Purification Technology*, 2020, **248**, 117038.

22. N. S. W. Zulkefeli, S. K. Weng and N. S. Abdul Halim, *Current Pollution Reports*, 2018, **4**, 84-92.

23. E. I. Oluwasola, A. L. Ahmad and N. F. Shoparwe, *Journal of Water Process Engineering*, 2023, **52**, 103508.

24. B. Wang, Y. Wang and T. Xu, *Advanced Materials Technologies*, 2023, **8**, 2300829.

25. K. Witt, E. Radzyminska-Lenarcik, A. Kosciuszko, M. Gierszewska and K. Ziuziakowski, *Polymers*, 2018, **10**, 134.

26. H. Cascon and S. Choudhary, *Separation Science and Technology*, 2013, **48**, 1616-1626.

27. A. Nath and A. Kumar, *Journal of membrane science*, 2014, **453**, 192-201.

28. H. I. Turgut, V. Eyupoglu, R. A. Kumbasar and I. Sisman, *Separation and Purification Technology*, 2017, **175**, 406-417.

29. D. Wang, R. W. Cattrall, J. Li, M. I. G. Almeida, G. W. Stevens and S. D. Kolev, *Separation and Purification Technology*, 2018, **202**, 59-66.

30. S. Bahrami, L. Dolatyari, H. Shayani-Jam and M. R. Yaftian, *Journal of Applied Polymer Science*, 2022, **139**, e52434.

31. D. Kazemi, M. R. Yaftian and S. D. Kolev, *Reactive and Functional Polymers*, 2021, **164**, 104935.

32. N. Ghaderi, L. Dolatyari, D. Kazemi, H. R. Sharafi, H. Shayani-Jam and M. R. Yaftian, *Journal of Applied Polymer Science*, 2022, **139**, 51480.

33. P. Szczepański, H. P. Guo, K. Dzieszkowski, Z. Rafiński, A. Wolan, K. Fatyeyeva, J. Kujawa and W. Kujawski, *Journal of Membrane Science*, 2021, **638**, 119674.

34. D. Wang, R. W. Cattrall, J. Li, M. I. G. Almeida, G. W. Stevens and S. D. Kolev, *Journal of Membrane Science*, 2017, **542**, 272-279.

35. S. Huang, J. Chen and D. Zou, *Journal of Rare Earths*, 2021, **39**, 1256-1263.

36. S. Bahrami, M. R. Yaftian, P. Najvak, L. Dolatyari, H. Shayani-Jam and S. D. Kolev, *Separation and Purification Technology*, 2020, **250**, 117251.

37. V. Eyupoglu, A. Unal, E. Polat, B. Eren and R. A. Kumbasar, *Separation and Purification Technology*, 2022, **303**, 122201.

38. B. Keskin, B. Zeytuncu-Gokoglu and I. Koyuncu, *Chemosphere*, 2021, **279**, 130604.

39. A. Nowik-Zajac, C. Kozłowski, and W. Walkowiak, *Physicochemical Problems of Mineral Processing*, 2010, **44**, 179-186.

40. R. Kumar, A. K. Pandey, A. Tyagi, G. Dey, S. V. Ramagiri, J. R. Bellare and A. Goswami, *Journal of colloid and interface science*, 2009, **337**, 523-530.

41. B. Wionczyk, W. A. Apostoluk,a nd K. Prochaska, *Analytica chimica acta*, 2001, **428**, 89-101.

42. J. D. Lamb, A. Y. Nazarenko and H. Tsukube, *Analytica chimica acta*, 1998, **373**, 167-173.

43. H. Dahdah, F. Sellami, S. Dekkouche, M. Benamor and O. Senhadji-Kebiche, *Polymer Bulletin*, 2023, **80**, 6495-6525.

44. M. Matsumoto , N. Kita and Y. Tahara , *Solvent Extraction Research and Development, Japan*, 2023, **30**, 177-181.

45. A. Kaya, C. Onac, H. K. Alpoguz, A. Yilmaz and N. Atar, *Chemical Engineering Journal*, 2016, **283**, 141-149.

46. S. P. Best, S. D. Kolev, J. R. P. Gabriel and R. W. Cattrall, *Journal of Membrane Science*, 2016, **497**, 377-386.

47. A. Yilmaz, G. Arslan, A. Tor and I. Akin, *Desalination*, 2011, **277**, 301-307.

48. B. Pospiech, *Physicochemical Problems of Mineral Processing*, 2013, **49**.

49. B. Pośpiech, *Separation Science and Technology*, 2012, **47**, 1413-1419.

50. X. Meng, Y. Long, Y. Tian, W. Li, T. Liu and S. Huo, *Hydrometallurgy*, 2021, **202**, 105615.

51. H. Arabi, S. Milani, H. Abolghasemi and F. Zahakifar, *Journal of Radioanalytical and Nuclear Chemistry*, 2021, **327**, 653-665.

52. M. d. L. Ballinas, E. Rodríguez de San Miguel, M. T. d. J. Rodríguez, O. Silva, M. Muñoz and J. De Gyves, *Environmental science & technology*, 2004, **38**, 886-891.

53. C. Cai, F. Yang, Z. Zhao, Q. Liao, R. Bai, W. Guo, P. Chen, Y. Zhang and H. Zhang, *Journal of Membrane Science*, 2019, **579**, 1-10.

54. L. Burger, *Nuclear Science and Engineering*, 1963, **16**, 428-439.

55. O. Tutkun and K. Kaparova, *Korean Journal of Chemical Engineering*, 2022, **39**, 1011-1019.

56. O. Kebiche-Senhadji, S. Tingry, P. Seta and M. Benamor, *Desalination*, 2010, **258**, 59-65.

57. D. Wang, J. Hu, Y. Li, M. Fu, D. Liu and Q. Chen, *Journal of Membrane Science*, 2016, **501**, 228-235.

58. Adigun, B.; Luo, H.; Wang, T.; Dai, S. Ionic liquid-enhanced recycling of lithium-ion battery black mass via heavy liquid centrifugal separation. *RSC advances* **2026**, *16* (1), 568-573.

59. M. O'Rourke, R. W. Cattrall, S. D. Kolev and I. D. Potter, *Solvent Extr. Res. Dev*, 2009, **16**, 1-12.

60. L. Chen, Y. Wu, H. Dong, M. Meng, C. Li, Y. Yan and J. Chen, *Separation and Purification Technology*, 2018, **197**, 70-85.

61. P. R. Danesi, *Separation Science and Technology*, 1984, **19**, 857-894.

62. T. Hanada, M. L. Firmansyah, W. Yoshida, F. Kubota, S. D. Kolev and M. Goto, *ACS omega*, 2020, **5**, 12989-12995.

CHAPTER THREE

MATERIALS AND METHODS

This chapter describes the membrane fabrication procedures, and experimental methods used to investigate the performance of PIMs for the separation and recovery of lithium-ion battery metals. PIMs used in this work were prepared using polymer matrices combined with carrier molecules and plasticizers to facilitate selective metal ion transport. Membrane fabrication procedures were designed to produce homogeneous films with reproducible thickness and structural properties. In addition to membrane synthesis, a series of analytical and characterization techniques were used to investigate membrane structure, stability, and transport performance. Metal ion transport experiments were conducted using a two-compartment diffusion cell to evaluate the separation of lithium, cobalt, nickel, and manganese from aqueous solutions. The concentrations of metal ions in both feed and receiving phases were monitored over time using inductively coupled plasma optical emission spectroscopy. Mechanical and structural characterization techniques were also used to evaluate membrane integrity and durability. These analyses provided insight into the relationship between membrane composition and mechanical stability, which is critical for long-term membrane operation. The methods described in this chapter establish the experimental framework used to evaluate PIMs throughout this dissertation.

3.1 Methods

3.1.1 Preparation of Polymer Inclusion Membrane

Polymer inclusion membranes were prepared using the solvent casting method, which is widely used for the fabrication of homogeneous membrane films. In a typical membrane preparation procedure, the polymer matrix, carrier molecule, and plasticizer were dissolved in an appropriate organic solvent to produce a homogeneous casting solution. The components were mixed under continuous stirring until a clear solution was obtained. The resulting solution was poured into a

glass casting dish and allowed to spread evenly across the surface. Solvent evaporation was carried out under controlled conditions to ensure uniform membrane formation. As the solvent evaporated, a thin polymer film containing the carrier and plasticizer was formed. After complete solvent evaporation, the membrane film was carefully removed from the casting surface and used for transport experiments. Membrane thickness was measured using a digital micrometer to ensure reproducibility among samples.

3.1.2 Layer-by-Layer Membrane Reinforcement

Layer-by-layer (LbL) modification of polymer inclusion membranes was performed to improve membrane mechanical stability and reduce carrier leaching during transport experiments. The membranes were sequentially immersed in aqueous solutions containing oppositely charged polyelectrolytes to deposit alternating layers on the membrane surface. In a typical procedure, the membrane was first immersed in a solution containing the cationic polyelectrolyte poly(diallyldimethylammonium chloride) (PDADMAC) for a predetermined period of time. The membrane was then rinsed with deionized water to remove loosely adsorbed polymer. Following rinsing, the membrane was immersed in an aqueous solution containing the anionic polyelectrolyte poly(sodium 4-styrenesulfonate) (PSS). This process resulted in the formation of a bilayer through electrostatic interactions between oppositely charged polymers. The deposition cycle was repeated multiple times to obtain the desired number of bilayers. After completion of the layer deposition process, the membranes were rinsed with deionized water and dried under ambient conditions prior to use in transport experiments.

3.1.3 Metal Ion Transport Experiments

Transport experiments were conducted using a two-compartment diffusion cell separated by the polymer inclusion membrane. One compartment contained the feed solution containing metal ions,

while the other contained the receiving solution designed to strip the metal ions from the carrier complex. The membrane was placed between the two compartments to create a barrier separating the feed and receiving phases. Both compartments were continuously stirred during the experiment to minimize concentration polarization at the membrane surface. Samples were periodically withdrawn from the receiving phase at predetermined time intervals to monitor metal ion transport. The concentrations of lithium, cobalt, nickel, and manganese in both feed and receiving solutions were determined using inductively coupled plasma optical emission spectroscopy. Transport experiments were conducted under controlled conditions to evaluate the influence of membrane composition, carrier type, and experimental parameters on metal ion transport.

3.1.4 Inductively Coupled Plasma Optical Emission Spectroscopy

Metal ion concentrations in feed and receiving solutions were determined using inductively coupled plasma optical emission spectroscopy (ICP-OES). Measurements were performed using a PerkinElmer Optima ICP-OES spectrometer (PerkinElmer Inc., USA). Calibration standards for lithium, cobalt, nickel, and manganese were prepared using certified standard solutions obtained from Sigma-Aldrich. Calibration curves were generated prior to sample analysis to ensure accurate quantification of metal concentrations. Samples collected during transport experiments were diluted appropriately using 2% HNO_3 before analysis.

3.2 Material Characterization

3.2.1 Scanning Electron Microscopy

The surface morphology of the membranes was examined using scanning electron microscopy (SEM). Imaging was performed using a field emission scanning electron microscope (Zeiss Auriga Crossbeam). Prior to imaging, membrane samples were mounted on aluminum stubs using

conductive carbon tape. The samples were coated with a thin layer of gold using a sputter coater to improve surface conductivity during imaging. SEM images were collected at different magnifications to observe membrane surface morphology and structural uniformity.

3.2.2 Fourier Transform Infrared Spectroscopy

Fourier transform infrared spectroscopy (FTIR) was used to characterize the chemical structure of the polymer inclusion membranes. FTIR spectra were collected using a Thermo Scientific Nicolet iS50 FTIR spectrometer. Spectra were recorded over a wavenumber range of 4000–500 cm^{-1}. FTIR analysis was used to confirm the presence of polymer matrix components, carriers, and plasticizers.

3.2.3 Nuclear Magnetic Resonance Spectroscopy

Nuclear magnetic resonance (NMR) spectroscopy was used to confirm the chemical structure of the synthesized ionic liquids. Proton and carbon NMR spectra were collected using a JEOL 400 YH NMR spectrometer ^{1}H and ^{13}C nuclei. Samples were prepared by dissolving the synthesized ionic liquid in appropriate deuterated solvents.

3.2.4 Thermogravimetric Analysis

Thermogravimetric analysis (TGA) was conducted to evaluate the thermal stability of the electrolyte samples. Measurements were performed using a TA Instruments TGA Q50 thermogravimetric analyzer (TA Instruments, USA) under a nitrogen atmosphere. Prior to heating, the samples were equilibrated isothermally at 20 °C for 30 minutes. The temperature was then increased from 20 °C to 600 °C at a heating rate of 10 °C min^{-1} under continuous nitrogen flow. The resulting weight loss profiles were used to assess the thermal stability and decomposition behavior of the membranes.

3.2.5 UV–Visible Spectroscopy

UV–visible spectroscopy was used to evaluate the leaching of membrane components from the polymer inclusion membranes during transport experiments. Measurements were carried out using a Thermo Scientific Evolution 300 UV–Vis spectrophotometer (Thermo Fisher Scientific, USA). Samples collected from the aqueous phases after membrane exposure were analyzed to detect the presence of dissolved membrane components, including carriers and plasticizers that may have leached into the solution.

3.2.6 Dynamic Mechanical Analysis

Dynamic mechanical analysis (DMA) was used to evaluate the mechanical properties of the membrane samples. Stress–strain measurements were conducted using a TA Instruments DMA Q800 dynamic mechanical analyzer (TA Instruments, USA). Membrane samples were cut into rectangular strips and mounted in the tensile clamp of the instrument.

Tensile testing was performed under controlled force mode with a ramping force rate of 0.1 N min^{-1}.

3.2.7 X-ray Diffraction

X-ray diffraction (XRD) was employed to analyze the crystalline structure and phase composition of the membrane samples. Diffraction patterns were collected using a PANalytical Empyrean X-ray diffractometer. Membrane samples were prepared by mounting flat sections onto the sample holder to ensure a uniform and smooth surface for analysis.

CHAPTER FOUR

COMPLEXATION-DRIVEN ION-EXCHANGE POLYMER INCLUSION MEMBRANES FOR SEPARATION OF COBALT AND NICKEL IONS FROM LITHIUM-ION VIA PROTON PUMPING

A version of this chapter was originally published by Babafemi Adigun, et al. as below: Adigun, B.; Thapaliya, B. P.; Luo, H.; Dai, S. Complexation-driven ion-exchange polymer inclusion membranes for separation of cobalt and nickel ions from lithium-ion via proton pumping. RSC Sustainability 2024, 2 (6), 1859-1867.

4.1 Abstract

Cobalt and nickel are vital components of lithium-ion battery (LIB) cathodes; their increasing demand requires efficient recovery from spent LIBs to foster a sustainable battery future. The limitations of current separation technologies necessitate the development of more cost-effective, efficient, and eco-friendly metal recovery methods. Herein, we developed a complexation-driven ion-exchange polymer inclusion membrane (IEPIM) by confining an ionic liquid (IL) and a protic extractant in a polymer host to separate cobalt and nickel ions from lithium ions. While past studies achieved selective separation of cobalt ions using basic extractants in aqueous chloride solutions, this study utilizes a protic extractant to achieve a multi-ion separation in aqueous solution. Our approach relies on proton pumping facilitated by the protic extractant, making the separation process effective while avoiding harmful organic solvents. The IEPIM made from 50% PVDF-HFP (poly(vinylidene fluoride-co-hexafluoropropylene)) as the polymer host, 30% Cyanex 301 (bis(2,4,4-trimethylpentyl) dithiophosphinic acid) as the protic extractant, and 20% [C_8mim][NTf2] (1-octyl-3-methylimidazolium bis(trifluoromethanesulfonyl)imide) as the plasticizer, efficiently separates Co^{2+} and Ni^{2+} from Li^{+} in aqueous solution, with over 90% transport efficiency for Co^{2+} and 73% for Ni^{2+}. The membrane maintained this efficiency through three cycles, indicating its stability. These results demonstrate that the IEPIM could be a viable alternative to conventional metal ion separation methods, offering an environmentally sustainable

and cost-effective strategy for recycling critical metals from spent lithium-ion batteries with the potential for industrial application in separation technology.

4.2 Introduction

The recovery of metals from waste, especially from expended LIBs, is critical for maintaining metal sustainability and environmental safety.[1,2] The demand for cobalt and nickel, key elements in LIB cathodes, has skyrocketed with the growth of the portable electronics and electric vehicle industries. This increase in demand poses challenges to their supply chains and has an environmental impact.[3–9] Conventional metal recovery methods, such as solvent extraction,[10,11] adsorption,[12,13] ion exchange,[14,15] and electrowinning,[16,17] come with significant drawbacks, including toxic waste creation, high costs, energy demands, and the need for large amounts of extractants. Therefore, there's a pressing need for an eco-friendly, efficient, and less extractant-dependent separation method to lessen environmental impact.

Polymer Inclusion Membranes (PIMs) provide a novel and continuous alternative to traditional metal separation techniques, offering efficiency and resource conservation. These membranes employ a selective approach, using a polymeric membrane infused with a specific extractant and a plasticizer to extract target metals from complex mixtures, like those found in spent battery leachates.[18,19] This method facilitates the selective transport of targeted metal ions, such as cobalt and nickel from complex mixtures, streamlining the process by combining extraction and stripping into one step. This reduces the need for extra separation phases, reduces extractant use, and minimizes environmental impact.[20,21]

PIMs have successfully recovered different metals; the key elements of PIMs, the polymer host, the extractant, and the plasticizer are essential for the membrane's effectiveness, stability, and

ability to transport materials. The polymer host, typically cellulose triacetate (CTA)[22–24] or poly(vinyl chloride) (PVC),[25,26] forms the membrane's structure and determines its physical and chemical attributes. Poly(vinylidene fluoride-co-hexafluoropropylene) (PVDF-HFP), though less common, offers notable advantages such as strong chemical resistance and high stability. The extractant is crucial in PIM-based metal ion transport, as it binds and carries the target metal through the membrane. Various extractants are utilized, including bis(2,4,4-trimethylpentyl) phosphinic acid (Cyanex 272), 2-ethylhexyl phosphoric acid mono-2-ethylhexyl ester (PC-88A), di(2-ethylhexyl)phosphoric acid (D2EHPA), and N,N-dioctyl-1-octanamine (Alamine 336).[27–29] The plasticizer contributes to the membrane's effectiveness by lessening the intermolecular forces of the polymer, which increases flexibility and permeability for better metal ion transport.[18,19] Common plasticizers include 2-nitrophenyl octyl ether (2-NPOE),[30,31] o-nitrophenyl pentyl ether (ONPPE),[32,33] and tris(2-ethylhexyl) phosphate (TEHP).[34,35] PIMs have been effectively used in the recovery of various metals. For instance, Fajar et al. successfully applied PIM for extracting platinum (Pt), palladium (Pd), and rhodium (Rh) from the leachate of spent automotive catalysts using the ionic liquid trioctyl(dodecyl) phosphonium chloride ($P_{88812}Cl$). Over 90% recovery of Pt and Pd with high purity was achieved.[36] Several other studies have concentrated on selectively separating metals from used batteries. In one such study, Pospiech employed PIM to differentiate cobalt from nickel and lithium in a chloride solution, using trisooctylamine (TIOA) as the extractant. This process transported 74.5% of Co(II) ions into the receiving solution within 24 hours.[37] Recently, ionic liquids (ILs) have gained recognition as efficient ionic liquid plasticizers (ILPs) in PIMs, attributed to their structural resemblance to conventional plasticizers and their unique non-volatile nature.[38,39] Guo et al., utilized ILs, specifically [Cnmim][PF_6], as plasticizers

in the transport of (Cr(VI)). It was found that these IL plasticizers enhanced the membrane's permeability coefficient, thereby improving Cr(VI) transport.[27]

Herein, we aim to address the challenges of the traditional separation process by eliminating the need for toxic organic solvents using an IEPIM. The IEPIM, composed of a polymer host (PVDF-HFP), an extractant (Cyanex 301), and a plasticizer ($[C_8mim][NTf_2]$), is designed to separate cobalt and nickel ions from lithium ions in aqueous solutions. The separation strategy is based on proton pumping, driven by the pH gradient between the feed and stripping solutions, and facilitates the metal ion transport through the membrane. Previous studies have successfully extracted cobalt ions using basic extractants in chloride-based aqueous solutions; however, our strategy involves using a protic extractant to separate multiple ions at once in an aqueous solution with the potential for further individual separation. The IEPIM effectively separates cobalt and nickel from lithium ions in aqueous media, achieving a remarkable transport efficiency exceeding 90% for cobalt and 73% for nickel. The IEPIM maintains this efficiency effectively across three successive cycles, showing good stability over successive use and potential for industrial applications. Our study is focused on creating an environmentally sustainable method for metal separation and recovery, aiming to reduce the environmental impact of conventional separation processes.

4.3 Materials and Methods

4.3.1 Materials

Poly(vinylidene fluoride-co-hexafluoropropylene) (PVDF-HFP, Mw~400,000, Mn~130,000, Sigma-Aldrich), bis(2,4,4-trimethylpentyl) dithiophosphinic acid (Cyanex 301, Solvay), acetone ($(CH_3)_2CO$, 99.5%, Fisher Chemical Company), lithium chloride (LiCl, 98.5%, Fisher Chemical Company), hydrochloric acid (HCl, 36%, Fisher Chemical Company), cobalt (II) chloride

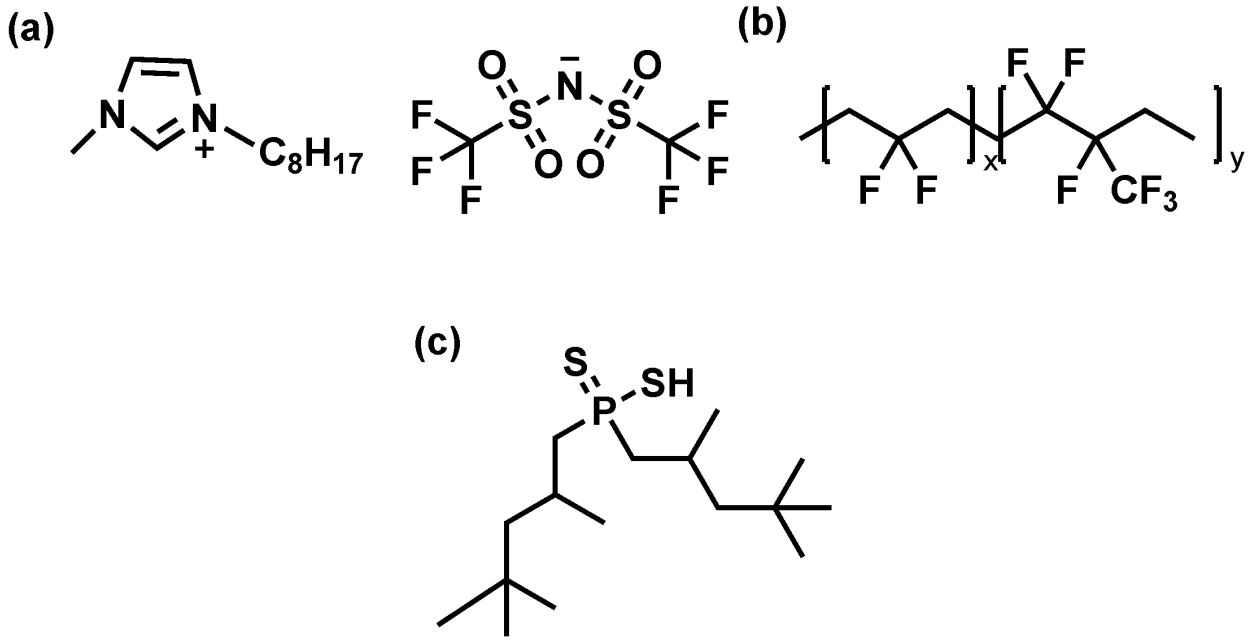

Figure 4.1 Chemical structures (a) [C_8mim][NTf_2], (b) PVDF-HFP, (c). Cyanex 301

($CoCl_2.6H_2O$, 98%, Alfa Aesar), nickel (II) chloride ($NiCl_2.6H_2O$, 98%, J.T Baker Chemical Company) were used as received. 1-Octyl-3-methylimidazolium bis(trifluoromethanesulfonyl)imide ([C_8mim][NTf_2]) was synthesized by modified procedure from literature.[41]

4.3.2 Membrane Preparation

The pure PVDF-HFP membrane was prepared by dissolving PVDF-HFP pellets in acetone, stirring overnight, and casting the solution onto a Petri dish. Then, the solvent was evaporated to get the membrane used as a reference material for comparative analysis. The IEPIM membrane was prepared by dissolving PVDF-HFP, Cyanex 301, and [C_8mim][NTf_2] in 5: 3 : 2 ratio by mass with a total weight of 0.2–0.3 g in 30 ml acetone. The solution was stirred overnight at 25 ± 0.6 °C to form a homogenous solution and then poured into a 6.5 cm diameter Petri dish. The solvent was

evaporated slowly over 24 hours, forming a membrane. The IEPIM membrane had a thickness of 45 ± 8 μm, as measured with a digital calliper (Mitutoyo 293-832-30 micrometer).

4.3.3 Extraction and Stripping Experiments

0.2 g of IEPIM was immersed in 30 mL of 1 mM Co^{2+} and Ni^{2+} solution and shaken at 200 rpm on an orbital shaker at 25 °C for 24 hours. 1 mL sample was periodically taken out for analysis and replaced with an equal amount of the original solution to keep the volume constant. The concentration of the metal ions in the solution was measured before and after the extraction by inductively coupled plasma optical emission spectroscopy (ICP-OES) (Agilent 5110). The extraction efficiency (E%) was calculated using Eq. 1 below.[28]

$$E(\%) = \frac{C_0^f - C_t^f}{C_0^f} \times 100 \qquad (1)$$

where 't' is the time (hours), the concentration of the metal ion in the feed solution at t = 0 (before extraction), at t > 0 (time of extraction) are denoted by C_0^f and C_t^f respectively.

Subsequently, the metal loaded IEPIM underwent a stripping process. It was placed in 30 mL of 2M HCl for another 24 hours. In a manner similar to the extraction phase, 1 mL aliquots were regularly taken from the solution, and replaced by an equal volume of the fresh solution to maintain the volume. The concentration of the metal ions in the stripping solution was again measured by ICP-OES. The stripping efficiency (S%) was calculated with Eq. 2 below.[28]

$$S(\%) = \frac{C_t^r}{C_{IEPIM}} \times 100 \qquad (2)$$

where t is time (hours), the concentration of the metal ion in the stripping solution at time t > 0 (the time of stripping) is denoted by C_t^r, The concentration of metal ion extracted into the membrane from the extraction experiment is denoted by C_{IEPIM}.

4.3.4 Mass Loss of IEPIM

Two IEPIMs with a mass of 0.3102 ± 0.0003 g were immersed in 50 mL of deionized water and left for 24 hours at room temperature. After 24 hours, they were removed from the solution, cleaned, dried in the oven for more than 24 hours at 50 °C, and weighed. The process was repeated for three cycles. The solution was analyzed using a UV-Vis spectrometer and ICP-OES.

4.3.5 Transport Experiments

The transport experiments involving the IEPIM were carried out using a jacketed glass compartment system. In this setup, the IEPIM was carefully placed between the compartments to ensure its contact with both the feed and stripping solutions. The surface area in contact with both the feed and stripping solutions is 3.14×10^{-4} m^2 (diameter 20 mm). The feed (100 mL of 0.1 mM Co^{2+}, $Ni^{2+,}$ Li^{+}) and stripping (100 mL of 2M HCl) solutions were stirred at 700 rpm using magnetic stir bars. 1 mL aliquots were extracted from the solution, and an equal volume of the original solution was added back to maintain the volume. The concentration of the metal ions in the solution was measured before and after the extraction by ICP-OES. The kinetics of the transport experiment is described by Eq. 3; the rate constant *k* (h^{-1}), initial flux J_0 ($mol\ m^{-2}\ s^{-1}$), permeability coefficient *P* ($m\ h^{-1}$) and the transport efficiency TE (%) were calculated using the following equations.[29]

$$In\left(\frac{C_t^f}{C_0^f}\right) = -kt \quad (3)$$

$$P = \left(\frac{V}{A}\right)k \quad (4)$$

$$J_0 = PC_0^f \quad (5)$$

$$TE\ (\%) = \frac{C_t^r}{C_0^f} \times 100 \quad (6)$$

where C_0^f is the concentration of the metal ions (mol L^{-1}) in the feed solution at t = 0, C_t^r is the concentration of the metal ions (mol L^{-1}) in the stripping solution at t > 0 (stripping time), V is volume (m^3) of the feed solution, A is the surface area (m^2) of the IEPIM in contact with the solutions.

4.4 Results and Discussion

4.4.1 Membrane Characterization

The surface morphology of the pure PVDF-HFP and IEPIM membranes was investigated using scanning electron microcopy (SEM), as shown in **Figure 4.2**. The SEM image of the pure PVDF membrane displayed a dense and rough surface, characterized by small, unevenly distributed pores (**Figure 4.2(a)**). This morphology is likely due to the solvent evaporation method used in membrane formation, which causes the development of these non-uniform pores. Upon incorporation of the extractant and plasticizer in fabricating the IEPIM, it was noted that the micropores became significantly filled (**Figure 4.2(b)**). This is presumed to arise from the penetration of the extractant and plasticizer into the pores

Before and after the transport experiments, the thermal analysis of pure PVDF-HFP and the IEPIM was examined. Thermogravimetric analysis (TGA) of pure PVDF-HFP, Cyanex 301, IEPIM before and after the transport experiments was examined as shown in **Figure 4.2(c)**. Pure PVDF-HFP and Cyanex 301 each exhibit a single-step thermal decomposition at approximately 480°C and 150°C, respectively. However, the IEPIM undergoes a two-step decomposition, starting at around 150°C due to the decomposition of the extractant and correlating with its proportion in the IEPIM, while the PVDF-HFP component continues to decompose at the same 480°C. These observations indicate that the IEPIM's

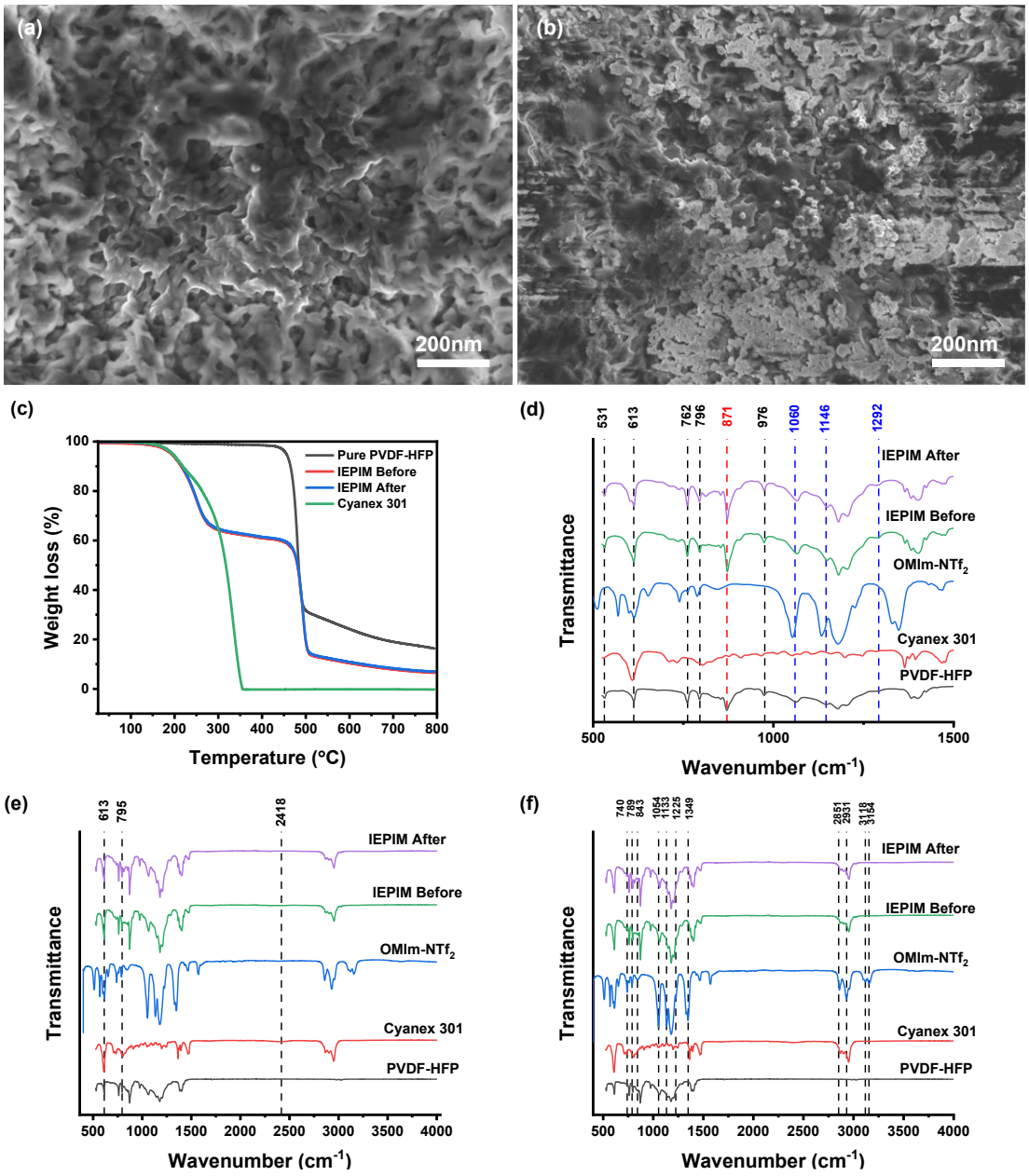

Figure 4.2 Top view SEM image of (a) pure PVDF-HFP membrane and (b) IEPIM, (c) Thermogravimetric analysis of Pure PVDF-HFP, Cyanex 301, IEPIM before, and after transport experiments. FTIR Spectra of pure PVDF-HFP membrane, Cyanex 301 [C_8mim][NTf_2] and IEPIM before and after use showing distinct peaks for (d) PVDF-HFP (e) Cyanex 301, and (f) [C_8mim][NTf_2].

thermal stability is maintained up to 150°C. The thermogravimetric analysis (TGA) of the IEPIM, conducted both before and after the extraction process was consistent, indicating that no residual metal ions remained in the membrane following the transport experiments. This finding confirms the membrane's efficiency in metal ion release during the transport process, highlighting its reusability without ion accumulation.

Fourier Transform Infrared (FTIR) spectroscopy was employed to identify the functional groups in the pure PVDF-HFP, Cyanex 301, and the IEPIM, covering a spectral range of 500 to 4000 cm^{-1}. In **Figure 4.2(d)**, distinctive peaks were observed, signifying both the crystalline and amorphous phases of the polymer in the FTIR spectra. Precisely, resonances at 531, 613, 762, 796, and 976 cm^{-1} correspond to the α-phase crystalline regions, while the peak at 871 cm^{-1} aligns with the amorphous phase of the polymer. Additional vibrational modes at 1060, 1146, and 1292 cm^{-1} can be attributed to the symmetric stretching of —CF groups, the stretching of —CF_2 moieties, and the symmetric stretching of —CF_3 bonds, respectively. In the FTIR spectra of Cyanex 301, major peaks are discerned at 613, 795, and 2418 cm^{-1}, corresponding to stretching bonds associated with P=S, S=P—SH, and S—H functionalities, respectively, as shown in **Figure 4.2(e)**. Although the 2418 cm^{-1} peak was less discernible in the combined spectra, its individual plotting (**(Figure S.1.))** made it more apparent.[41-44]

Similarly, the FTIR spectra of [C_8mim][NTf2], as shown in **Figure 4.2f**, exhibits peaks at 740, 789, 843, 1054, 1133, 1225, 1349 cm^{-1} which correspond to the symmetric bending of CF3, C–S & S–N stretching, in-plane bending C–H peak of imidazolium ring, S–N–S asymmetric stretching, symmetric stretching of CF_3; stretching of C–N within the imidazole ring and asymmetric deformation vibrations of SO_2 bonds, respectively. Peaks at 2859 – 2931 cm^{-1} correspond to the

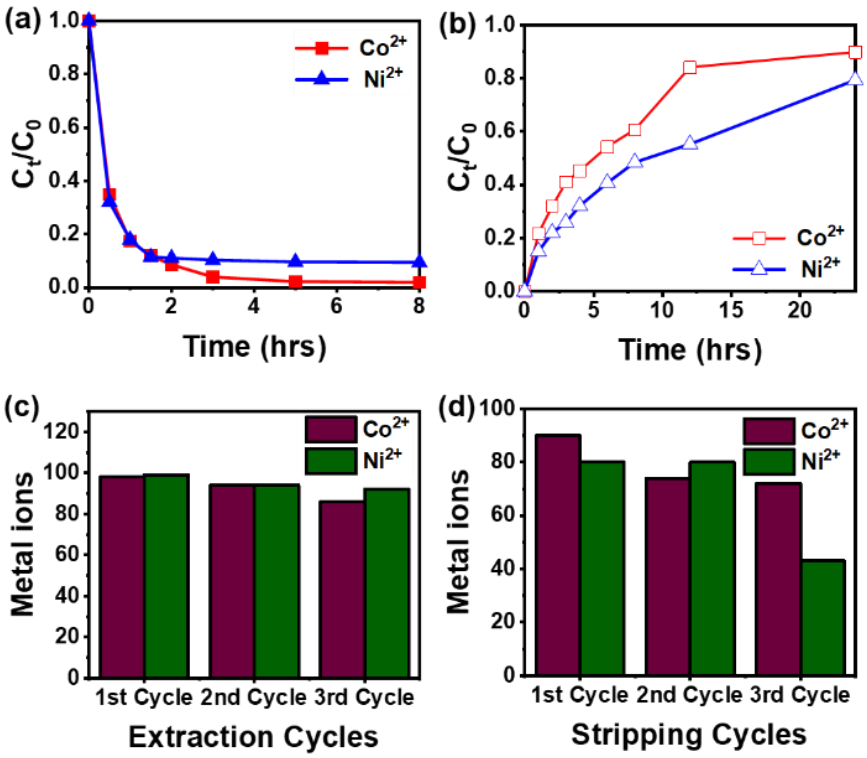

Figure 4.3 (a) Extraction of Co^{2+} and Ni^{2+} into IEPIM in the feed solutions. (b) Stripping of Co^{2+} and Ni^{2+} from IEPIM in the stripping solutions. Three cycles of (c) extraction of Co^{2+} and Ni^{2+} into IEPIM and (d) stripping Co^{2+} and Ni^{2+} from IEPIM

aliphatic stretching of C–H, and 3118 – 3154 cm^{-1} correspond to the C–H stretching specific to the imidazole ring.45 The IEPIM membrane's FTIR spectra showed the distinct peaks of its constituent materials, confirming their successful incorporation. Notably, the absence of specific peaks (3118 – 3154 cm^{-1}) in the IEPIM's spectra suggested possible inhibitions in the imidazole ring's vibrations after the membrane formation. Furthermore, no significant spectral changes were observed in the IEPIM membrane before and after metal ion transport, indicating the structural stability of the membrane throughout the process.

4.4.2 Extraction and stripping studies with cobalt (II) and nickel (II)

The IEPIM was immersed in 30 mL of 1 mM Co^{2+} and Ni^{2+} solutions for 8 hours. The normalized concentrations of Co^{2+} and Ni^{2+} in the feed solution are shown in **Figure 4.3a**. The Co^{2+} and Ni^{2+} concentrations rapidly reduced in the first 2 hours and reached equilibrium around 8 hours, after which the concentrations no longer decreased significantly. The IEPIM extracted 98% of Co^{2+} and 91% of Ni^{2+} in the feed solutions in 8 hours. The equation below (Eq. 7) describes the extraction mechanism of Co^{2+} and Ni^{2+} in solvent extraction studies with Cyanex 301 as the extractant. The mechanism involves a cationic exchange between the H+ and the metal ions, extracted by exchanging two protons with the extractant.

$$M^{2+}_{(aq)} + 2HA_{(mem)} \leftrightharpoons MA_{2(mem)} + 2H^{+}_{(aq)} \qquad (7)$$

Where *aq* and *mem* represent the aqueous and membrane phases, respectively, it was assumed that the extraction mechanism in solvent extraction is the same in the IEPIM system.

A 2M HCl solution was employed as the stripping solution for the stripping phase. This process, guided by the exact mechanism (Eq. 7), resulted in the stripping of significant amounts of Co^{2+} and Ni^{2+} from the IEPIM, as shown in **Figure 4.3b**. However, complete stripping of the metal ions was not achieved. Over 24 hours, the IEPIM stripped 90% of Co^{2+} and 79% of Ni^{2+}. After three cycles, there was a noticeable decrease in extraction efficiency for Co^{2+}; the extraction efficiency decreased from an initial 98% to 86%, while the stripping efficiency declined from 90% to 72%. In contrast, for Ni^{2+}, the extraction performance remained consistent, exceeding 90% after each cycle, while the stripping efficiency significantly declined from 80% to 43% (**Figure 4.3(c-d)**). This decline in performance is likely due to the loss of the extractant during the processes.

The performance drop of the IEPIM was investigated by evaluating its mass changes. The IEPIM was immersed in deionized water for 24 hours. **Figure 4.4a** shows the relative mass of the IEPIM

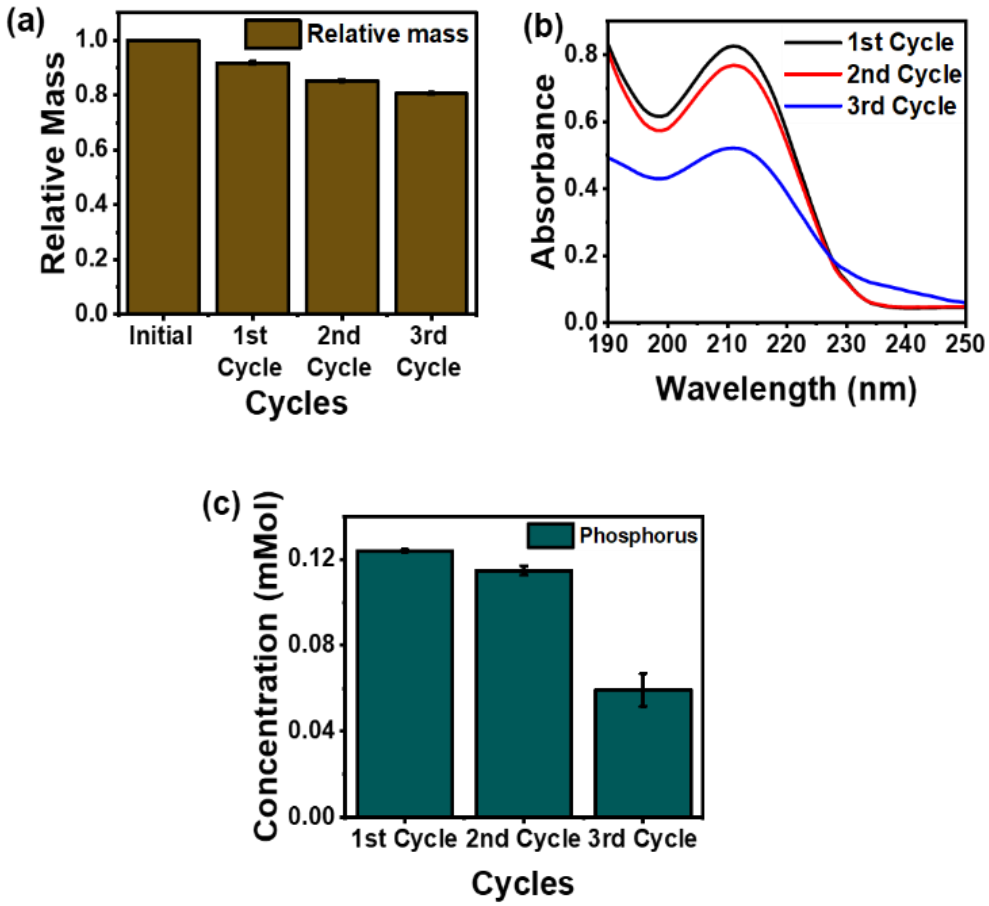

Figure 4.4 (a) Mass changes of IEPIM for three cycles (b) UV-Vis spectra showing imidazolium peaks (c) phosphorus concentration in the solution after immersion in deionized water.

after each cycle, where the relative mass is calculated as the ratio of the mass of the IEPIM after immersion (m) to the initial mass of the IEPIM (m_0). A notable mass loss of approximately 8% was observed following each cycle. To investigate the leakage of extractant and IL, analyses were conducted on the solution after each cycle using UV-Vis and ICP-OES. The UV-Vis spectra, depicted in **Figure 4.4b**, exhibits a characteristic peak at 211 nm corresponding to the imidazolium ring in C_8mim-NTf_2. Additionally, **Figure 4.4c** displays the phosphorus content in the solution

after each cycle, with a decrease in phosphorus concentration mirroring the trend seen in the UV-Vis spectra of the imidazolium ring. These observations indicate that the mass loss in the IEPIM is due to the leakage of extractant and IL from the membrane.

4.4.3 Membrane Transport of Co(II) and Ni(II) and separation from Li(I)

The transport experiments utilized an IEPIM membrane in a system designed to separate Co^{2+} and Ni^{2+} from Li^{+}. This system enabled concurrent extraction and stripping of these metal ions from the feed to the stripping solution. The extractant plays a significant role in facilitating the transport of ions across the IEPIM. Therefore, the effect of the extractant's concentration in the IEPIM was studied in the transport of Co^{2+} and Ni^{2+} across the IEPIM. The weight percent composition of the IEPIM varied from 0% to 30% by weight. In the experiments, a feed solution containing 0.1 mM of Li^{+}, Co^{2+}, and Ni^{2+} and a 2M HCl as the receiving solution. The rate constants (k) and the initial flux (J_0) of Co^{2+} and Ni^{2+} increased with an increasing extractant concentration (wt. % composition), as shown in

Figure 4.5 (a-c). The kinetic parameters of the transport of Co^{2+} and Ni^{2+} across the IEPIMs are summarized in **Table 4.1**. The most effective transport was observed with the 30 wt. % composition IEPIM, demonstrating the highest flux values with a flux of 1.58 and 1.51 $\mu mol \cdot m^{-2} \cdot s^{-1}$ for Co^{2+} and Ni^{2+}, respectively. These findings demonstrated that the extractant facilitates the transport of the ions, even at low concentrations. The optimal concentration for effective ion transport was established at 30 wt. % of the extractant and was used for the transport experiments in this work.

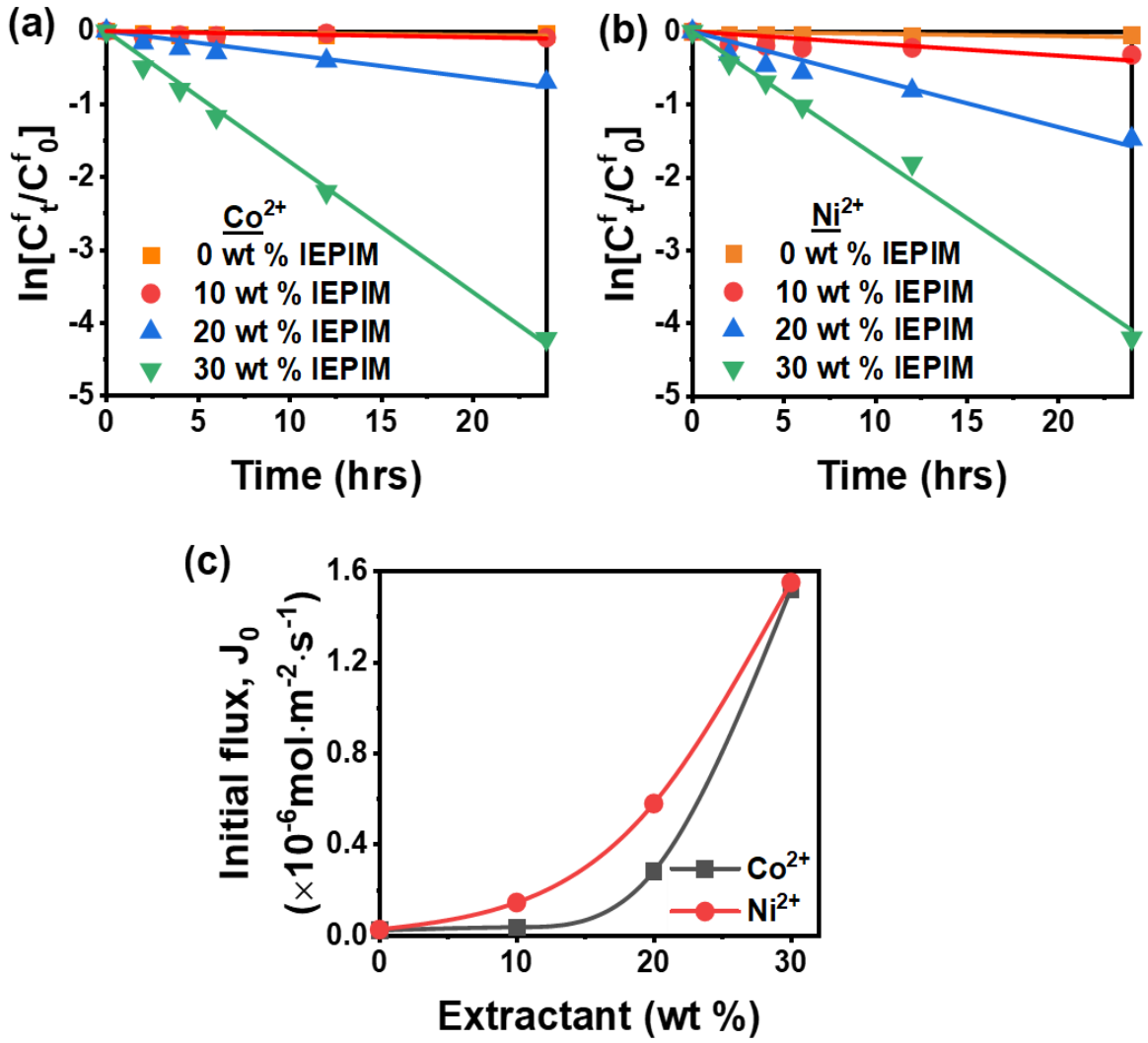

Figure 4.5 Kinetic plots of the (a) Transport of Co^{2+}, (b) Transport of Ni^{2+}, and (c) Initial flux at varying weight composition of the extractant across IEPIM in the feed solution.

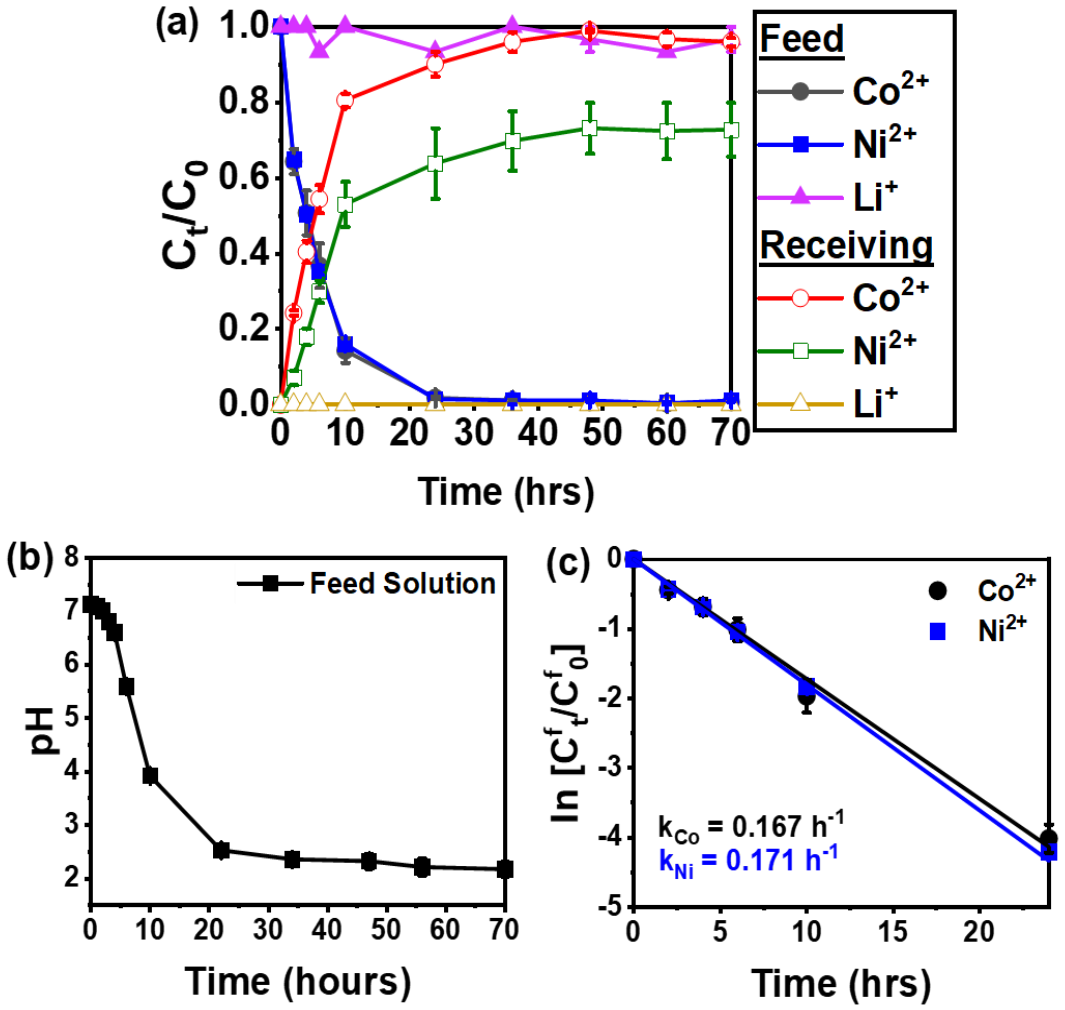

Figure 4.6 Transport of Co^{2+} and Ni^{2+} across an IEPIM in the feed and stripping solutions over time (b) Plot of pH in the feed solution over time (c) Kinetic plots of the transport of Co^{2+} and Ni^{2+} across the IEPIM in the feed solution.

Table 4.1 Co^{2+} and Ni^{2+} rate constant (k), permeability coefficient (P), and initial fluxes (J_0) for transport across IEPIM with varying weight compositions.

Extractant ***wt. (%)***	**Metal ions**	***k*** ***(h^{-1})***	***P*** ***($\times 10^{-6}$ $m \cdot s^{-1}$)***	***J_0*** ***($\times 10^{-6}$) $mol \cdot m^{-2} \cdot s^{-1}$)***	**Transport Efficiency** ***(%)***
0	Co^{2+}	0.00267	0.236	0.0236	0
	Ni^{2+}	0.00305	0.270	0.0270	1
10	Co^{2+}	0.00419	0.370	0.370	12
	Ni^{2+}	0.0166	1.46	0.146	19
20	Co^{2+}	0.0319	2.82	0.282	94
	Ni^{2+}	0.0656	5.80	0.580	67
30	Co^{2+}	0.167	15.8	1.580	95
	Ni^{2}	0.171	15.1	1.510	70

Figure 4.6a shows the successful transport of Co^{2+} and Ni^{2+} across the IEPIM, with a corresponding decrease in these ions in the feed solution and an increase in the stripping solution. At the same time, Li^{+} remained predominantly in the feed solution. After 70 hours, the IEPIM achieved a transport efficiency of 96% for Co^{2+} and 73% for Ni^{2+}. 4% of Li^{+} ions were extracted into the membrane but not subsequently transported into the receiving solution. The pH of the feed solution decreases over time, indicating the diffusion of protons across the IEPIM from the stripping solution to the feed solution **Figure 4.6b**. This process suggests that metal ion transport occurs via a cation exchange mechanism

Table 4.2 Co^{2+} and Ni^{2+} rate constant (k), permeability coefficient (P), and initial fluxes (J_0) for transport across IEPIM.

Metal ions	k (h^{-1})	P ($\times 10^{-6}$ $m \cdot s^{-1}$)	J_0 ($\times 10^{-6}$) $mol \cdot m^{-2} \cdot s^{-1}$)	Transport Efficiency (%)
Co^{2+}	0.167	14.8	1.48	96
Ni^{2+}	0.171	15.1	1.51	73

facilitated by proton pumping. From the plot of $In\ C_t^f / C_0^f$ against time for the feed solution in **Figure 4.6c**, the rate constant (k), permeability coefficient (P), and initial flux (J_0) were calculated using equations 3–5. These values are listed in **Table 4.2**.

4.4.4 Effect of Membrane Thickness on Transport of ions

The membrane's thickness is crucial in ion transport efficiency in the IEPIM. To investigate this, IEPIMs of identical composition but varying thicknesses, ranging from 45 ± 8μm to 104 ± 2μm, were examined. **Figure 4.7a** shows the initial flux of the ions across the IEPIM at different thicknesses. The initial flux of Ni^{2+} decreases linearly as the thickness of the IEPIM increases from 45 – 104 μm. However, for Co^{2+}, the initial flux reduces as the thickness increases from 45 μm to 71 μm and remains the same as the thickness increases from 71 to 104 μm. **Figures 4.7(b, c)** demonstrate the influence of membrane thickness on transport efficiency. Both Co_{2+} and Ni^{2+} transport efficiencies slightly decrease as the thickness increases from 45 to 71 μm, followed by a substantial drop from 71 to 104 μm, particularly for Ni^{2+}. In the transport involving the thickest version of the IEPIM (104μm), a notable delay was observed in the ion transport process. The Co^{2+} ions were detected in the receiving solution after a 2-hour interval, whereas the appearance of Ni^{2+} ions required a significantly longer duration of 24 hours. This observed delay in ion transport could

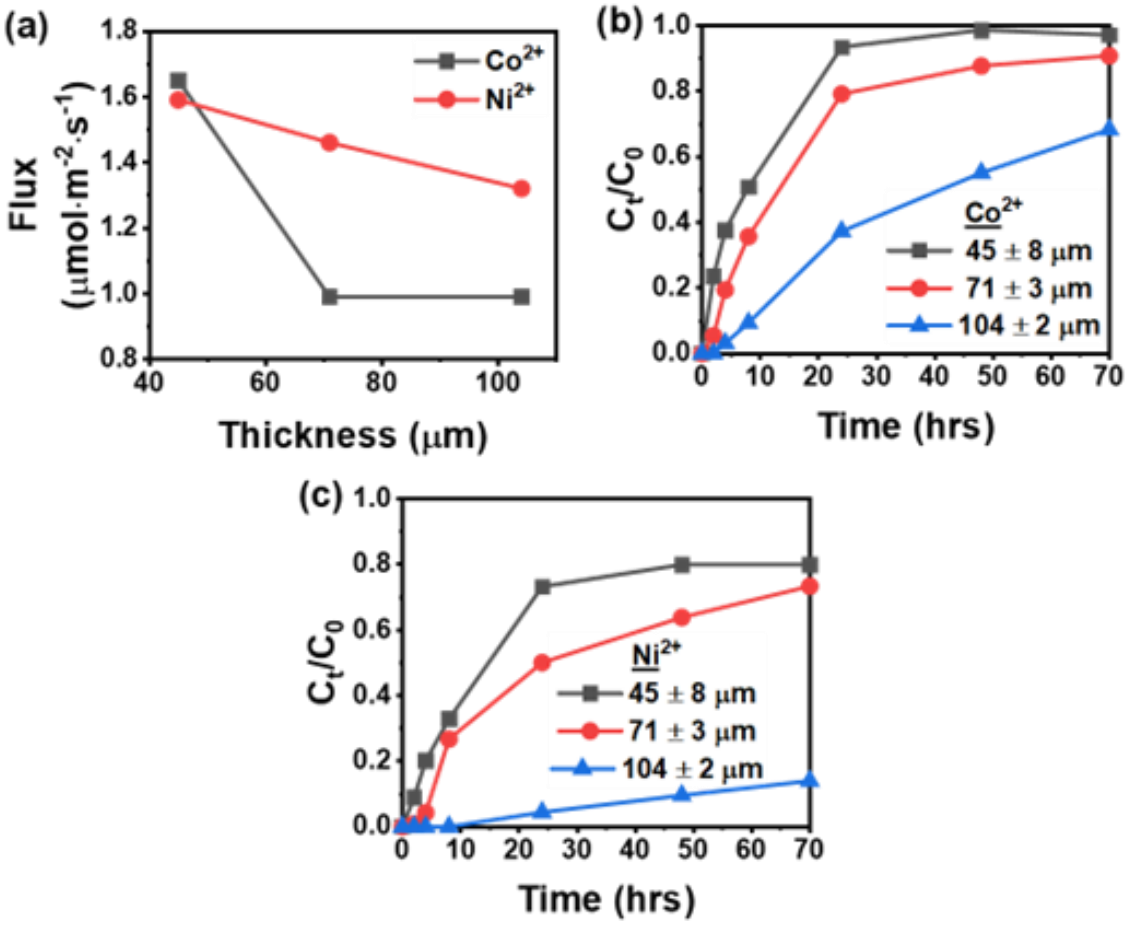

Figure 4.7 (a) Initial flux of Co^{2+} and Ni^{2+} (b) Transport efficiency of Co^{2+} (c) Transport efficiency of Ni^{2+} at different membrane thicknesses across IEPIM.

potentially be linked to the longer diffusion path necessitated by the increased thickness of the membrane. This finding highlights the membrane thickness's impact on ion transport efficiency in IEPIM systems.

4.4.5 Membrane Stability

The stability of the IEPIM was evaluated through three consecutive cycles of use, as shown in **Figure 4.8**, with both the feed and stripping solutions being replenished after each cycle. The

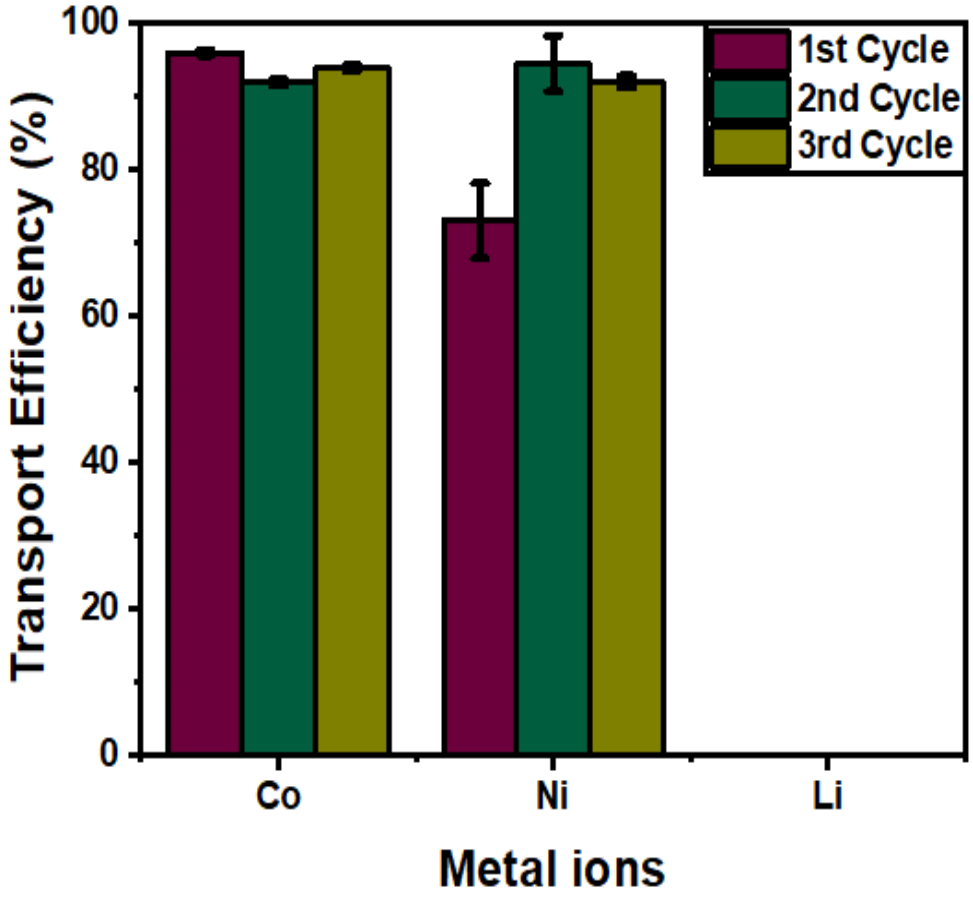

Figure 4.8 Transport efficiency of 3 transport cycles. Feed solution: 100 mL of 0.1 mM Li^{+}, Co^{2+}, and Ni^{2+}. Receiving Solution: 2M HCl. Membrane composition 50% wt. PVDF-co-HFP and 30% wt. Cyanex 301 and 20% wt. $[C_8mim][NTf_2]$.

rate constant (k), permeability coefficient (P), and initial fluxes (J_0) for each transport cycle across IEPIM are summarized in **Table 4.3**. The transport efficiency of Co^{2+} remained above 90% for all three cycles, while Ni^{2+} increased from 73% to 94% and 92% in the second and third cycles. However, the initial fluxes in the feed solution decreased after each cycle as shown by the

Table 4.3 Co^{2+} and Ni^{2+} rate constant (k), permeability coefficient (P), and initial fluxes (J_0) for transport across IEPIM for the three cycles.

Cycle	Metal ions	*k* (h^{-1})	*P* ($\times 10^{-6} m \cdot s^{-1}$)	J_0 ($\times 10^{-6} mol \cdot m^{-2} \cdot s^{-1}$)	*Transport Efficiency (%)*
1st	Co^{2+}	0.172	15.2	1.52	96
	Ni^{2+}	0.176	15.5	1.55	73
2nd	Co^{2+}	0.040	3.54	0.354	92
	Ni^{2+}	0.0592	5.23	0.523	94
3rd	Co^{2+}	0.0303	2.68	0.268	94
	Ni^{2+}	0.040	3.54	0.354	92

lower transport efficiency of both ions after 24 hours in **Figure S.2.** The transport efficiency of Co^{2+} and Ni^{2+} after 24 hours was 90%, 50%, and 41% for Co^{2+}, and 64%, 54%, and 39% for Ni^{2+} for the first, second, and third cycles, respectively. The IEPIM showed higher selectivity for Co^{2+} over Ni^{2+} in the first cycle but no significant difference in the later cycles.

4.4.6 Transport Mechanism

The potential transport mechanisms for cobalt and nickel ions through the IEPIM were deduced from their observed behaviors, as demonstrated in **Figure 4.9**. Initially, Co^{2+} and Ni^{2+} ions present in the feed solution were extracted into the membrane through ion exchange interactions with protons from the extractant at the interface between the feed solution and IEPIM and formed metal complexes with the extractant in the IEPIM. Subsequently, at the IEPIM-stripping solution

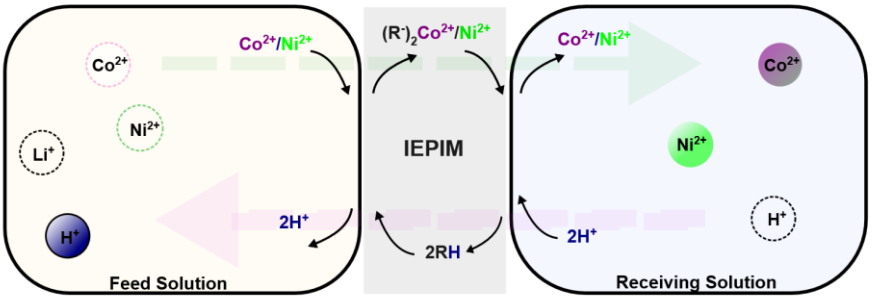

Figure 4.9 Plausible mechanism for transporting Co^{2+} and Ni^{2+} across IEPIM in this study.

interface, metal ions are released from these complexes and replaced by protons from the stripping solution, facilitated by proton pumping through the protic extractant.

This mechanism enables the concurrent transport of Co^{2+} and Ni^{2+} from the feed solution while moving protons from the receiving solution to the feed solution. The extractant's affinity for Co^{2+} and Ni^{2+}, characterized as soft metal ions, is due to its nature as a soft ligand, leading to the selective transport of these ions over hard ions like Li^{+}. The high acid concentration in the stripping solution ensures continuous proton transfer, as indicated by the pH decrease in the feed solution.

4.5 Conclusion

In summary, we have successfully demonstrated the transport of cobalt and nickel ions from lithium ions in aqueous media by using an IEPIM composed of Cyanex 301 as an extractant, PVDF-HFP as the polymer host, and $[C_8mim][NTf_2]$ as the plasticizer. The transport of the metal ions is facilitated by proton pumping through protons from the protic extractant in exchange for the metal ions. This environmentally benign and cost-effective approach eliminates the requirement for volatile solvents. The developed IEPIM successfully demonstrated transport efficiency exceeding 90% for Co^{2+} and 74% for Ni^{2+}. Furthermore, the membrane maintained its efficiency over successive operational cycles, surpassing 90% for Co^{2+} across three cycles and

Ni^{2+} showing 73% after the first cycle and 94% and 92% for the second and third cycles, respectively, indicating the membrane's stability. However, addressing potential concerns regarding the loss or leakage of extractant and ionic liquid is essential, which could be critical in practical extraction and back-extraction processes, warranting further investigation and optimization for real-world applications. These results underscore the IEPIM's potential as an appealing alternative to conventional metal ion separation methods. Successful integration on an industrial scale could revolutionize the separation landscape, promoting eco-friendliness, cost-effectiveness, and the efficient recycling of critical metal ions from spent LIBs.

References

1. M. Henckens, P. Driessen and E. Worrell, Resources, Conservation and recycling, 2014, 93, 1-8.

2. M. Reuter, C. Hudson, A. Van Schaik, K. Heiskanen, C. Meskers and C. Hagelüken, A report of the working group on the global metal flows to the international resource panel, 2013.

3. M. Li and J. Lu, Science, 2020, 367, 979-980.

4. N. Nitta, F. Wu, J. T. Lee and G. Yushin, Materials today, 2015, 18, 252-264.

5. M. S. Whittingham, Chemical reviews, 2004, 104, 4271-4302.

6. X. Zheng, Z. Zhu, X. Lin, Y. Zhang, Y. He, H. Cao and Z. Sun, Engineering, 2018, 4, 361-370.

7. A. Mayyas, D. Steward and M. Mann, Sustainable materials and technologies, 2019, 19, e00087.

8. E. A. Olivetti, G. Ceder, G. G. Gaustad and X. Fu, Joule, 2017, 1, 229-243.

9. B. E. Murdock, K. E. Toghill and N. Tapia-Ruiz, Advanced Energy Materials, 2021, 11, 2102028.

10. W. Yoshida, F. Kubota, Y. Baba, S. D. Kolev and M. Goto, ACS Omega, 2019, 4, 21122-21130.

11. X. Sun, H. Luo and S. Dai, Talanta, 2012, 90, 132-137.

12. Y. A. Aydın and N. D. Aksoy, Chemical Engineering Journal, 2009, 151, 188-194.

13. S. Gupta and B. Babu, Chemical Engineering Journal, 2009, 150, 352-365.

14. A. B. Botelho Junior, D. B. Dreisinger and D. C. Espinosa, Mining, Metallurgy & Exploration, 2019, 36, 199-213.

15. J.-c. Lee, H.-J. Hong, K. W. Chung and S. Kim, Separation and Purification Technology, 2020, 246, 116896.

16. A. Fathima, J. Y. B. Tang, A. Giannis, I. Ilankoon and M. N. Chong, Chemosphere, 2022, 298, 134340.

17. S. Hussaini and A. M. Tita, in Recycling Technologies for Secondary Zn-Pb Resources, Springer, 2023, pp. 403-459.

18. L. Nghiem, P. Mornane, I. Potter, J. Perera, R. Cattrall and S. Kolev, Journal of Membrane Science, 2006, 281, 7-41.

19. M. I. G. S. Almeida, R. W. Cattrall and S. D. Kolev, Journal of Membrane Science, 2012, 415-416, 9-23.

20. A. T. Fajar and M. Goto, Journal of Chemical Engineering of Japan, 2023, 56, 2153547.

21. B. Keskin, B. Zeytuncu-Gökoğlu and I. Koyuncu, Chemosphere, 2021, 279, 130604.

22. A. Kaya, C. Onac, A. Surucu, E. Karapinar, H. K. Alpoguz and B. Tabakci, Journal of Inclusion Phenomena and Macrocyclic Chemistry, 2014, 79, 103-111.

23. C. Cai, F. Yang, Z. Zhao, Q. Liao, R. Bai, W. Guo, P. Chen, Y. Zhang and H. Zhang, Journal of Membrane Science, 2019, 579, 1-10.

24. O. Kebiche-Senhadji, L. Mansouri, S. Tingry, P. Seta and M. Benamor, Journal of Membrane Science, 2008, 310, 438-445.

25. S. D. Kolev, Y. Baba, R. W. Cattrall, T. Tasaki, N. Pereira, J. M. Perera and G. W. Stevens, Talanta, 2009, 78, 795-799.

26. N.-S. Abdul-Halim, P. G. Whitten and L. D. Nghiem, Separation and Purification Technology, 2013, 119, 14-18.

27. L. Guo, Y. Liu, C. Zhang and J. Chen, Journal of Membrane Science, 2011, 372, 314-321.

28. W. Yoshida, Y. Baba, F. Kubota, S. D. Kolev and M. Goto, Journal of Membrane Science, 2019, 572, 291-299.

29. H. Dahdah, F. Sellami, S. Dekkouche, M. Benamor and O. Senhadji-Kebiche, Polymer Bulletin, 2023, 80, 6495-6525.

30. D. Wang, R. W. Cattrall, J. Li, M. I. G. Almeida, G. W. Stevens and S. D. Kolev, Journal of Membrane Science, 2017, 542, 272-279.

31. D. Wang, J. Hu, Y. Li, M. Fu, D. Liu and Q. Chen, Journal of Membrane Science, 2016, 501, 228-235.

32. E. Radzyminska-Lenarcik and M. Ulewicz, Polish Journal of Chemical Technology, 2015, 17, 51-56.

33. B. Pospiech, Archives of Metallurgy and Materials, 2015.

34. M. Monroy-Barreto, A. N. Bautista-Flores, N. M. Munguia Acevedo, E. R. de San Miguel and J. de Gyves, Industrial & Engineering Chemistry Research, 2021, 60, 3385-3396.

35. M. Macías and E. Rodríguez de San Miguel, Water, Air, & Soil Pollution, 2021, 232, 1-16.

36. A. T. Fajar, T. Hanada, M. L. Firmansyah, F. Kubota and M. Goto, ACS Sustainable Chemistry & Engineering, 2020, 8, 11283-11291.

37. B. Pospiech, Physicochemical Problems of Mineral Processing, 2022, 58.

38. M. Rahman and C. S. Brazel, Polymer Degradation and Stability, 2006, 91, 3371-3382.

39. M. P. Scott, C. S. Brazel, M. G. Benton, J. W. Mays, J. D. Holbrey and R. D. Rogers, Chemical Communications, 2002, 1370-1371.

40. P. Bonhote, A.-P. Dias, N. Papageorgiou, K. Kalyanasundaram and M. Grätzel, Inorganic chemistry, 1996, 35, 1168-1178.

41. Q. J. Guan, W. Sun, G. Y. Zhou, J. P. Liu and Z. G. Yin, Trans. Nonferrous Met. Soc. China, 2016, 26, 865-873.

42. T. Guoxin, Z. Yongjun, X. Jingming, Z. Ping, H. Tiandou, X. Yaning and Z. Jing, Inorganic Chemistry, 2003, 42, 735-741.

43. S. Khurana, S. Negi and A. Chandra, Polymer Testing, 2021, 96, 107118.

44. P. M. Shanthi, P. J. Hanumantha, T. Albuquerque, B. Gattu and P. N. Kumta, ACS Applied Energy Materials, 2018, 1, 483-494.

45. X. Xu, G. Van Eygen, C. Molina-Fernández, D. Nikolaeva, Y. Depasse, S. Chergaoui, Y. Hartanto, B. Van der Bruggen, J. A. Coutinho and A. Buekenhoudt, Journal of Membrane Science, 2023, 670, 121350

CHAPTER FIVE

TOTAL SEPARATION OF LITHIUM, COBALT, MANGANESE AND NICKEL ACROSS POLYMER INCLUSION MEMBRANES

A version of this chapter has been submitted for publication and is currently under review:

Adigun, B.; Thapaliya, B. P.; Luo, H.; Dai. Total Separation of Lithium, Cobalt, Manganese and Nickel across Polymer Inclusion Membranes

5.1 Abstract

The increasing global dependence on lithium-ion batteries (LIBs) for energy storage has raised concerns about the sustainable supply of critical metals like cobalt, nickel, lithium. Traditional mining practices pose significant environmental challenges, emphasizing the need for effective metal separation and recycling technologies. This study explores the application of polymer inclusion membranes (PIMs) as a promising alternative for low-waste operation. Herein, we developed and optimized a sequential separation process based on PIMs containing specific extractants for the selective recovery of Li^{+}, Co^{2+}, Mn^{2+}, and Ni^{2+} from simulated solutions and leachates derived from spent LIBs. Notably, our PIM technology achieved high metal recovery efficiencies and maintained performance over three cycles, establishing PIMs as a viable solution for critical metal recovery and promoting a circular economic approach to battery recycling.

5.2 Introduction

The transition to sustainable technologies has driven an unprecedented reliance on lithium-ion batteries (LIBs), which is crucial in electric vehicles, renewable energy storage systems, and a wide range of portable electronic devices.[1-3] These batteries are indispensable in the global push for a cleaner energy future, with production surging from 30 GWh in 2011 to 492 GWh in 2021 and projected to exceed 2–3.5 TWh by 2030.[4-6] Critical metals, including lithium (Li), cobalt (Co), nickel (Ni), and manganese (Mn), are essential to the performance of LIBs. Li contributes to ionic conductivity, enabling efficient charge transport within the battery. Co enhances structural and

thermal stability, providing safety and longevity under varying operating conditions,[7, 8] while Ni increases energy density, enabling higher storage capacities.[9, 10] Mn adds safety and stability, particularly in cathode chemistries like lithium manganese oxide and nickel manganese cobalt (NMC) systems, improving cycling stability and performance.[7, 11] Achieving an optimal balance of these elements is crucial for the development of high-performance LIBs, ensuring efficiency, safety, and durability. However, the limited availability and uneven distribution of these metals, coupled with environmental and geopolitical concerns, have created significant challenges for the sustainable development of LIBs.

The finite and uneven distribution of these critical metals poses significant risks to global supply chains, leading to supply chain vulnerabilities and price surge. In addition to supply chain concerns, the mining and refining of these metals have substantial environmental impacts such as the generation of significant amounts of waste and the release of pollutants into the environment. The reliance on these resources highlights the urgency of developing sustainable recycling methods to recover Li, Co, Ni, and Mn from spent LIBs.[12-16] Recycling metals from secondary sources like spent LIBs presents a practical solution to ensure the steady supply of critical materials while mitigating environmental pollutions. This approach reduces dependence on primary mining activities and minimizes the environmental footprint of battery disposal.[13, 17-21]

Polymer inclusion membranes (PIMs) have emerged as a promising alternative for metal recovery, offering high selectivity, reduced reliance on hazardous solvents, and operational scalability.[22-27] By embedding specific carrier molecules in a polymer matrix, PIMs facilitate selective transport of metal ions. PIMs are particularly effective due to their ability to incorporate specific carrier molecules that selectively bind to target metals within a polymer host. They have

shown remarkable efficacy in the selective separation and recovery of various metal ions.[26, 28-35] Kolev et al. investigated the use of PIMs made from cellulose triacetate (CTA), N-[N,N-di(2-ethylhexyl)aminocarbonylmethyl] glycine (D2EHAG), and dioctylphthalate for the selective extraction of cobalt from manganese.[36] Similarly, Pospiech demonstrated the separation of cobalt from nickel and lithium from a chloride medium with a PIM composed of CTA, trihexyl(tetradecyl)phosphonium thiosalicylate, and 2-nitrophenyl octyl ether.[37] Previous studies have demonstrated their potential for separating metals such as Co and Ni, but their application to sequentially recover Li, Co, Ni, and Mn from complex LIB leachates remains underexplored.

To address the challenges in recovering Li, Co, and Ni, our group previously employed PIMs with bis(2,4,4-trimethylpentyl) dithiophosphinic acid (Cyanex 301) as the carrier to successfully separate Co and Ni from Li. This process utilized ion exchange between the target metal ions and protons in the receiving solution, demonstrating the potential of PIMs for effective metal recovery.[38] Building on this foundation, this study aims to advance this approach by developing a sequential recovery strategy for Li, Co, and Ni. Utilizing the hard-soft acid-base (HSAB) theory, carriers were selected that can selectively bind to these metal ions based on their chemical properties for separation using PIMs.

Herein, for the first time, we report the successful sequential separation of all metal ions from both a simulated mixture solution of the metal ions and an NMC 622 leachate solution, achieving high recovery rates. A two-step sequential transport process was employed, in which the receiving solution from the initial transport step served as the feed solution for the subsequent step, facilitating the efficient separation of all metal ions. The innovation of this study lies in the application of PIMs within a sequential recovery framework, providing a sustainable and scalable

alternative to conventional extraction techniques. The performance of PIMs was assessed based on selectivity, transport efficiency, and long-term stability across multiple cycles. Additionally, thorough membrane characterization, including structural and thermal analyses, was conducted to validate the robustness and scalability of this method. By focusing on NMC 622 leachates, the results of this study demonstrate the potential of PIM technology as a sustainable and effective solution for recycling critical metals from LIBs. The findings underscore the transformative potential of PIM-based technologies for recovering critical metals, contributing to a circular economy and advancing global sustainability initiatives.

5.3 Materials and Methods

5.3.1 Materials

Trihexyltetradecylphosphonium chloride ($P_{66614}Cl$), bis(2-ethylhexyl) hydrogen phosphate (HDEHP) were purchased from Sigma Aldrich, bis(2,4,4-trimethylpentyl) dithiophosphinic acid (Cyanex 301) was purchased from Solvay, poly(vinylidene fluoride-co-hexafluoropropylene) (PVDF-co-HFP, Mw~400,000, Mn~130,000), lithium chloride (LiCl) and hydrochloric acid (HCl) were purchased from Fisher Chemical Company, cobalt (II) chloride ($CoCl_2.6H_2O$) was purchased from Alfa Aesar, nickel (II) chloride ($NiCl_2.6H_2O$) was purchased from J.T Baker Chemical Company, pristine NMC 622 cathode powder was obtained from Sigma Aldrich.

5.3.2 Preparation of Polymer Inclusion Membranes

Three PIMs were prepared for the sequential separation of Li, Co, Mn and Ni. The first PIM was prepared using PVDF-co-HFP (50 wt.% polymer host) and $P_{66614}Cl$ (50% wt. carrier). A total mass of 300 mg was dissolved in 10 mL of acetone and stirred overnight to obtain a homogenous solution. The resulting solution was then cast into a 6.5 cm diameter Petri dish, covered with filter

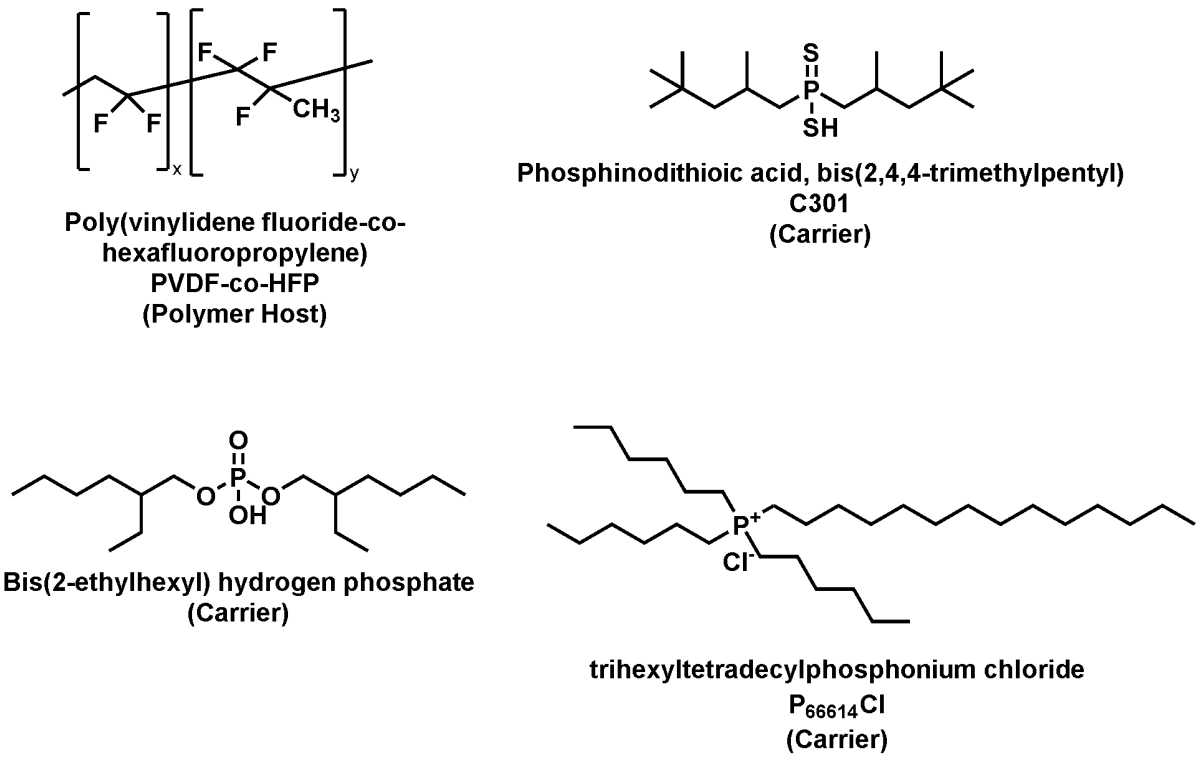

Figure 5.1 Chemical structures of polymer host and carriers.

paper and left to allow acetone evaporation under controlled conditions for 24 hours. The second PIM was prepared using the same procedure as the first, substituting $P_{66614}Cl$ with HDEHP as the carrier. The third PIM was prepared as reported in our previous study.[38] These PIMs were evaluated for their transport efficiency, stability, and selectivity during the separation experiments.

5.3.3 PIM Extraction and Stripping Experiments

The extraction performance of the PIM was evaluated for the extraction of Co^{2+} ion in different acidic concentrations. A PIM with $P_{66614}Cl$ as carrier with a mass of 300 mg was immersed in a flask containing 50 mL of 0.1 mM Co^{2+} and 0.1mM Ni^{2+} in deionized water and hydrochloric acid (HCl) solutions with 1 M, 3 M, 6 M, and 9 M concentrations. The extraction process was conducted

at 25°C for 24 hours under continuous agitation at 200 rpm using an orbital shaker. Following the extraction process, the metal-loaded PIM was gently dried and transferred to a fresh 50 mL stripping solution for the stripping experiment. This experiment was conducted under the same conditions as the extraction. The concentrations of Co^{2+} and Ni^{2+} in the feed solution and stripping solution was determined before and after extraction and stripping steps using inductively coupled plasma optical emission spectrometry (ICP-OES). The extraction efficiency (E%) and stripping efficiency (S%) was calculated using the equations below.[39]

$$E(\%) = \frac{C_0^f - C_t^f}{C_0^f} \times 100 \quad (1)$$

$$S(\%) = \frac{C_t^s}{C_0^f - C_t^f} \times 100 \quad (2)$$

where:

t = Time (hours)

C_0^f = Initial concentration of the metal ion (mol L^{-1}) in the feed solution before extraction.

C_t^f = Concentration of the metal ion in the feed solution at time t during the extraction process.

C_t^s Concentration of the metal ion in the stripping solution at time (t) during the stripping process.

5.3.4 PIM Transport Experiments

The separation performance was evaluated by a series of transport experiments. The PIM transport experiments were conducted using a double-jacketed glass compartment system with the PIM positioned between the feed and receiving solutions (100 mL, respectively). The membrane had a surface area of 20 mm in diameter in direct contact with both solutions. The concentrations

of metal ions in the feed and receiving solutions were measured before and after the transport process using ICP-OES. The kinetics of the transport experiments were evaluated using the following equations:[39]

$$In\left(\frac{C_t^f}{C_0^f}\right) = -kt \quad (3)$$

$$P = \left(\frac{V}{A}\right)k \quad (4)$$

$$J_0 = PC_0^f \quad (5)$$

$$RF\ (\%) = \frac{C_t^r}{C_0^f} \times 100 \quad (6)$$

where:

C_0^f = Initial concentration of the metal ion (mol L^{-1}) in the feed solution.

C_t^f = Concentration of the metal ion in the feed solution at time (*t*).

C_t^r = Concentration of the metal ion in the receiving solution

V = Volume of the feed solution (m^3),

A = surface area (m^2) of the PIM in contact with both the feed and the receiving solution. Parameters such as the rate constant (k), initial flux (J_0), permeability coefficient (*P*) and the recovery factor RF (%) were calculated to assess the transport efficiency and effectiveness of the PIMs.

5.4 Results and Discussion

This study evaluated the performance and selectivity a PIM system containing $P_{66614}Cl$ as the carrier for extracting cobalt (Co^{2+}) from hydrochloric acid solutions. It specifically examined how

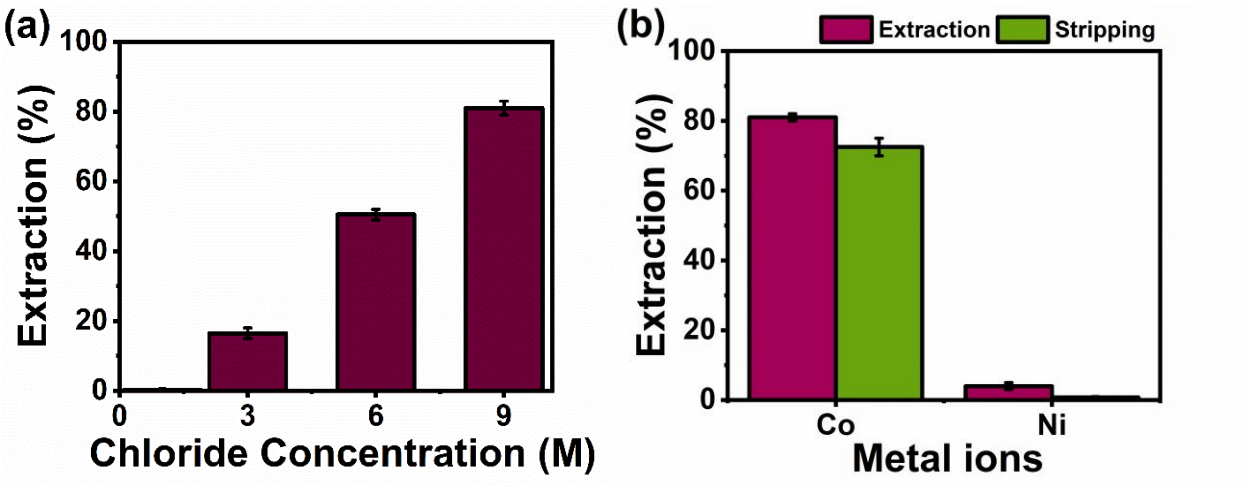

Figure 5.2 (a) Extraction percentage of Co^{2+} at different HCl concentration in the feed solution (b) Extraction and Stripping percentage of Co^{2+} and Ni^{2+} in 9M HCl.

changes in chloride ion concentration influence the extraction efficiency and selectivity of Co^{2+}, especially in the presence of nickel (Ni^{2+}) as a competing ion.

Figure 5.2a presents the extraction efficiency of Co^{2+} at varying HCl concentrations (0, 3, 6 and 9 M) using a PIM composed of 50% PVDF-co-HFP and 50% $P_{66614}Cl$ as the carrier. These results demonstrate that extraction efficiency increases with increasing HCl concentration in the feed solution. At low HCl concentrations between 0–3 M, the extraction efficiency was minimal, with an efficiency of 17% at 3 M HCl. However, as the chloride concentration exceeded 3 M, a significant increase in extraction efficiency was observed. At the highest tested concentration (9 M HCl), the extraction efficiency reached 81%, suggesting that higher chloride concentrations enhance Co^{2+} extraction into the membrane. The PIM was further evaluated for the extraction and stripping of $Co^{2+}$and Ni^{2+} in 9 M HCl, using deionized water as the stripping solution. **Figure 5.2(b)** shows the extraction behavior of both Co^{2+} and Ni^{2+}. The results demonstrate that Co^{2+} was preferentially extracted into the membrane, while Ni^{2+} remained predominantly in the feed

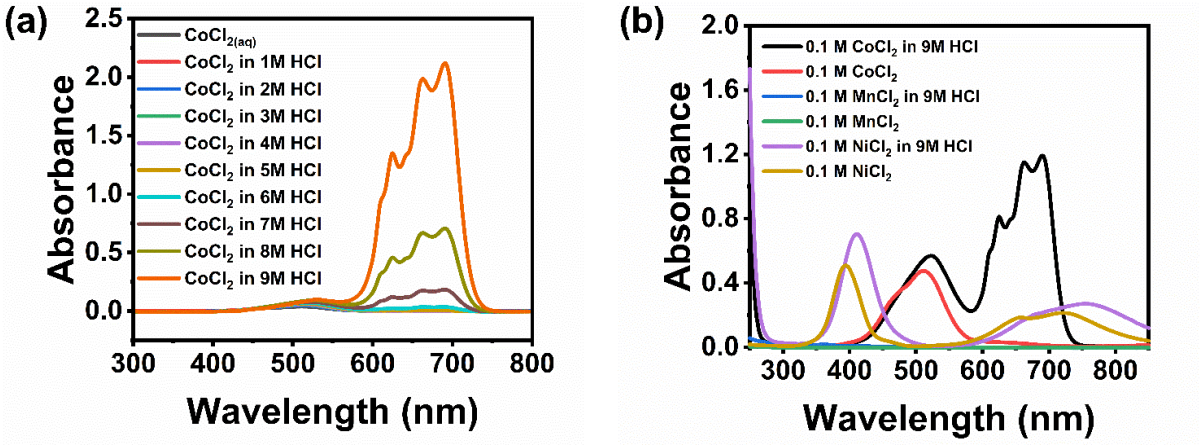

Figure 5.3 UV-Vis spectra of (a) cobalt-chloride complexes in concentrated chloride solution (b) cobalt, manganese and nickel chloride complexes in aqueous and 9 M HCl solution.

solution. Approximately 80% of Co^{2+} was extracted, whereas only 4% of Ni^{2+} was transferred into the membrane. The stripping efficiency was 73% for Co^{2+}, while Ni^{2+} stripping remained below 1%. These findings highlight the high selectivity and efficiency of the $P_{66614}Cl$-based PIM for Co^{2+} transport.

5.4.1 Effect of Chloride Ion Concentration on Selective Extraction of Cobalt

The extraction studies presented in **Figure 5.2** demonstrate the significant influence of chloride ion concentration on the efficiency of Co^{2+} extraction using PIMs. In aqueous solutions, Co^{2+} ions typically exist as hydrated cations. However, as the chloride ion concentration increases, cobalt-chloride complexes begin to form, enhancing their affinity for the carrier embedded in the PIM. The effect of chloride concentration on cobalt was evaluated using UV-Vis spectroscopy, as shown in **Figure 5.3(a)**. Cobalt-chloride complexes in hydrochloric acid solutions are driven by thermodynamic equilibrium, with equilibrium constants providing insight into the relative stability

of these species. Cobalt ions readily form anionic chloride-containing complex, $[CoCl_4]^{2-}$, whereas nickel primarily forms the cationic species $NiCl^+$. This difference in complexation behavior makes the selective separation of nickel from cobalt via anion-exchange methods.[40, 41] At 298 K, the logarithmic equilibrium constant (log K) for the formation of the tetrachlorocobalt(II) complex $[CoCl_4]^{2-}$ is relatively low, at –2.09.[42] In dilute solutions, $[CoCl_4]^{2-}$ formation is thermodynamically unfavorable, and cobalt exists mainly as hydrated Co^{2+} ions. However, increasing chloride concentration shifts the equilibrium toward $[CoCl_4]^{2-}$ formation. As a result, cobalt remains mostly as free Co^{2+} ions in solution when chloride levels are low. This thermodynamic trend is confirmed by UV-Vis spectroscopic data (**Figure 5.3a**). At low chloride concentrations (0–5 M), the UV-Vis spectrum exhibits a dominant absorption peak at 533 nm, which corresponds to the hydrated Co^{2+} species. This observation confirms that at these chloride levels, the available Cl- ions are insufficient to drive the formation of significant $[CoCl_4]^{2-}$ complexes, leading to low extraction efficiencies in separation processes. As the chloride concentration increases beyond 6 M, new absorption bands emerge at 626 nm, 664 nm, and 690 nm, characteristic of the tetrahedral $[CoCl_4]^{2-}$ complex. The appearance of these peaks suggests that at high chloride concentrations; the equilibrium shifts toward the formation of anionic cobalt-chloride species. This shift occurs due to the high chloride ion activity, which compensates for the thermodynamic limitation and drives complex formation. Furthermore, the increased presence of $[CoCl_4]^{2-}$ enhances its extraction efficiency by the PIM, as anion exchange occurs with chloride ions present in the carrier ($P_{66614}Cl$).

The proposed extraction mechanism can be described by the following equations:

$$\text{Extraction: } [CoCl_4^{2-}]_{feed} + 2[P_{66614}^{+}][Cl^-]_{mem} \leftrightarrow [P_{66614}^{+}]_2[CoCl_4^{2-}]_{mem} + 2[Cl^-]_{feed} \quad (7)$$

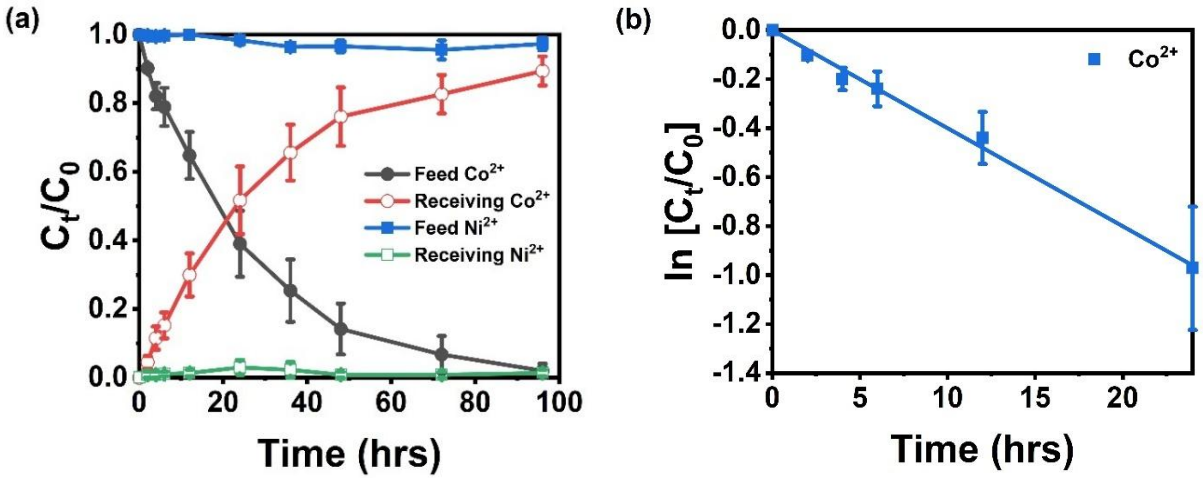

Figure 5.4 (a) Transport of Co^{2+} and Ni^{2+} across an PIM in the feed and receiving solutions over time (b) Kinetic plots of the transport of Co^{2+} PIM in the feed solution.

Stripping: $[P_{66614}^{+}]_2[CoCl_4^{2-}]_{mem} + H_2O_{rec} \leftrightarrow 2[P_{66614}^{+}][Cl^{-}]_{mem} + (CoCl_2)_{rec} + H_2O$ (8)

To assess the selectivity of the PIM for cobalt extraction in the presence of competing metal ions, UV-Vis spectra of Co^{2+}, Mn^{2+}, and Ni^{2+} solutions were analyzed in both deionized water and 9 M chloride solutions (**Figure 5.3(b)**). The spectra reveal that while cobalt undergoes speciation into extractable anionic complexes at high chloride concentrations, the UV-Vis spectra of nickel and manganese remain unchanged in both deionized water and concentrated chloride solutions. This indicates that Ni^{2+} and Mn^{2+} do not form anionic chloride complexes under these conditions, further highlighting the selectivity of the PIM system for cobalt extraction over nickel. The proposed extraction mechanism provides a strategy for designing PIM-based separation systems to recover cobalt ion in the presence of competing metal ions such as nickel.

5.4.2 Selective Membrane Separation of Co^{2+} from Ni^{2+}

Our previous study successfully demonstrated the effective separation of Co^{2+} and Ni^{2+} from Li^{+} using a PIM system.[38] Building on these findings, the present study focuses on achieving the selective separation of Co^{2+} from Ni^{2+}. A feed solution containing an equimolar mixture of Co^{2+} and Ni^{2+} (0.1 mM each) in 100 mL of 9 M HCl was used, with deionized water (100 mL) serving as the receiving solution. The transport efficiency and selectivity of the PIM were evaluated over a 96-hour period. As shown in **Figure 5.4(a)**, the concentration of Co^{2+} in the feed solution gradually decreased over time, while its concentration in the receiving phase increased proportionally, indicating effective transport of Co^{2+} across the membrane. In contrast, the Ni^{2+} concentration in both the feed and receiving solutions remained largely unchanged throughout the experiment, demonstrating the membrane's selectivity for Co^{2+}. By the end of the experiment, 90% of Co^{2+} had been selectively transported to the receiving solution, while 97% of Ni^{2+} remained in the feed solution. The transport kinetics of Co^{2+} were further analyzed by plotting In C^f_t/C^f_0 against time for the feed solution as shown in **Figure 5.4(b).** Using Equations 3–5, the rate constant (k), permeability coefficient (P), and initial flux (J_0) were calculated, with the results summarized in **Table 5.1**. Our PIM system achieved 90% Co recovery with only 1% Ni co-transport in a single stage, demonstrating excellent selectivity and efficiency. In contrast, conventional solvent extraction methods can reach ~95% Co extraction but often exhibit 5–6% Ni co-extraction at high extractant concentrations and require strict pH control and extensive organic solvent handling.[45, 46] Similarly, MOF-based adsorbents have reported high overall metal recoveries but generally show lower selectivity.[47] Compared to these approaches, our PIM method delivers comparable recovery with higher purity, improved selectivity, and significantly lower reagent consumption, highlighting its potential as a more sustainable and operationally simple alternative.

Table 5.1 The rate constant (k), permeability coefficient (P), and initial fluxes (J_0) for the transport of Co^{2+} across PIM

Metal ions	k (h^{-1})	P ($\mu m \cdot s^{-1}$)	J_0 ($\mu mol \cdot m^{-2} \cdot s^{-1}$)	*Transport Efficiency (%)*
Co^{2+}	0.0402	3.55	0.355	90

Table 5.2 Comparison of kinetic parameters (rate constant, permeability, initial flux, and recovery percentage) for the separation of Co^{2+} across different studies

Carrier	k (h^{-1})	P ($\mu m \cdot s^{-1}$)	J_0 ($\mu mol \cdot m^{-2} \cdot s^{-1}$)	Recovery Factor (%)	Ref
D2EHAG	0.076	2.3	1.1	100	[36]
TIOA	-	1.51	3.02	90.55	[43]
[PR4][TS]	0.151	3.34	66.8	91.6	[37]
DNNSA	0.019	1.956	1.991	97.8	[44]
$P_{66614}Cl$	0.040	3.55	0.355	90	This study

*All units are converted to k (h^{-1}), P ($\mu m \cdot s^{-1}$) and P ($\mu m \cdot s^{-1}$) for rate constant, permeability, and initial flux respectively.

D2EHAG: N-[N,N-di(2-ethylhexyl)aminocarbonylmethyl]glycine, TIOA: triisooctylamine, [PR4][TS]: trihexyl(tetradecyl)phosphonium

5.4.3 Sequential Membrane Separation of Co^{2+}, Ni^{2+} and Li^{+}

The overall aim of this research is to develop an effective strategy for the selective recovery of critical battery metals such as cobalt (Co), nickel (Ni), and lithium (Li) from spent LIBs, contributing to the affordable management of these valuable resources. This study employs a

sequential transport approach using PIMs to selectively separate these metals based on their chemical properties.

First Transport Sequence: Separation of Co^{2+} and Ni^{2+} from Li^{+}

In the first transport sequence, Co^{2+} and Ni^{2+} were separated from Li^{+} using a PIM with Cyanex 301 as the carrier. This process operated via a cation-exchange-facilitated complexation mechanism, where Co^{2+} and Ni^{2+} were transported from a feed solution containing 0.1 mM of Co^{2+}, Ni^{2+}, and Li^{+} into a receiving solution of 9 M HCl. The cation-exchange-facilitated complexation process is described by Equation 9:

$$M^{2+}_{(aq)} + 2HA_{(mem)} \quad \leftrightharpoons \quad MA_{2(mem)} + 2H^{+}_{(aq)} \qquad (9)$$

where, *aq* and *mem* represent the aqueous and membrane phases, respectively

After 96 hours, 91% of Co^{2+} and 88% of Ni^{2+} were successfully transported into the receiving solution, while 92% of Li^{+} remained in the feed solution **(Figure 5.5a)**. The high selectivity of the PIM for Co^{2+} and Ni^{2+} over Li^{+} is attributed to their stronger complexation with the Cyanex 301 carrier, driven by differences in charge density and binding affinity. This selectivity can be explained using Hard-Soft Acid-Base (HSAB) theory, which classifies metal ions based on their polarizability and interaction preferences. According to HSAB principles, Li^{+}, a hard acid, preferentially interacts with hard bases such as oxygen-containing ligands, resulting in weaker interactions with the soft donor atoms present in Cyanex 301. In contrast, Co^{2+} and Ni^{2+} are borderline acids that exhibit stronger affinities for the softer sulfur-containing ligands of Cyanex 301, facilitating their extraction into the membrane phase.[48, 49] The selective retention of Li^{+} in the feed solution highlights the system's effectiveness in separating Co^{2+} and Ni^{2+} from Li^{+}, providing the foundation for subsequent separation of Co^{2+} from Ni^{2+}.

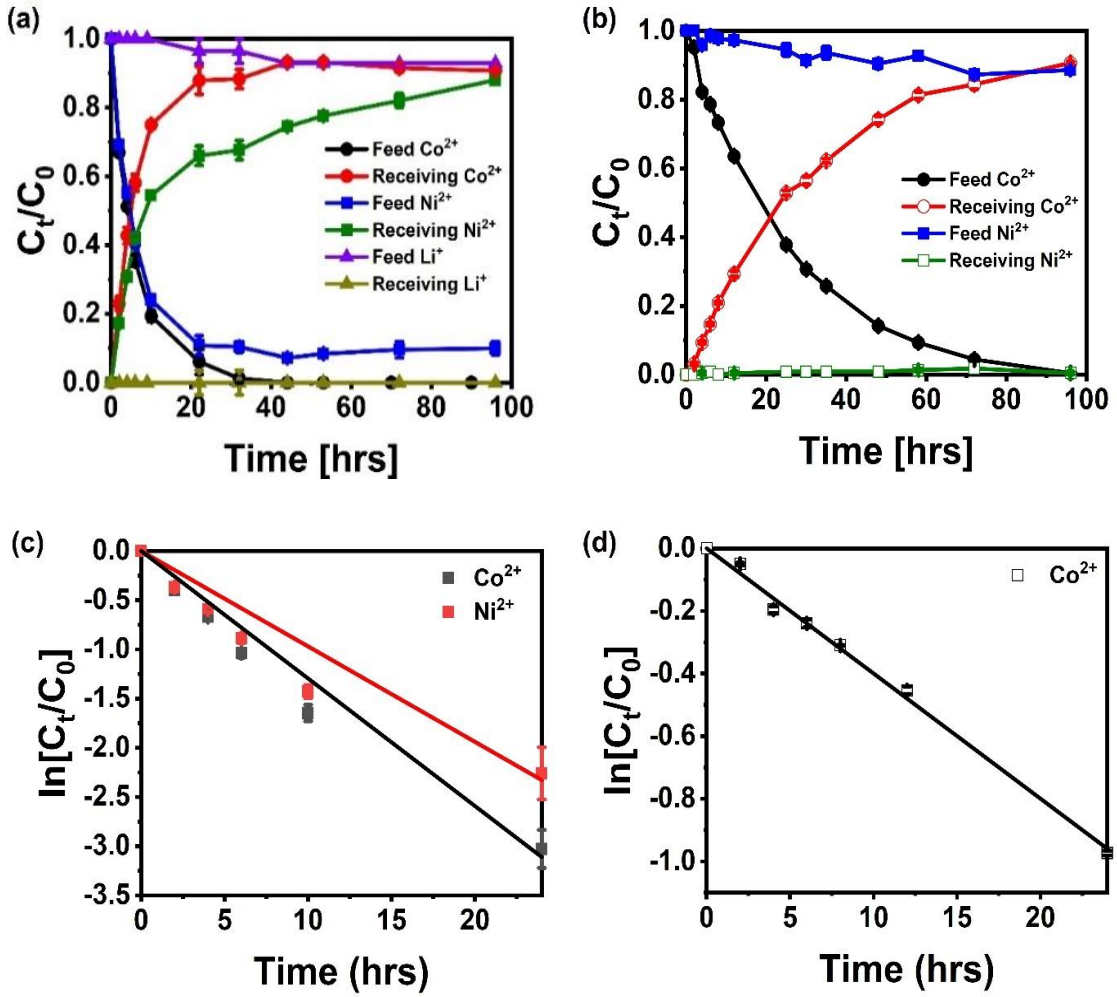

Figure 5.5 (a) First transport sequence of Co^{2+} and Ni^{2+} (b) Second transport sequence of Co^{2+} across a PIM in the feed and receiving solutions over time. Kinetic plots of (c) First transport sequence (d) Second transport sequence.

Second Transport Sequence: Separation of Co^{2+} from Ni^{2+}

In the second transport sequence, the Co^{2+} and Ni^{2+} mixture in the receiving solution was further separated using a PIM with $P_{66614}Cl$ as the carrier. This step aimed to selectively separate Co^{2+} from Ni^{2+} via an anionic exchange mechanism. In the presence of excess chloride ions in the 9 M HCl receiving solution, Co^{2+} formed tetrahedral cobalt-chloride complexes, $[CoCl_4]^{2-}$ which were

Table 5.3 First transport sequence for the separation of Co and Ni from Li

Metal ions	*k* (h^{-1})	*P* ($\mu m \cdot s^{-1}$)	J_0 ($\mu mol \cdot m^{-2} \cdot s^{-1}$)	*Recovery Factor* (%)
Co^{2+}	0.130	11.46	1.146	91
Ni^{2+}	0.097	8.57	0.857	88
Second transport sequence for the separation of Co from Ni				
Co^{2+}	0.040	3.53	0.3530	91

selectively transported across the membrane in the second transport sequence, as described by Equations (7) and (8): As shown in **Figure 5.5(b)**, 91% of Co^{2+} was selectively transported into the receiving solution, while 88% of Ni^{2+} remained in the feed solution, confirming the high selectivity of the system for cobalt extraction. The kinetic plot from the plot of In C^f_t/C^f_0 against time for the feed solution in **Figure 5.5(c-d)** was used to calculate the rate constant (*k*), permeability coefficient (*P*), and initial flux (J_0) for the transport eperiments. These values are summarized in **Table 5.3**.

5.4.4 Optimization of the Sequential Separation of Co, Ni, and Li

To optimize the sequential separation process and minimize the number of transport sequences required, a three-jacketed glass compartment system was built (**Figure 5.6**). This setup allowed for the simultaneous operation of two polymer inclusion membranes (PIMs), each with a different carrier, positioned between the compartments. This configuration facilitated the concurrent transport of Co^{2+}, Ni^{2+}, and Li^+ ions using Cyanex 301 and $P_{66614}Cl$ as membrane carriers. In the first transport step, Co^{2+} and Ni^{2+} were selectively transported from the feed solution into the first receiving solution (9 M HCl) using the Cyanex 301 PIM. As shown in **Figure 5.7**, the

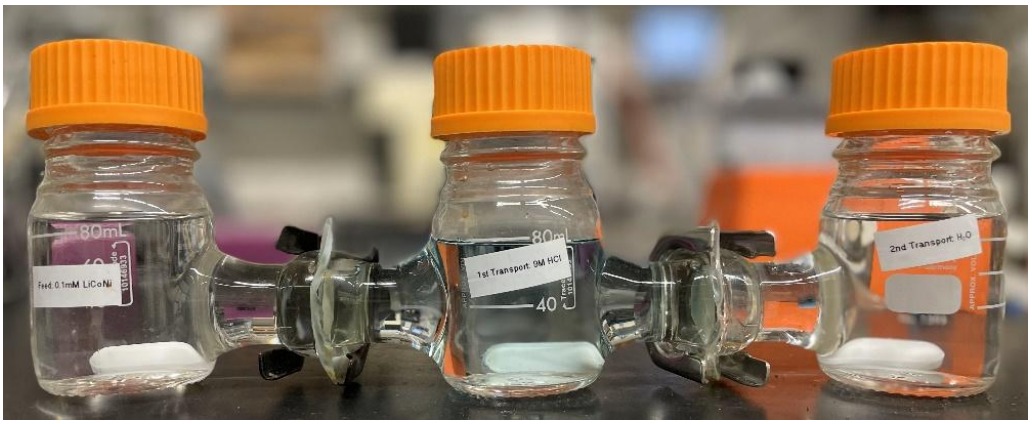

Figure 5.7 Picture of the 3- jacketed glass compartment for the optimized transport experiment.

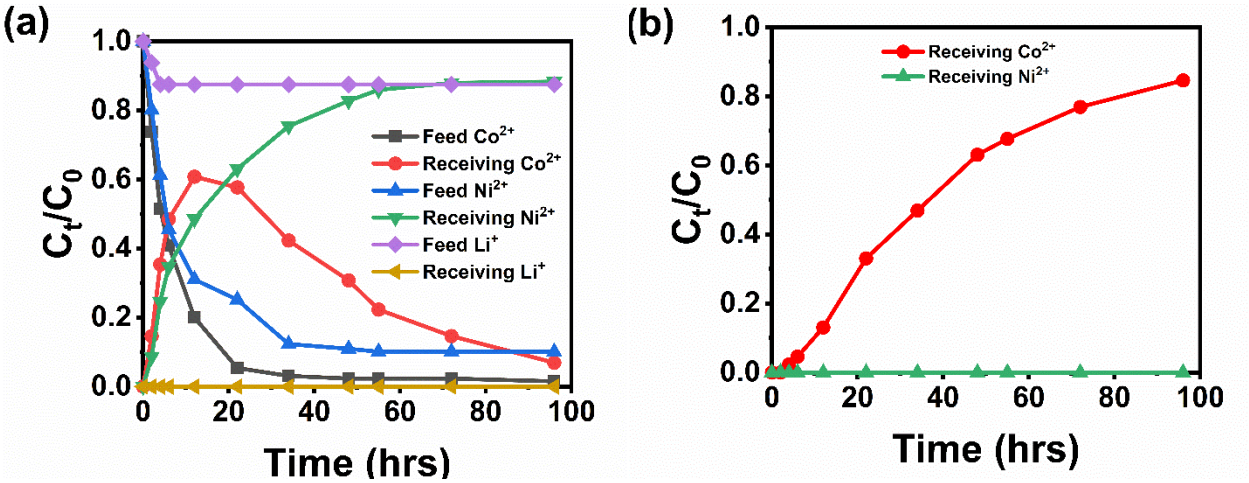

Figure 5.6 (a) 1st transport sequence separation of Co^{2+} and Ni^{2+} from Li^+ (b) 2nd transport sequence of Co^{2+} from Ni^{2+}

concentrations of both Co^{2+} and Ni^{2+} in the feed solution decreased over time, while their concentrations in the first receiving solution increased. However, after 24 hours, the concentration of Co^{2+} in the first receiving solution began to decline, coinciding with an increase in Co^{2+} concentration in the second receiving solution (deionized water). This transition marked the onset

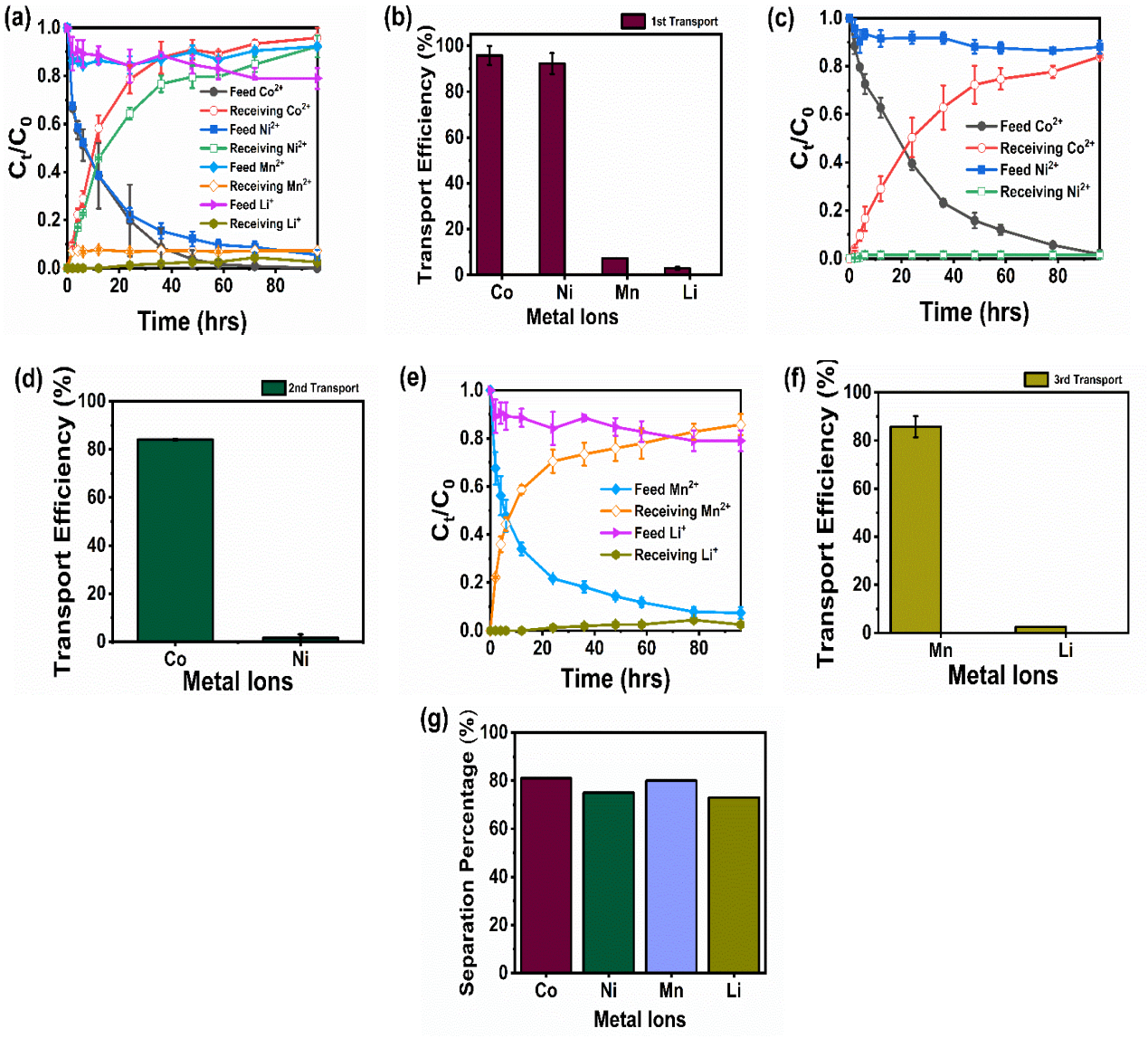

Figure 5.8 (a)1st transport sequence separation of Co^{2+} and Ni^{2+} from Li^+ and Mn^{2+} (b) Transport efficiency of the first transport sequence (c) 2nd transport sequence of Co^{2+} from Ni^{2+} (d) Transport efficiency of the second transport sequence. (e) 3rd transport sequence of Co^{2+} from Ni^{2+} (f) Transport efficiency of the third transport sequence. (g) Separation percentage of the metal ions.

of the second transport process, where Co^{2+} was selectively transported from the first receiving solution into the second receiving solution via the $P_{66614}Cl$ PIM. After 96 hours, the optimized two-step process achieved selective separation of the three target ions: 88% of Ni^{2+} was transported into the first receiving solution, 85% of Co^{2+} was transported into the second receiving solution, and 87% of Li^{+} remained in the feed solution. This simultaneous two-step transport strategy effectively streamlined the separation process by reducing both the number of steps and the overall separation time.

5.4.5 Sequential transport from NMC 622 leachate

Building on the successful sequential separation of Co^{2+}, Ni^{2+}, and Li^{+} from simulated solutions, this study further evaluated the practical applicability by employing pristine NMC 622 cathode powder. This approach was used to confirm that the optimized separation sequence developed under simulated conditions remains effective when applied to real NMC 622 leachates. The pristine powder used was free of PVDF binder and fluorinated electrolyte residues, therefore, HF generation was not a concern under our experimental conditions. To obtain metal ions from the pristine NMC 622 cathode powder, acid leaching was performed using aqua regia as the leaching agent. A known mass of NMC 622 powder was added to freshly prepared aqua regia ($HCl:HNO_3$ = 3:1, v/v) and the leachate was diluted and used as the feed solution. The leachate, containing 0.5 mM of NMC 622, was prepared for a series of transport experiments designed to evaluate the effectiveness of tailored PIMs with Cyanex 301, HDEHP, and P66614Cl as carriers for the separation of the cathode materials. In the first transport sequence, Co^{2+} and Ni^{2+} were separated from Mn^{2+} and Li^{+} using a PIM with Cyanex 301 as the carrier. Co^{2+} and Ni^{2+} were transported from the feed solution into the receiving solution of 100ml of 9M HCl over 96 hours as shown in **Figure 5.8(a, b)**. The process achieved high transport efficiencies of 96% for Co^{2+} and 92% for

Ni^{2+}, while 93% of Mn^{2+} and 97% of Li^{+} remained in the feed solution. The second transport sequence aimed to separate Co^{2+} from Ni^{2+} using a PIM with $P_{66614}Cl$ as the carrier. In this step, the receiving solution from the first transport experiment served as the feed solution, with deionized water used as the receiving solution. As shown in **Figures 5.8(c, d)** 84% of Co^{2+} was selectively transported into the receiving solution, while 88% of Ni^{2+} remained in the feed solution. In the third transport sequence, the feed solution from the first transport experiment was used as the feed solution for the third transport for the separation of Mn^{2+} from Li^{+} using a PIM with HDEHP as the carrier and 2M HCl as the receiving solutionCo^{2+} was selectively transported into the receiving solution, while 88% of Ni^{2+} remained in the feed solution. In the third transport sequence, the feed solution from the first transport experiment was used as the feed solution for the third transport for the separation of Mn^{2+} from Li^{+} using a PIM with HDEHP as the carrier and 2M HCl as the receiving solution. **Figures 5.8(e, f)** show that Mn^{2+} was selectively transported with an efficiency of 86%, while 97% of Li^{+} remained in the feed solution. This step completed the sequential recovery of all target metals. The transport efficiencies for all three steps are summarized in **Figure 5.8(g).** The separation percentages of the recovered metal ions were 81%, 80%, 75%, and 73% for Co^{2+}, Mn^{2+}, Ni^{2+}, and Li^{+}, respectively. These results highlight the effectiveness of the sequential transport system in isolating critical metals with high efficiency. An alternative strategy for the separation of these metals could involve initially recovering the monovalent Li^{+} ions from the feed solution, followed by selective separation of the remaining divalent ions (Co^{2+}, Ni^{2+}, and Mn^{2+}). This reverse approach would require the use of a carrier capable of preferentially transporting Li^{+} in the presence of divalent transition metals. However, achieving a high separation factor under such conditions can be challenging, as Li^{+}, a hard acid interacts weakly with most carriers that typically favor the softer or borderline divalent cations.

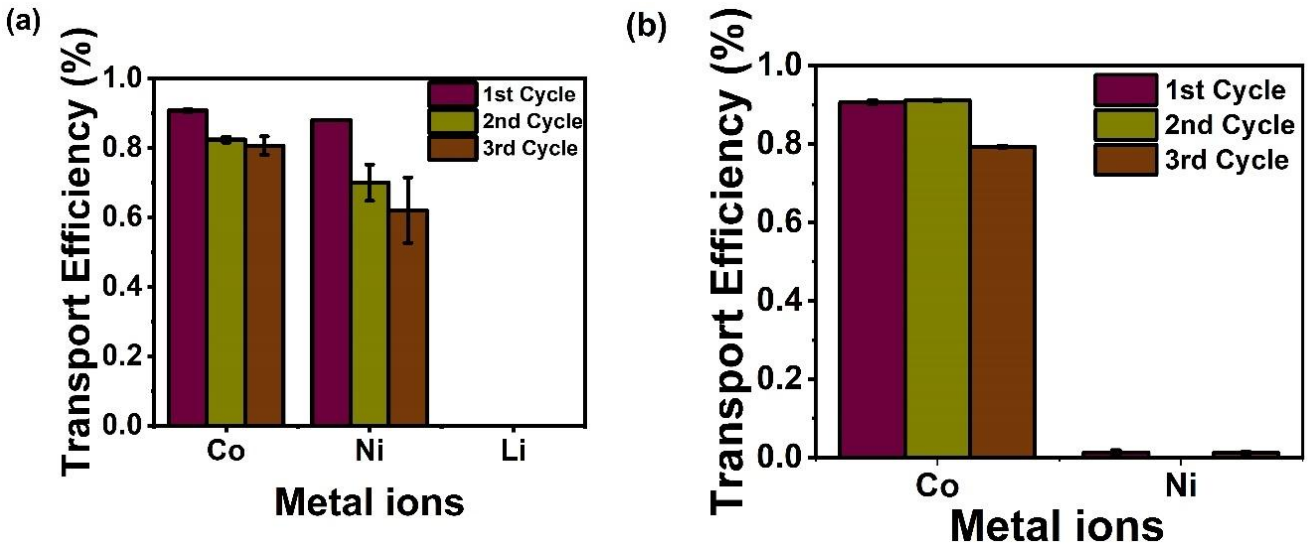

Figure 5.9 Stability of membrane after (a) 1st transport sequence (b) 2nd transport sequence.

Consequently, while Li^+ first recovery presents an intriguing alternative pathway, its implementation would necessitate the design or use of carrier molecules with high affinity and selectivity toward Li^+ to achieve efficient and sustainable separation.

5.4.6 Membrane Stability

The stability of PIMs is critical for their application in the sequential separation of metal ions, particularly in industrial and real-world recycling scenarios. In this study, the stability of PIMs containing Cyanex 301, and $P_{66614}Cl$ as carriers was assessed under prolonged operation and repeated use. The membranes were subjected to three consecutive 96-hour transport experiments for both the first and second transport sequence in a continuous operation reusing the same membrane and changing the feed and receiving solution after each cycle to investigate their chemical integrity, transport efficiency, and reusability. The transport efficiency of Co^{2+} and Ni^{2+} in the first transport sequence progressively declined, decreasing from 91% in the first cycle to 82% and 81% in the second and third cycles,

respectively (**Figure 5.9**). In the second transport sequence, transport efficiency remained stable at 91% for the first two cycles but dropped to 80% in the third cycle. To further evaluate the stability of the membrane, potential leaching of the carrier was assessed by monitoring changes in membrane mass and measuring phosphorus concentrations after immersion in solutions representative of the feed and receiving phases. Membrane samples were immersed in deionized water and 9M HCl for 4 days. The initial mass of each membrane sample was recorded prior to immersion. After the 4-day period, the membranes were removed, thoroughly rinsed with deionized water, and dried to a constant weight. The final mass of each membrane was then measured, with any mass loss suggesting potential leaching of membrane components. The results are summarized in **Figure S.3** and **Table S.1**, showed that the mass loss of the PIM with $P_{66614}Cl$ was minimal compared to that of the Cyanex 301 PIM, suggesting lower carrier leaching in the $P_{66614}Cl$ membrane. To further quantify carrier loss, phosphorus concentrations in the immersion solutions were analyzed ICP-OES. After four days, the phosphorus concentrations in the immersion solutions from the Cyanex 301 PIM and $P_{66614}Cl$ PIM were approximately 7 ppm and 3 ppm, respectively. The detected phosphorus concentration originates from the partial dissolution of the organophosphorus carrier (Cyanex 301) upon prolonged contact with the aqueous phase. This leaching correlates with the observed decline in transport efficiency from 91% to ~80% after four days. The leaching process occurs when components of the PIM, particularly the extractant molecules, diffuse out of the membrane matrix into the contacting solution. The loss of these organophosphorus species reduces the number of available carrier sites within the membrane, thereby decreasing the efficiency of ion transport. To mitigate this effect and improve membrane longevity, several strategies are being considered. These include using analogues of organophosphorus extractants that exhibit stronger affinity for the polymer phase and applying

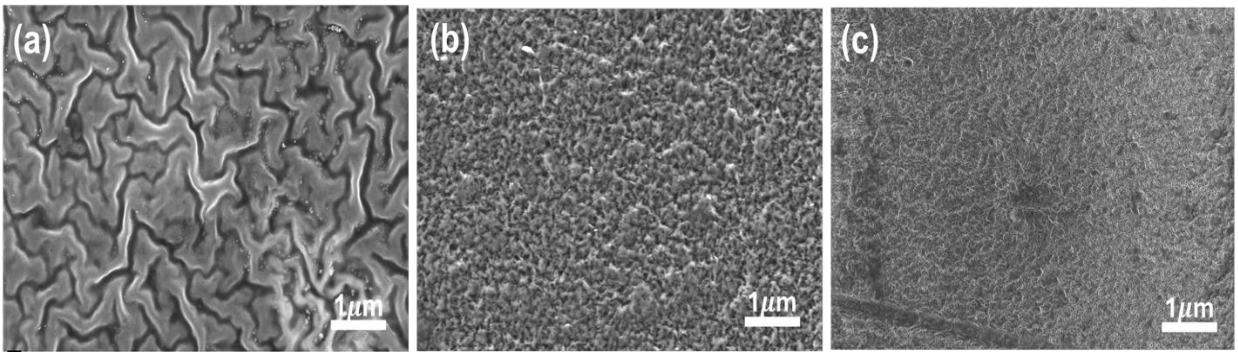

Figure 5.11 SEM images of (a) $P_{66614}Cl$ PIM (b) Cyanex 301 PIM (c) HDEHP PIM.

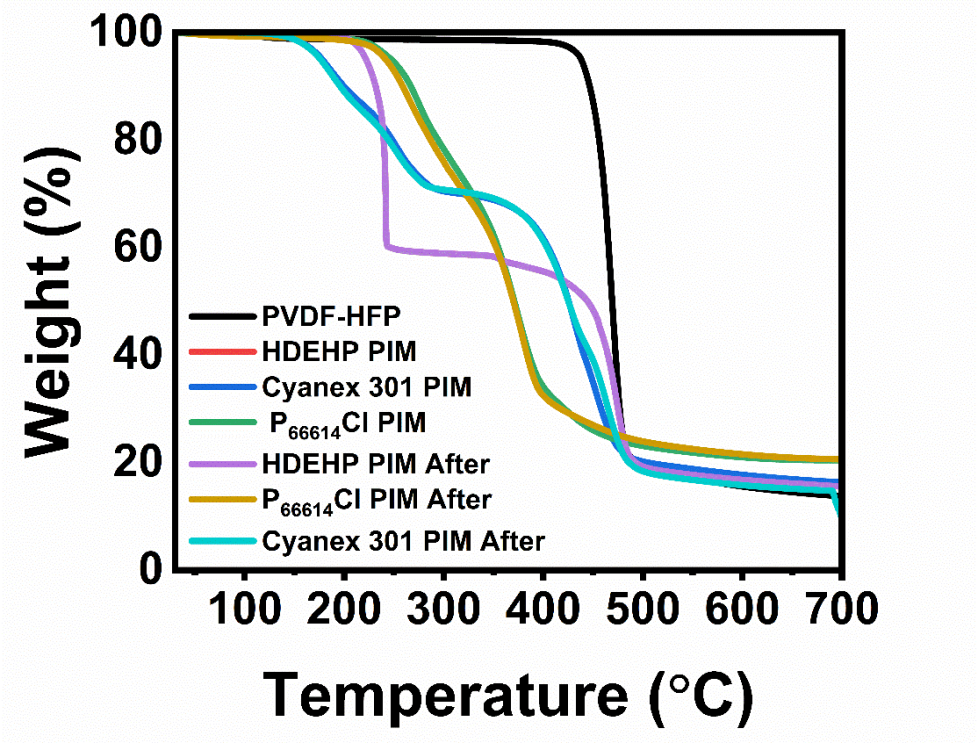

Figure 5.10 Thermogravimetric analysis of PVDF-HFP, HDEHP PIM, Cyanex 301 PIM and $P_{66614}Cl$ PIM.

protective surface coatings to minimize leaching during extended operation. These findings indicate that the PIM with $P_{66614}Cl$ exhibits superior stability, with lower carrier leaching than the

Cyanex 301-based membrane, highlighting its potential for extended use in metal ion separation processes.

5.4.7 Membrane Characterization

The PIMs used in this study were characterized using scanning electron microscopy (SEM), thermogravimetric analysis (TGA), and Fourier-transform infrared spectroscopy (FTIR). SEM was employed to examine the surface morphology and microstructure of the PIMs. As shown in **Figure 5.10**, the SEM images revealed a uniform and dense membrane structure, indicating the successful incorporation of the carrier agents into the polymer matrix. The surface of the PIM containing $P_{66614}Cl$ exhibited cracks, while the surface of the PIMs with Cyanex 301 and HDEHP appeared rough and dense, which may be attributed to solvent evaporation during membrane preparation. The surface morphology of the membranes didn't change much after the transport experiments suggesting structural integrity was largely maintained after repeated use (**Figure S.4**). TGA was performed to assess the thermal stability of the PIMs. The membranes were heated under a nitrogen atmosphere, with the weight loss recorded as a function of temperature. **Figure 5.11** presents the thermal decomposition data for pure PVDF-co-HFP, Cyanex 301 PIM, $P_{66614}Cl$ PIM and HDEHP PIM before and after the transport experiments over a temperature range of 30–800°C. The PVDF-co-HFP and $P_{66614}Cl$ based PIMs exhibited single-step decomposition at 480°C and 300°C, respectively while sCyanex 301 and HDEHP based PIMs underwent two-step decomposition at 200°C and 250°C. The high decomposition temperatures indicate that the PIMs possess substantial thermal stability, remaining stable well above their operational temperature range. The distinct weight loss steps correspond to the degradation of the polymer host and carrier molecules confirmed the successful formulation of the membranes. Additionally, no changes in the thermal stability of the membranes were observed after use.

Figure S.5 presents the FTIR analysis of PVDF-co-HFP, $P_{66614}Cl$, HDEHP, Cyanex 301 and their PIMs. In **Figure S.5(a)**, the FTIR spectra of Cyanex 301 reveal key peaks at 613, 795, and 2418 cm^{-1}, corresponding to the stretching vibrations of P=S, S=P–SH, and S–H bonds. HDEHP exhibuted peaks at 889, 1230 and 1030 cm^{-1} assigned to P–O, P=O and P–O–C functional groups, respectively.[50, 51] Furthermore, the FTIR spectrum of $P_{66614}Cl$ demonstrates distinct peaks at 1457 cm^{-1} and 2918 cm^{-1}, which are associated with P–C stretching and aliphatic C–H stretching vibrations.[52, 53] In **Figure S.5.(b)**, the FTIR spectra of the polymer hosts highlight its crystalline and amorphous phases. Peaks at 531, 762, 796, and 976 cm^{-1} correspond to the α-phase crystalline regions, while the amorphous phase is represented by the peak at 871 cm^{-1}. Additional vibrational modes observed at 1060, 1146, and 1292 cm^{-1} correspond to the symmetric stretching of –CF groups, $–CF_2$ units, and $–CF_3$ bonds, respectively.[38, 54, 55] The presence of key corresponding to both the polymer host and the carrier molecules in the PIM spectra confirmed their successful integration into the membrane structure. Together, these characterization techniques provided comprehensive insight into the structural, thermal, and chemical properties of the PIMs demonstrating their stability and suitability for metal ion separation applications.

5.5 Layer-by-Layer Reinforcement of Polymer Inclusion Membranes

Polymer inclusion membranes (PIMs) have demonstrated significant potential for the selective separation and recovery of metal ions due to their tunable composition, ease of fabrication, and high selectivity. However, despite these advantages, the long-term operational stability of PIMs remains a critical challenge that limits their practical application in continuous separation processes. One of the primary limitations is the gradual loss of membrane components, particularly carriers and plasticizers, through leaching into the surrounding aqueous phases. This loss not only

reduces membrane efficiency but also alters transport behavior and compromises reproducibility over extended operation. To address these limitations, a Layer-by-Layer (LbL) assembly approach was explored as a strategy to enhance the mechanical stability and structural integrity of PIMs. LbL assembly is a well-established surface modification technique based on the sequential deposition of oppositely charged species, typically polyelectrolytes, onto a substrate through electrostatic interactions, hydrogen bonding, or other intermolecular forces. This technique enables the formation of thin, conformal multilayer films with controlled thickness and composition at the nanoscale.[56-60] The application of LbL assembly to PIM systems is motivated by its ability to introduce a secondary structural framework at the membrane interface without significantly altering the bulk membrane composition. The deposited multilayer coating can serve as a protective barrier that limits the outward diffusion of membrane components, thereby mitigating carrier and plasticizer leaching. In addition, the multilayer structure can enhance mechanical strength by reinforcing the membrane surface and improving resistance to deformation and structural failure.[61-65]

The key motivation for integrating LbL with PIMs was:

- To enhance mechanical robustness through formation of a surface-confined multilayer network
- To reduce carrier and plasticizer leaching by creating a diffusion barrier
- To improve membrane integrity under operational conditions

The LbL approach was investigated as a post-fabrication modification strategy to evaluate its effectiveness in enhancing membrane stability while maintaining acceptable transport performance. The goal was not only to improve membrane durability but also to understand the trade-offs associated with introducing interfacial multilayer structures in PIM systems. The

outcomes of this investigation provide insight into the design considerations required for developing robust and high-performing membranes for long-term metal ion separation applications.

5.5.1 LbL Deposition Procedure

The Layer-by-Layer (LbL) assembly of polyelectrolyte multilayers on polymer inclusion membranes (PIMs) was performed using a sequential dip-coating method involving the alternate adsorption of oppositely charged polyelectrolytes. A cationic solution of poly(diallyldimethylammonium chloride) (PDADMAC) and an anionic solution of poly(styrene sulfonate) (PSS) were prepared in deionized (DI) water at concentrations of 0.1 wt%, The LbL deposition process consisted of sequential immersion of the membrane into the PDADMAC solution for 10 seconds, followed by rinsing in DI water for 10 seconds to remove weakly adsorbed polymer chains. The membrane was subsequently immersed in the PSS solution for an equivalent duration, followed by a second rinsing step. This sequence constituted one bilayer deposition cycle (PDADMAC/PSS). The process was repeated for a defined number of cycles (10 bilayers), yielding membranes denoted as PIM–10LbL, respectively. Following the final deposition cycle, the membranes were thoroughly rinsed with DI water and dried under ambient conditions 24 hours to remove residual moisture.

5.5.2 Characterization

Dynamic Mechanical Analysis (DMA) was employed to evaluate the mechanical properties of pristine and Layer-by-Layer (LbL)-modified polymer inclusion membranes (PIMs), with the aim of quantifying the impact of multilayer deposition on membrane stiffness, strength, and flexibility. Mechanical reinforcement is a critical factor in determining membrane durability under operational conditions, particularly for systems containing plasticizers and mobile carrier species

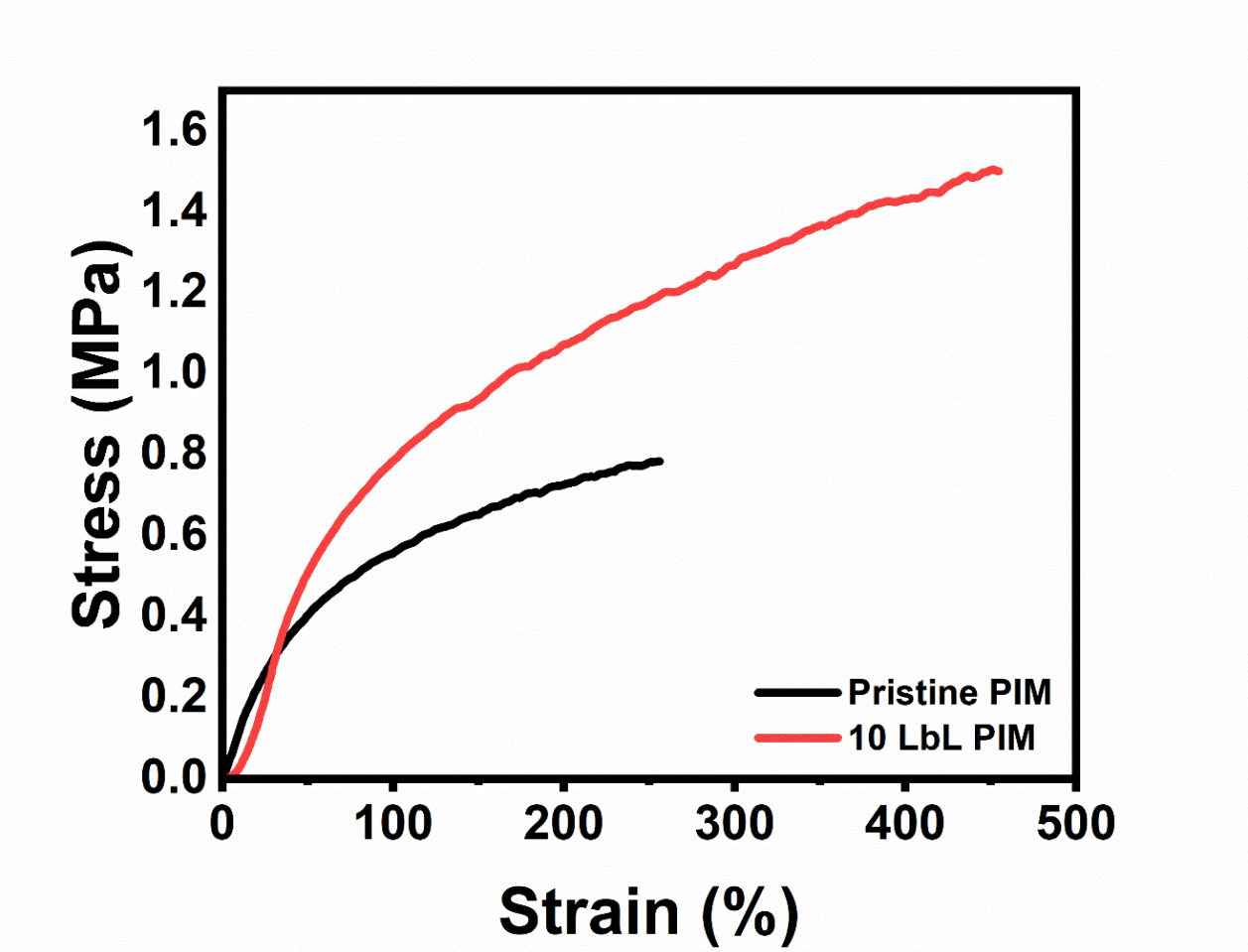

Figure 5.12 DMA Analysis of Pristine PIM and LbL PIM

that inherently reduce structural integrity. **Figure 5.12** shows the stress–strain measurements were conducted under controlled force mode using a dynamic mechanical analyzer, and the resulting profiles were used to extract key mechanical parameters, including Young's modulus, tensile strength, and elongation at break. These parameters provide insight into the elastic behavior, resistance to deformation, and failure characteristics of the membranes.Dynamic mechanical analysis revealed that the 10LbL membrane exhibited substantially improved mechanical performance relative to the pristine PIM. The Ionogel showed an apparent Young's modulus of approximately 1.19 MPa, a maximum stress of 0.784 MPa, and a maximum strain of 256.2%,

Table 5.4. Mechanical properties of pristine PIM and LbL PIM

Material	Young Modulus (MPa)	Tensile Strength (MPa)	Maximum Strain (%)
Pristine PIM	1.19	0.784	256.2
LbL PIM	1.31	1.505	454.9

with a toughness of 1.445 MJ m^{-3}. In contrast, the 10LbL membrane reached a maximum stress of 1.505 MPa and a maximum strain of 454.9%, with a toughness of 4.724 MJ m^{-3}. Although the initial low-strain region of the 10LbL curve displayed a toe region and therefore a reduced apparent modulus when calculated strictly from the first few percent strain, the main deformation region showed a higher effective modulus of about 1.31 MPa. These results indicate that the LbL treatment significantly improved the strength, extensibility, and energy absorption capacity of the membrane. The enhanced mechanical response is attributed to the formation of an interfacial multilayer network that improves cohesion and stress distribution during deformation. Overall, the DMA results demonstrate that the Layer-by-Layer assembly strategy is effective in enhancing the mechanical robustness of polymer inclusion membranes. The observed improvements in stiffness and strength indicate that LbL coatings can significantly reinforce membrane structure and improve resistance to mechanical degradation.

5.5.2 Evaluation of Polymer Inclusion Membrane Leaching

The stability of polymer inclusion membranes was further evaluated by investigating the leaching of membrane components into the aqueous phase. Leaching of plasticizers and carrier molecules is a well-known limitation of PIM systems, as it leads to gradual loss of functionality, reduced transport efficiency, and poor long-term operational stability. Both membranes were immersed in

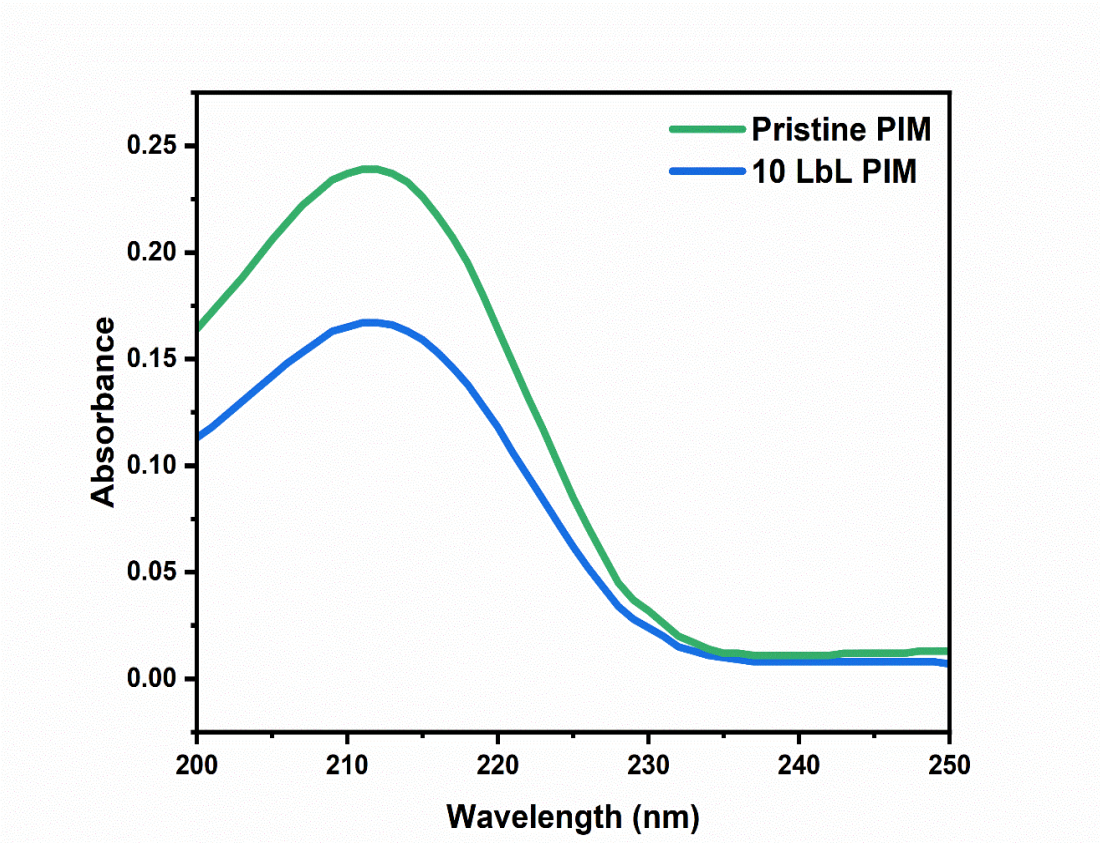

Figure 5.13 UV–Vis spectra of leached components from Pristine PIM and 50 LbL PIM

water solution for 24 hours and the solution analyzed using UV-Vis. The UV–Vis spectra of the solution after 24 hours show distinct absorbance profiles for both the pristine PIM and the LbL PIM. Both spectra exhibit a characteristic absorbance band in the range of approximately 200–230 nm, which can be attributed to the presence of 1-Methyl-3-octylimidazolium bis(trifluoromethylsulfonyl)imide (plasticizer) in the membrane. The pristine PIM exhibits a significantly higher absorbance intensity, with a peak absorbance of approximately 0.24 at around 210–215 nm. In contrast, the LbL PIM shows a lower absorbance peak of approximately 0.16–0.17 within the same wavelength region. The higher absorbance observed for the pristine PIM indicates a greater concentration of leached species in solution, confirming that the pristine

membrane is more susceptible to component loss. The reduced absorbance intensity observed for the LbL-modified membrane demonstrates that the Layer-by-Layer coating effectively suppresses the leaching of membrane components. This improvement can be attributed to the formation of a dense polyelectrolyte multilayer at the membrane surface, which acts as a protective barrier that limits the diffusion of carrier molecules and plasticizers from the membrane into the surrounding solution. The strong electrostatic interactions within the multilayer structure further contribute to the retention of membrane constituents by reducing their mobility. The difference in leaching behavior between the two membranes is consistent with the mechanical properties observed from DMA analysis. These findings highlight an important advantage of the LbL strategy in improving membrane stability. Reduced leaching is critical for maintaining consistent membrane performance over extended operational periods, particularly in applications involving continuous ion separation

5.5.3 Impact of Layer-by-Layer Reinforcement on Ion Transport

The transport behavior of metal ions across polymer inclusion membranes was evaluated for both the pristine membrane and the LbL modified membrane to assess the influence of mechanical reinforcement on separation performance. While the LbL strategy significantly improved the mechanical properties of the membrane, as demonstrated by DMA analysis, its effect on ion transport revealed a clear trade-off between structural stability and transport efficiency. The pristine membrane exhibited relatively higher ion transport rates, consistent with its more flexible structure and higher polymer chain mobility. The presence of plasticizer within the pristine membrane enhances free volume within the membrane matrix, facilitating the diffusion of the

metal–carrier complex across the membrane phase. As a result, the flux of ions through the pristine membrane was comparatively higher.

In contrast, the LbL-modified membrane demonstrated a noticeable reduction in transport rates. The deposition of polyelectrolyte multilayers on the membrane surface introduces an additional barrier to mass transfer, effectively increasing the diffusion path length and resistance to transport. This reduction in flux can be attributed to several interrelated factors. First, the LbL coating forms a denser and more compact surface layer, which restricts the mobility of the carrier–metal complex. The strong electrostatic interactions between oppositely charged polyelectrolytes in the multilayer structure reduce free volume and limit the permeability of the membrane surface. This structural densification hinders the diffusion step, which is often the rate-limiting stage in polymer inclusion membrane

transport. Second, the multilayer coating may partially block or reduce the accessibility of

active carrier sites at the membrane interface. Since ion transport in PIMs relies on the formation of carrier–metal complexes at the feed/membrane interface, any restriction at this interface can slow down the overall transport process. The presence of the LbL layer can therefore introduce an additional kinetic barrier to complexation and decomplexation processes.

5.6 Conclusion

This study demonstrated the effective use of polymer inclusion membranes (PIMs) for the selective recovery of critical metals such as cobalt, nickel, manganese, and lithium from both simulated solutions and real NMC 622 leachates. The successful separation under complex, multicomponent conditions highlight the robustness and practical applicability of PIM systems beyond simplified laboratory models. Membranes incorporating carriers such as $P_{66614}Cl$, Cyanex

301, and HDEHP achieved high recovery efficiencies, while mechanistic insights confirmed the important role of chloride ions in enhancing cobalt selectivity. These findings establish PIMs as promising, low-energy, and environmentally friendly alternatives to conventional hydrometallurgical processes, with strong potential for integration into scalable recycling technologies. To address the critical challenge of membrane stability, a Layer-by-Layer (LbL) reinforcement strategy was investigated. The LbL-modified membranes exhibited significantly improved mechanical strength and toughness, confirming the effectiveness of multilayer assembly in enhancing structural integrity. In addition, UV–Vis analysis demonstrated reduced leaching of membrane components, indicating improved retention of carriers and plasticizers and suggesting enhanced long-term operational stability. However, these improvements were accompanied by a reduction in ion transport rates. The LbL coating introduced additional resistance to mass transfer by reducing free volume, restricting carrier mobility, and increasing diffusion path length. This highlights a fundamental trade-off between membrane stability and transport performance, where enhanced durability comes at the expense of flux. Overall, this work establishes PIMs as a viable platform for sustainable metal recovery from lithium-ion battery waste while demonstrating that LbL modification is an effective strategy for improving membrane durability. Future efforts should focus on optimizing membrane composition and multilayer design to minimize transport resistance while maintaining mechanical stability and reducing leaching. Achieving this balance will be critical for advancing PIM technology toward practical, long-term applications in battery recycling and resource recovery.

References

(1) Di Lecce, D.; Verrelli, R.; Hassoun, J. Lithium-ion batteries for sustainable energy storage: recent advances towards new cell configurations. *Green Chemistry* **2017**, *19* (15), 3442-3467.

(2) Khan, F. N. U.; Rasul, M. G.; Sayem, A.; Mandal, N. K. Design and optimization of lithium-ion battery as an efficient energy storage device for electric vehicles: A comprehensive review. *Journal of Energy Storage* **2023**, *71*, 108033.

(3) Gao, Y.; Pan, Z.; Sun, J.; Liu, Z.; Wang, J. High-energy batteries: beyond lithium-ion and their long road to commercialisation. *Nano-micro letters* **2022**, *14* (1), 94.

(4) Frith, J. T.; Lacey, M. J.; Ulissi, U. A non-academic perspective on the future of lithium-based batteries. *Nature Communications* **2023**, *14* (1), 420.

(5) McKerracher, C.; Izadi-Najafabadi, A.; O'Donovan, A.; Albanese, N.; Soulopolous, N.; Doherty, D.; Boers, M.; Fisher, R.; Cantor, C.; Frith, J. Electric vehicle outlook 2020. *Bloomberg New Energy Finance* **2020**, (July).

(6) Li, Z. A Review of the Current Status of Global Electric Vehicle Charging Infrastructure Development. *International Journal of Global Economics and Management* **2024**, *3* (3), 123-134.

(7) Chu, B.; Guo, Y.-J.; Shi, J.-L.; Yin, Y.-X.; Huang, T.; Su, H.; Yu, A.; Guo, Y.-G.; Li, Y. Cobalt in high-energy-density layered cathode materials for lithium ion batteries. *Journal of Power Sources* **2022**, *544*, 231873.

(8) Li, M.; Lu, J. Cobalt in lithium-ion batteries. *Science* **2020**, *367* (6481), 979-980.

(9) Zheng, X.; Cai, Z.; Sun, J.; He, J.; Rao, W.; Wang, J.; Zhang, Y.; Gao, Q.; Han, B.; Xia, K. Nickel-rich layered oxide cathodes for lithium-ion batteries: Failure mechanisms and modification strategies. *Journal of Energy Storage* **2023**, *58*, 106405.

(10) Zeng, X.; Zhan, C.; Lu, J.; Amine, K. Stabilization of a high-capacity and high-power nickel-based cathode for Li-ion batteries. *Chem* **2018**, *4* (4), 690-704.

(11) Wei, H.-x.; Tang, L.-b.; Yan, C.; He, Z.-j.; Mao, J.; Dai, K.; Wu, X.-w.; Jiang, J.-b.; Zheng, J.-c. Lithium-rich manganese-based cathode materials with highly stable lattice and surface enabled by perovskite-type phase-compatible layer. *Nano Energy* **2021**, *88*, 106288.

(12) Li, P.; Luo, S.; Zhang, L.; Liu, Q.; Wang, Y.; Lin, Y.; Xu, C.; Guo, J.; Cheali, P.; Xia, X. Progress, challenges, and prospects of spent lithium-ion batteries recycling: a review. *Journal of Energy Chemistry* **2024**, *89*, 144-171.

(13) Lv, W.; Wang, Z.; Cao, H.; Sun, Y.; Zhang, Y.; Sun, Z. A critical review and analysis on the recycling of spent lithium-ion batteries. *ACS Sustainable Chemistry & Engineering* **2018**, *6* (2), 1504-1521.

(14) Lehtimäki, H.; Karhu, M.; Kotilainen, J. M.; Sairinen, R.; Jokilaakso, A.; Lassi, U.; Huttunen-Saarivirta, E. Sustainability of the use of critical raw materials in electric vehicle batteries: A transdisciplinary review. *Environmental Challenges* **2024**, *16*, 100966.

(15) Niri, A. J.; Poelzer, G. A.; Zhang, S. E.; Rosenkranz, J.; Pettersson, M.; Ghorbani, Y. Sustainability challenges throughout the electric vehicle battery value chain. *Renewable and Sustainable Energy Reviews* **2024**, *191*, 114176.

(16) Yang, Y.; Okonkwo, E. G.; Huang, G.; Xu, S.; Sun, W.; He, Y. On the sustainability of lithium ion battery industry–A review and perspective. *Energy Storage Materials* **2021**, *36*, 186-212.

(17) Hantanasirisakul, K.; Sawangphruk, M. Sustainable reuse and recycling of spent Li-ion batteries from electric vehicles: chemical, environmental, and economical perspectives. *Global Challenges* **2023**, *7* (4), 2200212.

(18) Roy, J. J.; Cao, B.; Madhavi, S. A review on the recycling of spent lithium-ion batteries (LIBs) by the bioleaching approach. *Chemosphere* **2021**, *282*, 130944.

(19) Ordoñez, J.; Gago, E. J.; Girard, A. Processes and technologies for the recycling and recovery of spent lithium-ion batteries. *Renewable and Sustainable Energy Reviews* **2016**, *60*, 195-205.

(20) Okonkwo, E. G.; Wheatley, G.; He, Y. The role of organic compounds in the recovery of valuable metals from primary and secondary sources: a mini-review. *Resources, Conservation and Recycling* **2021**, *174*, 105813.

(21) Garole, D. J.; Hossain, R.; Garole, V. J.; Sahajwalla, V.; Nerkar, J.; Dubal, D. P. Recycle, recover and repurpose strategy of Spent Li-ion Batteries and catalysts: current status and future opportunities. *ChemSusChem* **2020**, *13* (12), 3079-3100.

(22) Zante, G.; Boltoeva, M.; Masmoudi, A.; Barillon, R.; Trébouet, D. Supported ionic liquid and polymer inclusion membranes for metal separation. *Separation & Purification Reviews* **2022**, *51* (1), 100-116.

(23) Jha, R.; Rao, M. D.; Meshram, A.; Verma, H. R.; Singh, K. K. Potential of polymer inclusion membrane process for selective recovery of metal values from waste printed circuit boards: A review. *Journal of Cleaner Production* **2020**, *265*, 121621.

(24) Almeida, M. I. G.; Cattrall, R. W.; Kolev, S. D. Recent trends in extraction and transport of metal ions using polymer inclusion membranes (PIMs). *Journal of Membrane Science* **2012**, *415*, 9-23.

(25) Keskin, B.; Zeytuncu-Gökoğlu, B.; Koyuncu, I. Polymer inclusion membrane applications for transport of metal ions: A critical review. *Chemosphere* **2021**, *279*, 130604.

(26) Zulkefeli, N. S. W.; Weng, S. K.; Abdul Halim, N. S. Removal of heavy metals by polymer inclusion membranes. *Current Pollution Reports* **2018**, *4*, 84-92.

(27) Wu, N.; Almeida, M. I. G.; Simeonova, S.; Spassov, T. G.; Rangelov, A.; Cattrall, R. W.; Datcheva, M.; Kolev, S. D. Preparation and characterization of very thin polymer inclusion membranes (PIMs) and their application to the transport of thiocyanate. *Journal of Membrane Science* **2023**, *668*, 121249.

(28) Wang, D.; Cattrall, R. W.; Li, J.; Almeida, M. I. G.; Stevens, G. W.; Kolev, S. D. A poly (vinylidene fluoride-co-hexafluoropropylene)(PVDF-HFP)-based polymer inclusion membrane (PIM) containing LIX84I for the extraction and transport of Cu (II) from its ammonium sulfate/ammonia solutions. *Journal of Membrane Science* **2017**, *542*, 272-279.

(29) Eyupoglu, V.; Unal, A.; Polat, E.; Eren, B.; Kumbasar, R. A. An efficient cobalt separation using PVDF-co-HFP based ultrafiltration polymer inclusion membrane by room temperature ionic liquids. *Separation and Purification Technology* **2022**, *303*, 122201.

(30) Wang, B.; Liu, F.; Zhang, F.; Tan, M.; Jiang, H.; Liu, Y.; Zhang, Y. Efficient separation and recovery of cobalt (II) and lithium (I) from spent lithium ion batteries (LIBs) by polymer inclusion membrane electrodialysis (PIMED). *Chemical Engineering Journal* **2022**, *430*, 132924.

(31) Szczepański, P.; Guo, H.; Dzieszkowski, K.; Rafiński, Z.; Wolan, A.; Fatyeyeva, K.; Kujawa, J.; Kujawski, W. New reactive ionic liquids as carriers in polymer inclusion membranes for transport and separation of Cd (II), Cu (II), Pb (II), and Zn (II) ions from chloride aqueous solutions. *Journal of Membrane Science* **2021**, *638*, 119674.

(32) Wang, D.; Hu, J.; Li, Y.; Fu, M.; Liu, D.; Chen, Q. Evidence on the 2-nitrophenyl octyl ether (NPOE) facilitating Copper (II) transport through polymer inclusion membranes. *Journal of Membrane Science* **2016**, *501*, 228-235.

(33) Pospiech, B. Hydrometallurgical recovery of cobalt (II) from acidic chloride solutions by transport through polymer inclusion membranes. *Physicochemical Problems of Mineral Processing* **2013**, *49*.

(34) Specht, C.; Cattrall, R. W.; Spassov, T. G.; Spassova, M. I.; Kolev, S. D. Polymer inclusion membranes as substrates for controlled in-situ gold nanoparticle synthesis. *Reactive and Functional Polymers* **2018**, *130*, 81-89.

(35) Xu, L.; Zeng, X.; He, Q.; Deng, T.; Zhang, C.; Zhang, W. Stable ionic liquid-based polymer inclusion membranes for lithium and magnesium separation. *Separation and Purification Technology* **2022**, *288*, 120626.

(36) Baba, Y.; Kubota, F.; Goto, M.; Cattrall, R. W.; Kolev, S. D. Separation of cobalt (II) from manganese (II) using a polymer inclusion membrane with N-[N, N-di (2-ethylhexyl) aminocarbonylmethyl] glycine (D2EHAG) as the extractant/carrier. *Journal of Chemical Technology & Biotechnology* **2016**, *91* (5), 1320-1326.

(37) Pospiech, B. Separation of Co from Ni and Li from chloride media using polymer inclusion membrane system with thiosalicylate based ionic liquid. *Physicochemical Problems of Mineral Processing* **2022**, *58* (6).

(38) Adigun, B.; Thapaliya, B. P.; Luo, H.; Dai, S. Ionic liquid-based extraction of metal ions via polymer inclusion membranes: a critical review. *RSC Sustainability* **2024**.

(39) Yoshida, W.; Baba, Y.; Kubota, F.; Kolev, S. D.; Goto, M. Selective transport of scandium (III) across polymer inclusion membranes with improved stability which contain an amic acid carrier. *Journal of Membrane Science* **2019**, *572*, 291-299.

(40) Lee, M.-S.; Oh, Y.-J. Chemical equilibria in a mixed solution of nickel and cobalt chloride. *Materials transactions* **2005**, *46* (1), 59-63.

(41) Lee, M.-s.; Oh, Y.-j. Estimation of thermodynamic properties and ionic equilibria of cobalt chloride solution at 298 K. *Materials Transactions* **2004**, *45* (4), 1317-1321.

(42) Pan, P.; Susak, N. J. Co (II)-chloride and-bromide complexes in aqueous solutions up to 5 m NaX and 90 C: Spectrophotometric study and geological implications. *Geochimica et Cosmochimica Acta* **1989**, *53* (2), 327-341.

(43) Pośpiech, B.; Walkowiak, W. Separation of copper (II), cobalt (II) and nickel (II) from chloride solutions by polymer inclusion membranes. *Separation and Purification Technology* **2007**, *57* (3), 461-465.

(44) Shirzad, M.; Karimi, M.; Abolghasemi, H. Polymer inclusion membranes with dinonylnaphthalene sulfonic acid as ion carrier for Co (II) transport from model solutions. *Desalination and Water Treatment* **2019**, *144*, 185-200.

(45) Wang, J.; Wang, C.; Zhang, Q. Efficient extraction and recovery of Co (II) and Ni (II) from spent ChCl-EG deep eutectic solvent via solvent extraction: A mechanism and performance study. *Journal of Environmental Chemical Engineering* **2025**, *13* (3), 116671.

(46) Mubarok, M.; Hanif, L. Cobalt and nickel separation in nitric acid solution by solvent extraction using Cyanex 272 and Versatic 10. *Procedia Chemistry* **2016**, *19*, 743-750.

(47) Nour, A.; Iqbal, W.; Navarro-Alapont, J.; Ferrando-Soria, J.; Magarò, P.; Elliani, R.; Tagarelli, A.; Maletta, C.; Mastropietro, T. F.; Pardo, E. Efficient Nickel and Cobalt Recovery by

Metal–Organic Framework-Based Mixed Matrix Membranes (MMM-MOFs). *ACS Sustainable Chemistry & Engineering* **2024**, *12* (32), 12014-12028.

(48) Ayers, P. W. The physical basis of the hard/soft acid/base principle. *Faraday Discussions* **2007**, *135*, 161-190.

(49) Ho, T.-L. Hard soft acids bases (HSAB) principle and organic chemistry. *Chemical Reviews* **1975**, *75* (1), 1-20.

(50) Yang, Z.; Yuan, G.; Duan, X.; Liang, S.; Sun, G. HDEHP assisted solvothermal synthesis of monodispersed REPO 4 (RE= La–Lu, Y) nanocrystals and their photoluminescence properties. *New Journal of Chemistry* **2020**, *44* (11), 4386-4393.

(51) Shu, Q.; Khayambashi, A.; Wang, X.; Wei, Y. Studies on adsorption of rare earth elements from nitric acid solution with macroporous silica-based bis (2-ethylhexyl) phosphoric acid impregnated polymeric adsorbent. *Adsorption Science & Technology* **2018**, *36* (3-4), 1049-1065.

(52) Witschard, G.; Griffin, C. Infrared absorption characteristics of alkyl and aryl substituted phosphonium salts. *Spectrochimica Acta* **1963**, *19* (11), 1905-1910.

(53) Cholico-Gonzalez, D.; Avila-Rodriguez, M.; Cote, G.; Chagnes, A. Chemical properties of trihexyl (tetradecyl) phosphonium chloride and bis (2, 4, 4-trimethylpentyl) phosphinic acid mixtures: Interaction study by FT-IR and NMR spectroscopies. *Journal of Molecular Liquids* **2013**, *187*, 165-170.

(54) Khurana, S.; Negi, S.; Chandra, A. Effect of surface modification of dispersoid on hybrid polymer electrolyte. *Polymer Testing* **2021**, *96*, 107118.

(55) Parangusan, H.; Ponnamma, D.; Al-Maadeed, M. A. A. Stretchable electrospun PVDF-HFP/Co-ZnO nanofibers as piezoelectric nanogenerators. *Scientific reports* **2018**, *8* (1), 754.

(56) Thapaliya, B. P.; Popov, I.; Dai, S. Layer-by-Layer Assembly Strategy for Reinforcing the Mechanical Strength of an Ionogel Electrolyte without Affecting Ionic Conductivity. ACS Applied Energy Materials 2020, 3 (2), 1265-1270. DOI: 10.1021/acsaem.9b01932 (acccessed 2021-06-10T18:35:52).

(57) Joseph, N.; Ahmadiannamini, P.; Hoogenboom, R.; Vankelecom, I. F. J. Layer-by-layer preparation of polyelectrolyte multilayer membranes for separation. Polym. Chem. 2014, 5 (6), 1817-1831. DOI: 10.1039/c3py01262j (acccessed 2021-06-10T18:39:57).

(59) Zhang, X.; Chen, H.; Zhang, H. Layer-by-layer assembly: from conventional to unconventional methods. Chem. Commun. 2007, (14), 1395-1405. DOI: 10.1039/b615590a (acccessed 2021-07-15T18:48:08).

(60) Fu, Y.; Li, S.-J.; Xu, J.; Yang, M.; Zhang, J.-D.; Jiao, Y.-H.; Zhang, J.-C.; Zhang, K.; Jia, Y.-G. Facile and Efficient Approach to Speed up Layer-by-Layer Assembly: Dipping in Agitated Solutions. Langmuir 2011, 27 (2), 672-677. DOI: 10.1021/la104524k (acccessed 2021-07-16T15:55:21).

(61) Li, Y.; Wang, X.; Sun, J. Layer-by-layer assembly for rapid fabrication of thick polymeric films. Chemical Society Reviews 2012, 41 (18), 5998. DOI: 10.1039/c2cs35107b (acccessed 2021-07-16T16:01:11).

(62) Decher, G.; Hong, J.-D. Buildup of ultrathin multilayer films by a self-assembly process, 1 consecutive adsorption of anionic and cationic bipolar amphiphiles on charged surfaces. Makromolekulare Chemie. Macromolecular Symposia 1991, 46 (1), 321-327. DOI: 10.1002/masy.19910460145 (acccessed 2021-08-02T21:05:49).

(63) Kotov, N. A. Layer-by-layer self-assembly: The contribution of hydrophobic interactions. Nanostructured Materials 1999, 12 (5-8), 789-796. DOI: 10.1016/s0965-9773(99)00237-8 (acccessed 2021-08-02T21:06:43).

(64) Shimazaki, Y.; Mitsuishi, M.; Ito, S.; Yamamoto, M. Preparation of the Layer-by-Layer Deposited Ultrathin Film Based on the Charge-Transfer Interaction. Langmuir 1997, 13 (6), 1385-1387. DOI: 10.1021/la9609579 (acccessed 2021-08-02T21:13:37).

(65) Cini, N.; Tulun, T.; Decher, G.; Ball, V. Step-by-Step Assembly of Self-Patterning Polyelectrolyte Films Violating (Almost) All Rules of Layer-by-Layer Deposition. Journal of the American Chemical Society 2010, 132 (24), 8264-8265. DOI: 10.1021/ja102611q (acccessed 2021-08-02T21:14:22).

(58) Richardson, J. J.; Cui, J.; Bjornmalm, M.; Braunger, J. A.; Ejima, H.; Caruso, F. Innovation in Layer-by-Layer Assembly. Chem Rev 2016, 116 (23), 14828-14867. DOI: 10.1021/acs.chemrev.6b00627

CHAPTER SIX

IONIC LIQUID-ENHANCED RECYCLING OF LITHIUM-ION BATTERY BLACK MASS VIA HEAVY LIQUID CENTRIFUGAL SEPARATION

A version of this chapter was originally published by Babafemi Adigun, et al. as below:

Adigun, B.; Luo, H.; Wang, T.; Dai, S. Ionic liquid-enhanced recycling of lithium-ion battery black mass via heavy liquid centrifugal separation. *RSC advances* **2026**, *16* (1), 568-573.

6.1 Abstract

The increasing global dependence on lithium-ion batteries (LIBs) for energy storage has raised concerns about the sustainable supply of critical metals like cobalt, nickel, lithium. Traditional mining practices pose significant environmental challenges, emphasizing the need for effective metal separation and recycling technologies. This study explores the application of polymer inclusion membranes (PIMs) as a promising alternative for low-waste operation. Herein, we developed and optimized a sequential separation process based on PIMs containing specific extractants for the selective recovery of Li^{+}, Co^{2+}, Mn^{2+}, and Ni^{2+} from simulated solutions and leachates derived from spent LIBs. Notably, our PIM technology achieved high metal recovery efficiencies and maintained performance over three cycles, establishing PIMs as a viable solution for critical metal recovery and promoting a circular economic approach to battery recycling. Direct recycling of lithium-ion batteries (LIBs) is of great significance to supply chain security and environmental protection by restoring spent battery materials to their original purpose without destroying their chemical structure. One of the key processes for direct recycling is to separate valuable anode and cathode active materials from black mass. This study evaluates ionic liquid-enhanced Heavy Liquid Centrifugal Separation (HLCS) as an efficient method for separating LIB black mass into its constituent anode and cathode materials. The optimized HLCS process achieved a separation efficiency of over 95%, yielding a graphite-rich upper layer and an NMC-rich lower layer. Characterization by thermogravimetric analysis (TGA), X-ray diffraction (XRD),

and inductively coupled plasma-optical emission spectroscopy (ICP-OES) confirmed the purity and structural integrity of the recovered fractions. The addition of N-Methyl-2-pyrrolidone and ionic liquid 1-Ethyl-3-methylimidazolium bromide decoupled entangled particles, while subsequent treatment of the anode layer with 1-(2,3-dihydroxypropyl)-3-methylimidazolium chloride further enhanced separation purity. The recycled graphite exhibited comparable battery performance to pristine graphite. These results demonstrate HLCS as a promising LIB recycling strategy, advancing sustainable battery manufacturing.

6.2 Introduction

Lithium-ion batteries (LIBs) are at the forefront of the energy transition towards more sustainable power sources powering everything from portable electronics to electric vehicles (EVs). Their high energy density, long lifespan, and versatility make them a preferred choice for a wide range of applications.[1-5] The rapid expansion of the electric vehicle (EV) market, along with the widespread use of LIBs in portable electronics, has precipitated unprecedented growth in the LIB industry. However, the end-of-life management of these batteries presents significant environmental challenges and opportunities for resource recovery.[6, 7] Lithium battery recycling emerges as a critical solution to mitigate these environmental impacts, offering a pathway to recover valuable materials, such as lithium, cobalt, and nickel, thereby diminishing the demand for resource extraction and reducing the overall environmental burden.[8, 9] Beyond environmental considerations, the strategic importance of lithium battery recycling extends to enhancing material sustainability and economic resilience. Many of the raw materials integral to LIBs are sourced from geopolitically sensitive regions, subjecting supply chains to potential disruptions. By

establishing robust recycling capabilities, we can alleviate dependence on uncertain raw material supplies, fostering a more stable and sustainable battery supply chain.[10, 11]

Lithium battery recycling is currently dominated by three primary technologies: pyrometallurgy, hydrometallurgy, and direct recycling. Pyrometallurgical processes, involving high-temperature smelting, are favored for their operational robustness and ability to recover valuable metals such as cobalt, nickel, and copper. However, this method is energy intensive.[12-17] Hydrometallurgical processes offer a more environmentally benign alternative, using aqueous solutions to leach metals from battery waste. This method allows for the selective recovery of metals, including lithium, though it requires precise chemical management and can produce hazardous wastewater if not properly controlled.[18-20] Direct recycling stands out for its innovative approach and distinguishes itself from conventional recycling methods by aiming to preserve the structural and chemical integrity of cathode and anode materials for reuse in new batteries. The process involves several key steps: disassembly of spent batteries, separation and purification of electrode materials, and their direct reintroduction into new battery manufacturing. Unlike pyrometallurgical and hydrometallurgical processes, which primarily recover metal constituents through smelting and chemical leaching, direct recycling targets the preservation of valuable electrochemical properties of the active materials.[21, 22] Despite these advantages of direct recycling, the handling of black mass remains a bottleneck for scalable direct recycling systems. During shredding, graphite, carbon black, and cathode active material often form dense agglomerates due to strong PVDF binding, leading to poor particle separation, contamination, and reduced phase purity during separation steps. Many physical separation technologies such as froth flotation,[27, 28] magnetic separation[29-31] are highly sensitive to surface chemistry, particle size distribution, and residual binder content. This complexity drives the need for hybrid approaches that combine physical

Table 6.1. Quick comparison table of ILs for separation and purification.

Ionic Liquid	Method	Application	Ref.
1-decyl 3-methylimidazolium bis (trifluoromethylsulfonyl) imide	Solvent Extraction	Diluent	23
1-butyl-3-methylimidazolium tetrafluoroborate ([BMIm][BF_4])	Binder Dissolution	PVDF Binder Removal	24
1-(2,3-Dihydroxypropyl)-3-methylimidazolium chloride ([DHPMim][Cl])	Metal Dissolution	Selective metal-oxide dissolution	25
tri(hexyl)tetradecyl phosphonium chloride [P_{66614}][Cl]	Supported IL Membrane	Extractant	26

separation with targeted chemical assistance to enhance selectivity and yield.

In the process of direct recycling, a physical separation approach is employed to disassemble the battery into its constituent parts. This process generally starts with the mechanical destruction of batteries through methods like shredding or crushing. This step is followed by a classification procedure that segregates components based on their size. The larger fragments, which include plastics and current collectors, are isolated from the finer materials known as the black mass. The black mass is particularly significant as it comprises the active material from both the anode and cathode, including graphite, polyvinylidene fluoride (PVDF), carbon black, and lithium transition

metal oxides, in addition to traces of aluminum and copper from the current collectors.[32-34] Various methodologies aimed at improving the efficiency and sustainability of recycling processes. One such method, gravity separation, has emerged as a potentially viable technique for the separation of black mass components in LIBs. Heavy liquid centrifugal separation (HLCS) is a method that leverages the differences in density between the various components of the black mass to achieve separation. Black mass, the residue obtained after the mechanical processing of spent LIBs, contains a mixture of cathode and anode materials, including valuable metals such as lithium, cobalt, nickel, and manganese, as well as graphite. The principle of HLCS involves the use of fluid dynamics and the differential settling rates of particles to segregate materials based on their density.[35, 36] Heavy liquid (HL) separation techniques have been utilized to separate anode and cathode materials. Specifically, cathode active materials such as lithium cobalt oxide (LCO) and lithium nickel manganese cobalt oxide (NMC) have densities ranging from 4.5 to 5.0 g/cm^3, significantly higher than the density of graphite, which is 2.26 g/cm^3. By employing heavy liquids with densities between 2.26 - 4.50 g/cm^3, it is possible to achieve effective separation of these two types of materials when mixed.[25, 37, 38] Al-Shammari et al. utilized sodium polytungstate (SPT) as a heavy liquid for the recovery of graphite from mixed spent LIB powders. The recovered graphite delivered a specific capacity that is nearly identical to that of commercial graphite, demonstrating its excellent electrochemical performance and retention of functional integrity.[39] Their practical efficiency was constrained by particle entanglement, incomplete binder removal, and sluggish settling dynamics. These limitations underscore the need for intelligent modification of the liquid medium to promote dispersion and minimize interparticle adhesion.[40]

Ionic liquids (ILs) have rapidly emerged as versatile functional materials in battery recycling due to their ability to disrupt PVDF adhesion, leaching of metal ions and act as selective extractants

for recovering metal ions from spent batteries. Recent studies have demonstrated that ILs can dissolve PVDF binder, enabling easier detachment of cathode particles. Zeng et al. demonstrated that the ionic liquid 1-butyl-3-methylimidazolium tetrafluoroborate ([BMIm][BF_4]), when heated to 180 °C under continuous stirring (300 rpm), effectively cleaved the PVDF binder.[24, 41] ILs have also been used as extractants for cobalt and lithium from spent batteries.[26, 42-44] Wang et al. employed an ionic liquid system composed of 1-butyl-3-methylimidazolium bis(trifluoromethylsulfonyl)imide ([BMIm][NTf_2]), 2-thenoyltrifluoroacetone (HTTA), and trioctylphosphine oxide (TOPO) to efficiently extract and recover valuable transition metals from spent lithium-ion batteries.[45] Their multipurpose functionality, tunable physicochemical properties, and chemical stability under battery-recycling conditions position ILs as effective enhancers that can improve physical separation processes without degrading the active materials.

In this study, we investigate the direct recycling of lithium-ion black mass using ionic liquid enhanced heavy liquid centrifugal separation to selectively recover anode and cathode active materials from black mass. Bromoform, a high-density organic liquid with an intermediate density between the cathode and anode materials, was employed as the dense medium to facilitate the separation. However, the separation performance of pure bromoform is limited by the complex composition and entangled particles in black mass. By choosing ionic liquids and NMP as additives, the formulated heavy liquids exhibited excellent performance for black mass separation, generating NMC and graphite products with high purities of over 95%. The recycled graphite was treated with IL to remove residual cathode materials from the graphite, enabling electrochemical performance comparable to pristine anode material. These emerging synergies between HLCS and ionic-liquid chemistry provide a promising route to enhance the selectivity and recovery of high-value components during direct recycling.

6.3 Materials and Methods

6.3.1 Materials

The spent black mass used in this study was procured from commercial vendors supplying mechanically shredded and sieved lithium-ion battery waste composed of graphite as the anode material and lithium nickel-cobalt-manganese oxide (NMC) as the cathode material consistent with the composition confirmed by ICP-OES (Table S1). N-Methyl-2-pyrrolidone (NMP, ≥ 99%, Sigma-Aldrich), bromoform (96% Aldrich Chemical Company), 1-Ethyl-3-methylimidazolium bromide (C_2mimBr, 98%, Thermo Scientific), 1-(2,3-dihydroxypropyl)-3-methylimidazolium chloride prepared as synthesized in literature.[25]

6.3.2 Methods

Separation of the anode and cathode Layer

The black mass was first ground using a mortar and pestle until no visible lumps remained. The resulting material was then sieved through a 150 μm mesh to obtain a fine, uniform powder suitable for separation. A heavy liquid mixture was prepared using bromoform (BF) and/or a combination of bromoform, IL, and NMP. The black mass and liquid mixture were combined at a mass-to-volume ratio of 1:4 (corresponding to 2 g black mass, 360 μL NMP, 1 mL ionic liquid, and 7 mL bromoform). The mixture was sonicated for 20 minutes to ensure uniform particle dispersion, followed by stirring for 5 hours to enhance the interaction between the heavy liquid and the electrode particles. After treatment, the mixture was centrifuged at 5000 rpm for 3 minutes, resulting in clear separation of two solid layers due to the density difference between the cathode and anode materials. The bottom layer (cathode-rich fraction) and the upper layer (graphite-rich fraction) were carefully collected using a separatory funnel. Both layers were rinsed with acetone and deionized water to remove any residual bromoform and ionic liquid, then dried under vacuum

overnight at 70 °C. The dried products were subsequently used for thermogravimetric analysis (TGA), X-ray diffraction (XRD), and electrochemical testing.

6.3.3 Characterization

The half-cell tests were performed using lithium foil disks as counter and reference electrodes. The anode slurry, containing pristine or recycled graphite, carbon black, and PVDF, in a mass ratio of 92:2:6 with NMP, was coated onto copper foil. Coin cells were assembled in an argon-filled glovebox using Celgard 2320 membrane as the separator. The electrolyte is 1.2 M $LiPF_6$ in 30:70 wt.% ethylene carbonate/ethyl methyl carbonate.

The composition of the separated layers was determined using thermogravimetric analysis (TGA), where the recovered anode and cathode layers from the separation were heated above the thermal decomposition temperature of the anode material at a scanning rate of 10 °C min^{-1} in the temperature range of 25−900 °C under an air atmosphere. The residual mass percentage of the sample at 900 °C corresponds to the mass fraction of the cathode, whereas the weight loss percentage represents the fraction of graphite present in each layer. The chemical composition and purity of the recovered electrode materials were analyzed using inductively coupled plasma-optical emission spectroscopy (ICP-OES) and X-ray diffraction (XRD).

6.4 Results and Discussion

6.4.1 Separation of cathode/anode mixture

To evaluate the separation of cathode and anode materials, a heavy liquid with a density higher than that of the anode material but lower than that of the cathode material was utilized. The cathode and anode active materials have densities of approximately 4.7 g/cm³ and 2.3 g/cm³, respectively. For effective separation, bromoform/ionic liquid/NMP solution, with a density of 2.7 g/cm³, was

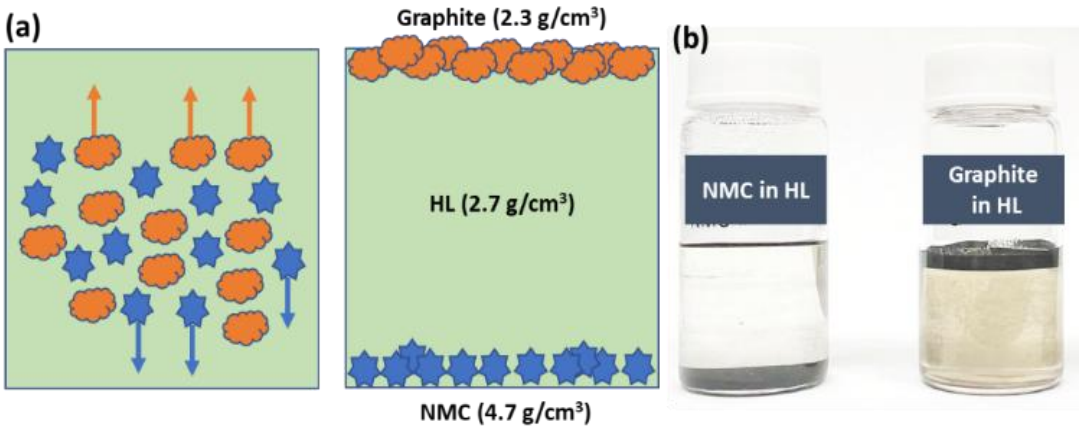

Figure 6.2 (a) Illustration of NMC/Graphite separation in HL. (b) Photos of NMC and Graphite in HL.

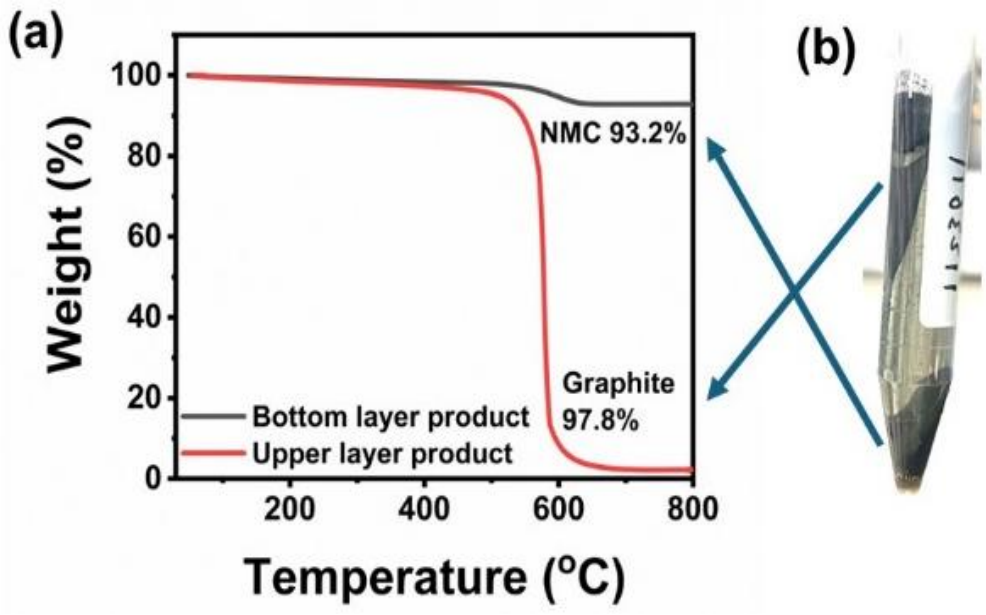

Figure 6.1. (a) TGA curves of the separated bottom and upper layers. (b) Photo of graphite/NMC mixtures after centrifugal separation.

chosen as the heavy liquid, falling within the density range between the cathode and anode active materials. A mixture of pristine graphite anode and NMC cathode materials was prepared for this study. Equal masses (1g each) of NMC cathode and graphite anode were combined with bromoform as a heavy liquid. The mixture was sonicated for 20 minutes and subsequently stirred for 5 hours to ensure thorough dispersion. It was then subjected to centrifugation at 5000 rpm for 3 minutes. Due to differences in specific densities, the graphite floated to the surface while the NMC cathode settled at the bottom. This separation process enables the complete recovery of the anode active material from the cathode using a separatory funnel. **Figure 6.1(a)** illustrates the separation of a cathode/anode mixture using a heavy liquid. **Figure 6.1(b)** shows the distribution of the cathode and anode within the heavy liquid, highlighting their displacement as a function of density differences. The separation performance was evaluated through TGA and XRD of the separated electrode materials, namely graphite (anode layer) and NMC cathode (cathode layer).

Figure 6.2a presents the TGA analysis of the cathode/anode mixture following its separation into distinct layers. The bottom layer, primarily composed of cathode material, exhibits a 6.8% weight loss upon heating beyond the thermal decomposition temperature of the anode material, indicating that cathode active material constitutes approximately 93.2% of this layer. The upper layer, predominantly consisting of anode material, undergoes a 97.8% weight loss, corresponding to the proportion of anode active material. A control experiment using pure bromoform for the separation of NMC/graphite exhibited much lower purity for graphite (85%) and NMC (79%) products (**Figure S.6.(a)**), which highlights the advantages of ionic liquid and NMP additives in improving the separation performance of heavy liquids.

To further analyze the composition of the cathode/anode mixture before and after separation, X-ray diffraction (XRD) was performed on both the mixed and separated layers. **Figure S.6.(b, c)**

presents the XRD patterns of pristine graphite and the NMC cathode, with characteristic diffraction peaks observed at 26.4° and 18.8°, respectively, confirming the presence of these phases. Following the separation of the cathode/anode mixture in bromoform, **Figures S.6.(d, e)** display the XRD patterns of the upper layer (anode layer) and the bottom layer (NMC cathode layer). The XRD pattern of the separated anode layer (**Figure S.6.(d)**) predominantly exhibits the graphite peak, along with a minor peak indicating residual NMC cathode. Similarly, the XRD pattern of the separated cathode layer (**Figure S.6.(e)**) reveals major peaks of the NMC cathode and graphite, aligning with the TGA data presented in **Figure S.6.(a)**. These results suggest that the separation process does not achieve complete phase purity, as some cathode material remains in the anode layer and vice versa. To enhance the efficiency of the separation, N-methyl-2-pyrrolidone (NMP) and the ionic liquid 1-ethyl-3-methylimidazolium bromide (C_2mimBr) were introduced in conjunction with the heavy liquid. These additives can help dissolve active materials typically bound by polymeric binders such as polyvinylidene fluoride (PVDF) and facilitate the dispersion of solid particles in the liquid phase, preventing agglomeration. **Figure S.7.** presents the XRD patterns of the separated anode and cathode layers after incorporating additives (NMP, C_2mimBr, and a combination of both) into the heavy liquid. The objective was to evaluate the impact of these additives on improving phase separation. The XRD patterns of the anode layer (**Figures S.7. (a–c)**) suggest that the addition of NMP, C_2mimBr, or their combination had minimal impact on improving the separation of anode material, as no significant enhancement was observed compared to using the heavy liquid alone. Peaks corresponding to residual cathode material remain present, suggesting that the additives had a limited effect on further purifying the anode layer. The cathode layer exhibited a marked improvement in separation efficiency upon the addition of the additives. Compared to using the heavy liquid alone, the incorporation of NMP and C_2mimBr led to a

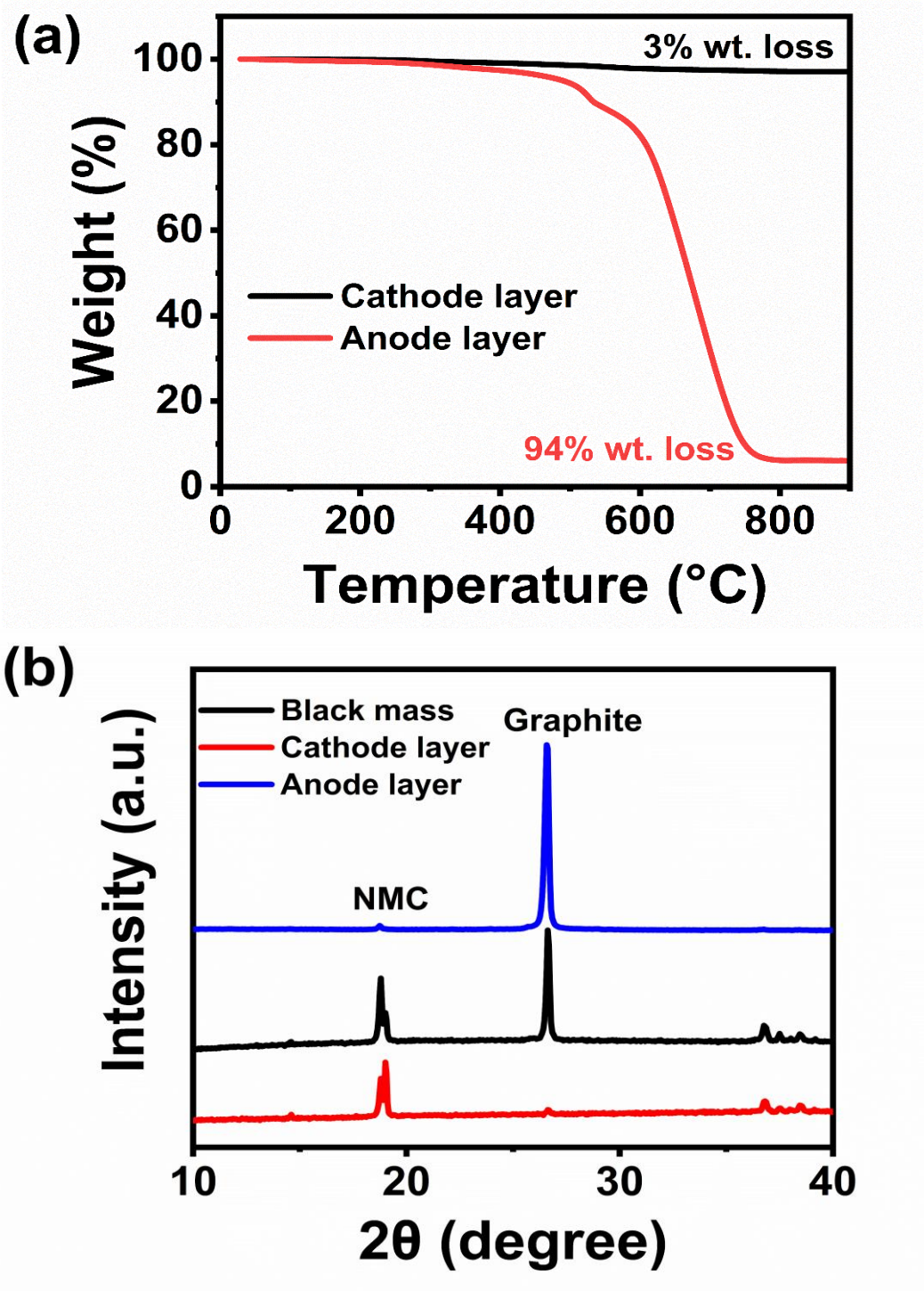

Figure 6.3 (a) TGA curves of bottom and upper layer products from black mass. (b) XRD patterns of black mass and bottom/upper layer products.

substantial reduction in the intensity of peaks corresponding to anode material in the cathode layer (**Figure S.7.(d-e)**). Among the tested conditions, the combined use of NMP and C_2mimBr resulted in the most effective separation (**Figure S.7.(f)**), indicating their synergistic role in enhancing the removal of residual anode material from the cathode fraction.

6.4.2 Separation of Black Mass

The composition of the NMC cathode and metal content in the black mass was determined using inductively coupled plasma–optical emission spectroscopy (ICP-OES), is presented in **Table S.2**. Based on these results, the NMC cathode in the black mass was calculated to have a composition of $LiNi_{0.39}Mn_{0.27}Co_{0.38}O_2$. To evaluate the effectiveness of the separation process under real-world conditions, black mass from spent batteries was subjected to cathode/anode separation using a combination of NMP and C_2mimBr as additives in the heavy liquid. 10 g of black mass was separated into cathode and anode active materials. The TGA of the separated layers is shown in **Figure 6.3(a).** The cathode layer exhibited only a 3% weight loss upon heating beyond the thermal decomposition temperature of the anode material, indicating that it consisted of approximately 97% cathode active material. Conversely, the anode layer demonstrated a 94% weight loss, confirming a 94% composition of anode-active material. Further characterization using X-ray diffraction (XRD) provided additional insights into the separation efficiency. **Figure 6.3(b)** presents the XRD pattern of the black mass before separation, displaying characteristic peaks for both graphite and the NMC cathode at nearly equal intensities. After separation, the XRD pattern of the anode layer predominantly exhibited the graphite peak, with only a minor peak corresponding to the NMC cathode, indicating minimal cathode contamination. Similarly, the XRD pattern of the cathode layer revealed strong peaks for the NMC cathode, with either a negligible or nearly undetectable graphite peak, signifying the effective removal of anode material

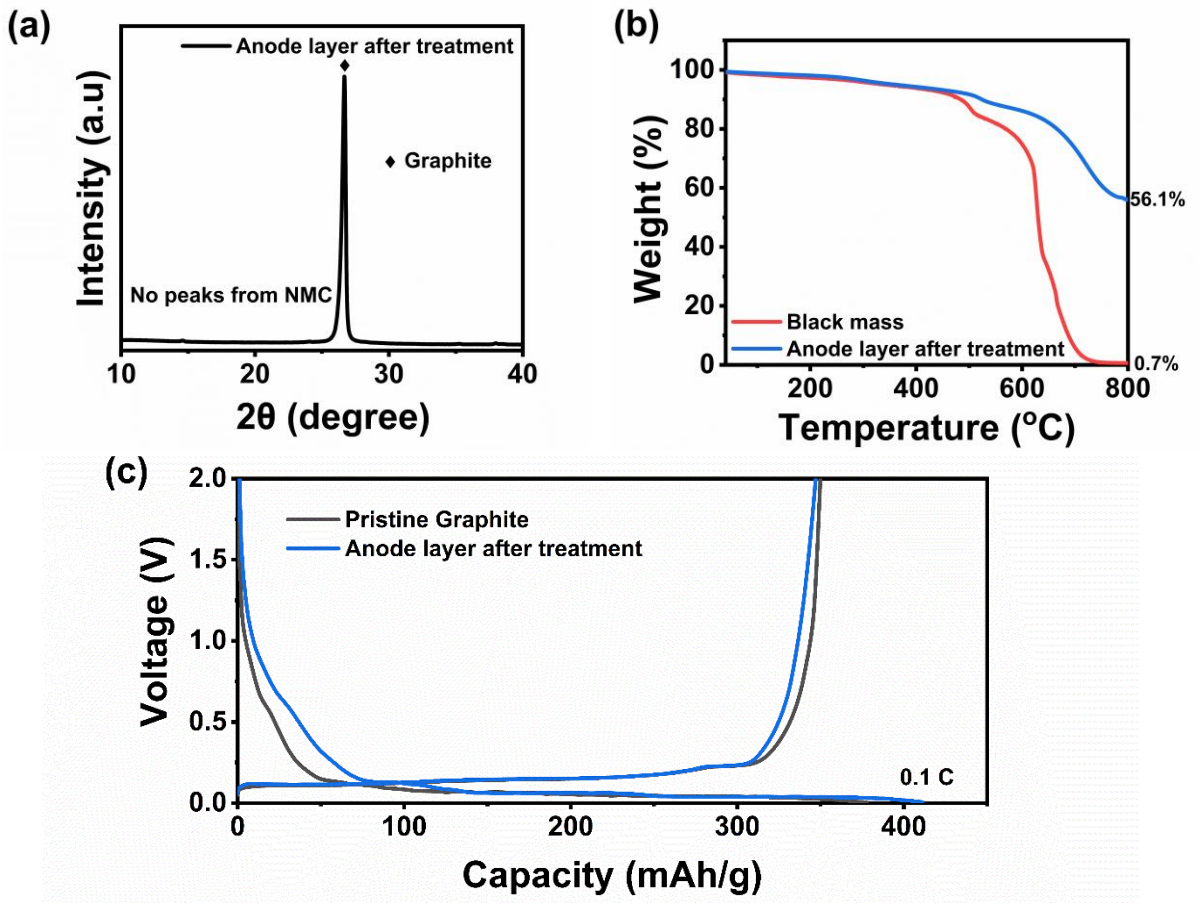

Figure 6.4 (a) XRD patterns of anode layer from black mass after treatment with ionic liquids. (b) TGA curves of black mass and anode layer products from black mass after treatment with ionic liquids. (c) The first charge/discharge curves of graphite|Li

from the cathode fraction. The separation process achieved an 85% recovery of the total electrode active materials. Of this, 28% corresponded to anode material (predominantly graphite), while 57% consisted of cathode active material (NMC), as detailed in **Table S.3.** The total recovery rate (85%) was determined using the actual mass of black mass (10 g) introduced into the HLCS process. The sum of the recovered anode and cathode fractions correspond to 8.5 g, equivalent to 85% of the total mass input. These results demonstrate that the formulated

Bromoform/NMP/C_2mimBr heavy liquid significantly enhances cathode/anode separation, leading to a high-purity recovery of both active materials.

To further improve the purity of the anode layer and eliminate residual cathode material, the separated anode fraction underwent additional treatment with 1-(2,3-dihydroxypropyl)-3-methylimidazolium chloride, an ionic liquid (IL) known for its effectiveness in dissolving metal oxides.[25] The IL was introduced to the anode layer at a mass ratio of 5:1 (IL to anode material), and the mixture was subjected to continuous stirring at 120°C for 12 hours. Following the treatment, the solid fraction was thoroughly washed with ethanol and deionized water to remove any residual IL and impurities. The effectiveness of this purification step was evaluated using X-ray diffraction (XRD). As shown in **Figure 6.4(a)**, the XRD pattern of the anode layer after IL treatment revealed the complete disappearance of cathode-related peaks, confirming the successful removal of residual cathode material. The TGA analysis of the anode exhibits more than 99% weight loss corresponding to the percentage of graphite in the anode layer further confirming the removal of the cathode materials from the anode layer (**Figure 6.4(b)**). The recovered graphite after the purification step with IL was used as anode active materials for graphite|Li half-cell battery tests. The recovered graphite exhibited almost identical charge/discharge curves to pristine graphite (**Figure6.4(c)**). The ionic liquid purification step effectively eliminates cross-contamination between graphite and NMC layers, reducing cathode residues in the anode fraction to <1 wt%. The recycled graphite shows identical charge/discharge behavior to pristine graphite, indicating no internal short-circuit risk.

6.5 Conclusions

This study highlights the potential of ionic liquid-enhanced Density Liquid Centrifugal Separation (HLCS) using bromoform for direct recycling of lithium-ion battery (LIB) black mass. The method effectively exploits density differences to achieve selective separation of graphite from NMC cathode materials achieving high-purity fractions. The use of ionic liquid C_2mimBr and NMP as additives improve cathode separation but has minimal effect on anode purification, implying that factors like particle wettability and surface interactions influence the process efficiency. Further treatment with ionic liquid 1-(2,3-dihydroxypropyl)-3-methylimidazolium chloride effectively removes residual cathode material from the separated anode layer. These results highlight the potential of HLCS as a cost-effective and energy-efficient method for directly recycling black mass, contributing to the advancement of a more sustainable LIB manufacturing

References

1. N. Nitta, F. Wu, J. T. Lee and G. Yushin, *Materials today*, 2015, **18**, 252-264.

2. T.-O. Folayan, A. L. Lipson, J. L. Durham, H. Pinegar, D. Liu and L. Pan, *Energy Technology*, 2021, **9**, 2100468.

3. A. Manthiram, *Nature communications*, 2020, **11**, 1550.

4. X.-n. Zhu, C.-c. Nie, S.-s. Wang, Y. Xie, H. Zhang, X.-j. Lyu, J. Qiu and L. Li, *Journal of Cleaner Production*, 2020, **248**, 119235.

5. W. Li, E. M. Erickson and A. Manthiram, *Nature Energy*, 2020, **5**, 26-34.

6. F. Duarte Castro, M. Vaccari and L. Cutaia, *Critical Reviews in Environmental Science and Technology*, 2022, **52**, 2060-2103.

7. E. Mossali, N. Picone, L. Gentilini, O. Rodrìguez, J. M. Pérez and M. Colledani, *Journal of environmental management*, 2020, **264**, 110500.

8. W. Zhang, C. Xu, W. He, G. Li and J. Huang, *Waste Management & Research*, 2018, **36**, 99-112.

9. M. Chen, X. Ma, B. Chen, R. Arsenault, P. Karlson, N. Simon and Y. Wang, *Joule*, 2019, **3**, 2622-2646.

10. W. Liu, X. Li, C. Liu, M. Wang and L. Liu, *Resources Policy*, 2023, **80**, 103183.

11. A. Hira, *International Journal*, 2025, **80**, 217-245.

12. X. Zhang, L. Li, E. Fan, Q. Xue, Y. Bian, F. Wu and R. Chen, *Chemical Society Reviews*, 2018, **47**, 7239-7302.

13. B. Huang, Z. Pan, X. Su and L. An, *Journal of power sources*, 2018, **399**, 274-286.

14. W. Lv, Z. Wang, H. Cao, Y. Sun, Y. Zhang and Z. Sun, *ACS Sustainable Chemistry & Engineering*, 2018, **6**, 1504-1521.

15. G. Harper, R. Sommerville, E. Kendrick, L. Driscoll, P. Slater, R. Stolkin, A. Walton, P. Christensen, O. Heidrich and S. Lambert, *nature*, 2019, **575**, 75-86.

16. B. Makuza, Q. Tian, X. Guo, K. Chattopadhyay and D. Yu, *Journal of Power Sources*, 2021, **491**, 229622.

17. M. Zhou, B. Li, J. Li and Z. Xu, *ACS ES&T Engineering*, 2021, **1**, 1369-1382.

18. E. Asadi Dalini, G. Karimi, S. Zandevakili and M. Goodarzi, *Mineral Processing and Extractive Metallurgy Review*, 2021, **42**, 451-472.

19. A. Chagnes and B. Pospiech, *Journal of Chemical Technology & Biotechnology*, 2013, **88**, 1191-1199.

20. Y. Yao, M. Zhu, Z. Zhao, B. Tong, Y. Fan and Z. Hua, *ACS Sustainable Chemistry & Engineering*, 2018, **6**, 13611-13627.

21. H. Ji, J. Wang, J. Ma, H.-M. Cheng and G. Zhou, *Chemical Society Reviews*, 2023, **52**, 8194-8244.

22. S. Sloop, L. Crandon, M. Allen, K. Koetje, L. Reed, L. Gaines, W. Sirisaksoontorn and M. Lerner, *Sustainable Materials and Technologies*, 2020, **25**, e00152.

23. G. Zante, A. Masmoudi, R. Barillon, D. Trébouet and M. Boltoeva, *Journal of Industrial and Engineering Chemistry*, 2020, **82**, 269-277.

24. X. Zeng and J. Li, *Journal of Hazardous Materials*, 2014, **271**, 50-56.

25. Y. Hu, M. Yang, Q. Dong, X. Zou, J. Yu, S. Guo and F. Yan, *Energy & Environmental Science*, 2024, **17**, 4238-4247.

26. G. Zante, M. Boltoeva, A. Masmoudi, R. Barillon and D. Trébouet, *Separation and Purification Technology*, 2020, **252**, 117477.

27. A. Vanderbruggen, N. Hayagan, K. Bachmann, A. Ferreira, D. Werner, D. Horn, U. Peuker, R. Serna-Guerrero and M. Rudolph, *Acs Es&t Engineering*, 2022, **2**, 2130-2141.

28. L. Verdugo, L. Zhang, B. Etschmann, W. Bruckard, J. Menacho and A. Hoadley, *Separation and Purification Technology*, 2023, **311**, 123241.

29. F. Mennik, N. İ. Dinç and F. Burat, *Results in Engineering*, 2023, **17**, 100868.

30. Z. Hu, J. Liu, T. Gan, D. Lu, Y. Wang and X. Zheng, *Separation and Purification Technology*, 2022, **297**, 121486.

31. W. Ding, S. Bao, Y. Zhang, C. Xin, B. Chen, J. Li, B. Liu, Y. Xia, X. Hou and K. Xu, *Journal of Cleaner Production*, 2024, **438**, 140798.

32. P. Xu, D. H. Tan, B. Jiao, H. Gao, X. Yu and Z. Chen, *Advanced Functional Materials*, 2023, **33**, 2213168.

33. Y. Lu, K. Peng and L. Zhang, *Acs Es&T Engineering*, 2022, **2**, 586-605.

34. H. Wang, S. Burke, R. Yuan and J. F. Whitacre, *Journal of Energy Storage*, 2023, **60**, 106616.

35. Y. Zhang, Y. He, T. Zhang, X. Zhu, Y. Feng, G. Zhang and X. Bai, *Journal of Cleaner Production*, 2018, **202**, 736-747.

36. H. Al-Shammari and S. Farhad, *Resources, Conservation and Recycling*, 2021, **174**, 105749.

37. R. Zhan and L. Pan, 2018.

38. K. D. Kepler, F. Tsang, R. Vermeulen and P. HAILEY, *Journal*, 2017.

39. H. Al-Shammari, S. Alharbi and M. B. A. Bashir, *International Journal of Energy Research*, 2025, **2025**, 8690843.

40. J. J. Roy, D. M. Phuong, V. Verma, R. Chaudhary, M. Carboni, D. Meyer, B. Cao and M. Srinivasan, *Carbon Energy*, 2024, **6**, e492.

41. A. Li, Z. Sun, C. Lv and Z. Fu, *Separation and Purification Technology*, 2025, 135193.

42. P. Meshram and N. Agarwal, *RSC advances*, 2025, **15**, 8321-8334.

43. R. Morina, D. Merli, P. Mustarelli and C. Ferrara, *ChemElectroChem*, 2023, **10**, e202201059.

44. L. Xu, C. Chen and M.-L. Fu, *Hydrometallurgy*, 2020, **197**, 105439.

45. K. Wang, G. Zhang, M. Luo and J. Li, *Chemical Engineering Journal*, 2023, **472**, 145006.

CHAPTER SEVEN

CONCLUSIONS AND RECOMMENDATIONS

7.1 Conclusion

This dissertation presents a comprehensive investigation into the development and optimization of polymer inclusion membranes for the selective separation and recovery of critical battery metal ions, including lithium, cobalt, nickel, and manganese. The growing demand for lithium-ion batteries has intensified the need for sustainable and efficient metal recovery technologies. In this context, polymer inclusion membranes were explored as a low-waste, tunable, and energy-efficient alternative to conventional hydrometallurgical separation processes. The results of this work demonstrate that carefully designed PIM systems can achieve selective and efficient separation of target metal ions from complex aqueous mixtures. Through systematic variation of membrane composition, including polymer matrix, carrier type, and ionic liquid plasticizers, it was shown that membrane performance is strongly governed by the chemical affinity between the carrier and the target metal ion, as well as the physicochemical properties of the membrane phase.

In particular, the use of extractants such as Cyanex 301, HDEHP, and $P_{66614}Cl$ ionic liquids enabled selective transport and separation of transition metals from lithium-containing systems. The developed membranes achieved high recovery efficiencies for cobalt, nickel, manganese, and lithium, with values exceeding 80% under optimized conditions. Furthermore, the sequential separation strategy demonstrated in this work highlights the capability of PIMs to process multicomponent systems, including realistic NMC 622 leachates, thereby bridging the gap between simplified laboratory systems and practical battery recycling applications.

Mechanistic investigations confirmed that ion transport across PIMs is governed by carrier-mediated processes involving reversible complexation, diffusion of the metal–carrier complex, and subsequent decomplexation at the receiving interface. The transport behavior was further influenced by factors such as chloride ion concentration, membrane thickness, and carrier loading, which collectively determine flux, permeability, and selectivity. These findings provide important insights into the design principles required for optimizing membrane performance. In addition to separation efficiency, this work also addressed the critical issue of membrane stability, which remains one of the primary challenges limiting the long-term application of PIMs. Although PIMs exhibit improved stability compared to conventional liquid membranes, their performance can degrade over time due to the gradual loss of membrane components. In particular, the leaching of carriers and plasticizers into the aqueous phase represents a significant limitation, as it reduces membrane efficiency, alters transport behavior, and limits reusability. This phenomenon is driven by interactions between membrane components and the feed or receiving solutions, especially under acidic or chemically aggressive conditions. Experimental observations in this work indicate that while the developed PIM systems maintained performance over several cycles, long-term stability under extended operation and industrial conditions requires further improvement. The retention of carrier molecules within the polymer matrix is therefore a key design consideration for advancing PIM technology toward practical applications.

Overall, this dissertation establishes polymer inclusion membranes as a viable and sustainable platform for the recovery of critical battery metals. By demonstrating high selectivity, operational simplicity, and compatibility with complex feed streams, this work contributes to the development of membrane-based separation technologies that support circular economy strategies for lithium-ion battery materials.

7.2 Recommendations and Future Work

Despite the promising performance of polymer inclusion membranes demonstrated in this study, several challenges remain that must be addressed to enable their widespread application in industrial-scale metal recovery processes.

7.2.1 Mitigation of Membrane Component Leaching

One of the most critical challenges identified in this work is the leaching of carriers and plasticizers from the membrane phase into the surrounding aqueous environment. This process leads to a gradual decline in membrane performance, reduced selectivity, and loss of active transport functionality over time. As reported in previous studies, leaching is influenced by the chemical compatibility between membrane components and the contacting solutions, as well as the structural integrity of the polymer matrix.

Future work should focus on strategies to enhance carrier and plasticizer retention within the membrane, improving chemical stability and minimizing leaching will be essential for achieving long-term membrane performance and enabling continuous operation.

7.2.2 Toward Scalable and Integrated Membrane Systems

For practical implementation, future studies should also explore scaling PIM fabrication to larger membrane areas, integrating PIMs into continuous flow or module-based systems coupling PIM technology with complementary processes such as electrodialysis or solvent extraction.

7.3 Final Perspective

This work demonstrates that polymer inclusion membranes offer a compelling pathway toward sustainable critical metal recovery. However, the long-term success of this technology will depend on overcoming stability limitations, particularly those associated with component leaching and

structural degradation. The exploration of Layer-by-Layer reinforcement in this study provides valuable insight into the design of more durable membrane systems, even though trade-offs in transport performance were observed. These findings emphasize the importance of integrated design strategies that simultaneously optimize stability, selectivity, and transport efficiency. Continued advancements in membrane chemistry, materials engineering, and process integration will be essential for translating polymer inclusion membranes from laboratory-scale systems to industrial applications, thereby contributing to the development of sustainable and circular energy technologies.

APPENDIX

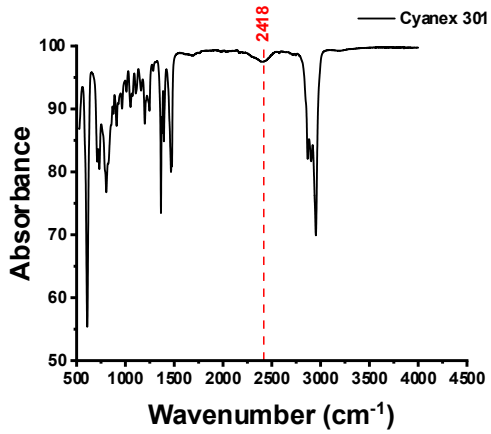

Figure S.1 FTIR Spectra of Cyanex 301 showing the peak corresponding to S—H stretching bonds.

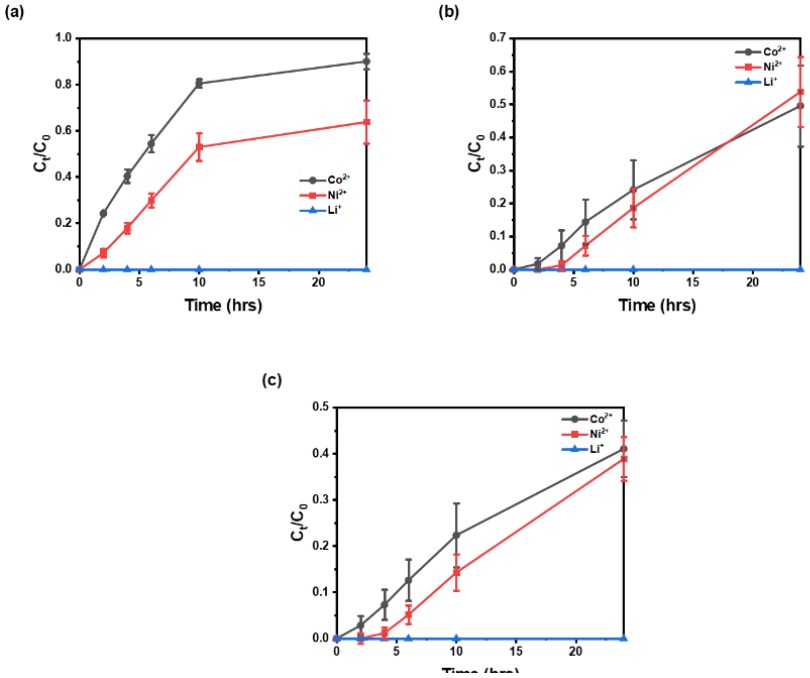

Figure S.2 Transport of Co^{2+}, Ni^{2+} and Li^{+} after 24 hours across IEPIM for three cycles:

(a) 1st cycle, (b) 2nd cycle, (c) 3rd cycle

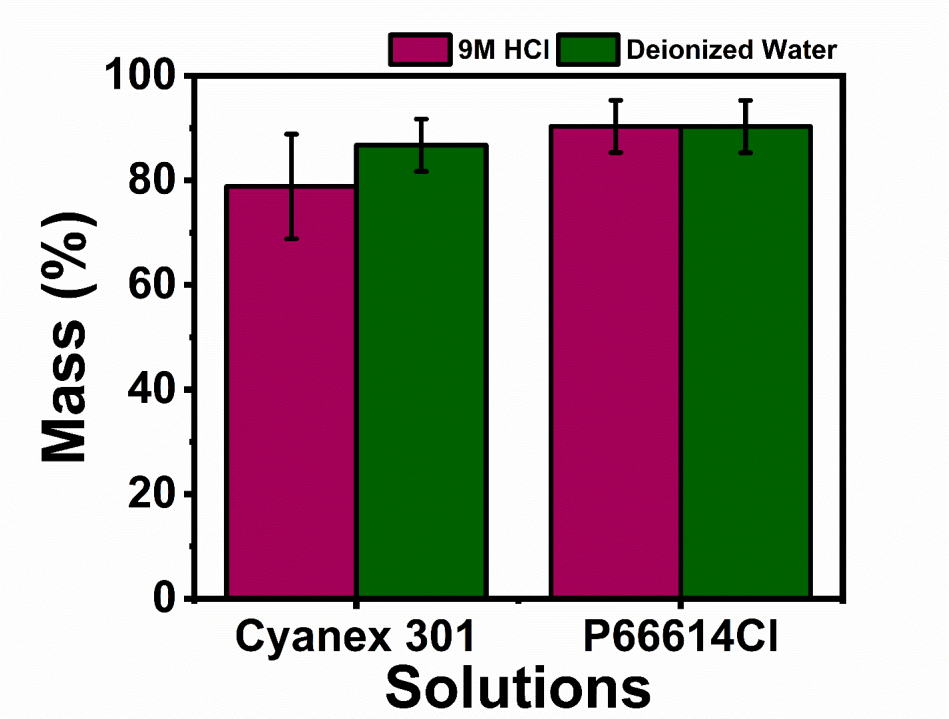

Figure S.3 Mass changes of the PIMs after immersion in 9 M HCl and deionized water for 4 days with constant shaking.

Table S.1 Phosphorous concentrations in the immersed solution.

Solution	**P concentration (ppm)**	
	PIM $P_{66614}Cl$	**PIM Cyanex 301**
9 M HCl	2.45	6.46
Deionized water	2.98	7.91

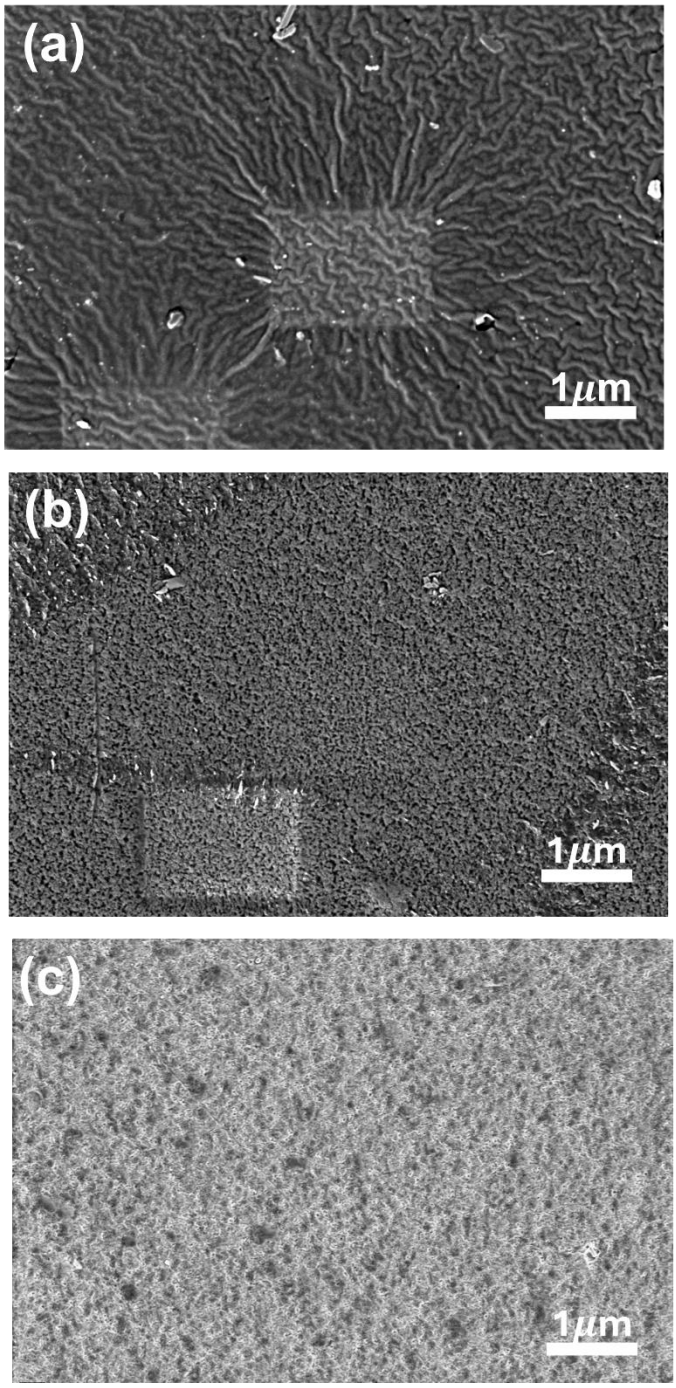

Figure S.4 SEM images of (a) $P_{66614}Cl$ PIM (b) Cyanex 301 PIM (c) HDEHP PIM after transport experiments.

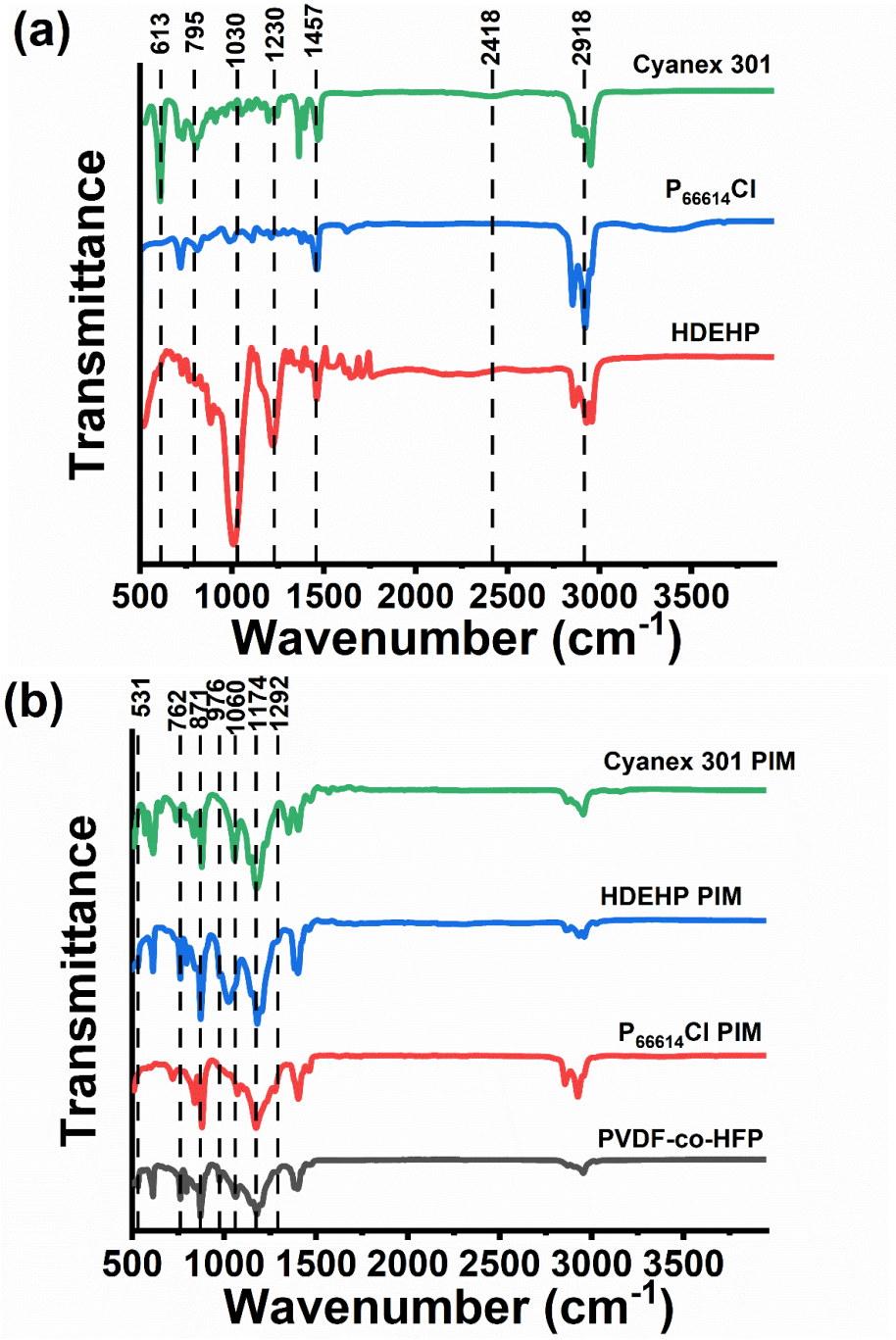

Figure S.5 FTIR analysis of (a) Cyanex 301, $P_{66614}Cl$, HDEHP (b) Pure PVDF-co-HFP, $P_{66614}Cl$ PIM, HDEHP PIM and Cyanex 301 PIM.

Table S.2 Metal composition of black mass determined by ICP-OES.

Element	Al	Co	Cu	Fe	Li	Mn	Ni
wt(%)	0.52	19.06	0.08	0.12	48.19	13.14	18.89

Table S.3 Yield and composition of separated electrode active materials from black mass.

Material	Mass (g)	Yield (%)	Graphite (%)	NMC (%)
Black Mass	10	85	28	57

The total recovery rate (85%) was determined using the actual mass of black mass (10 g) introduced into the HLCS process. The sum of the recovered anode and cathode fractions correspond to 8.5 g, equivalent to 85% of the total mass input.

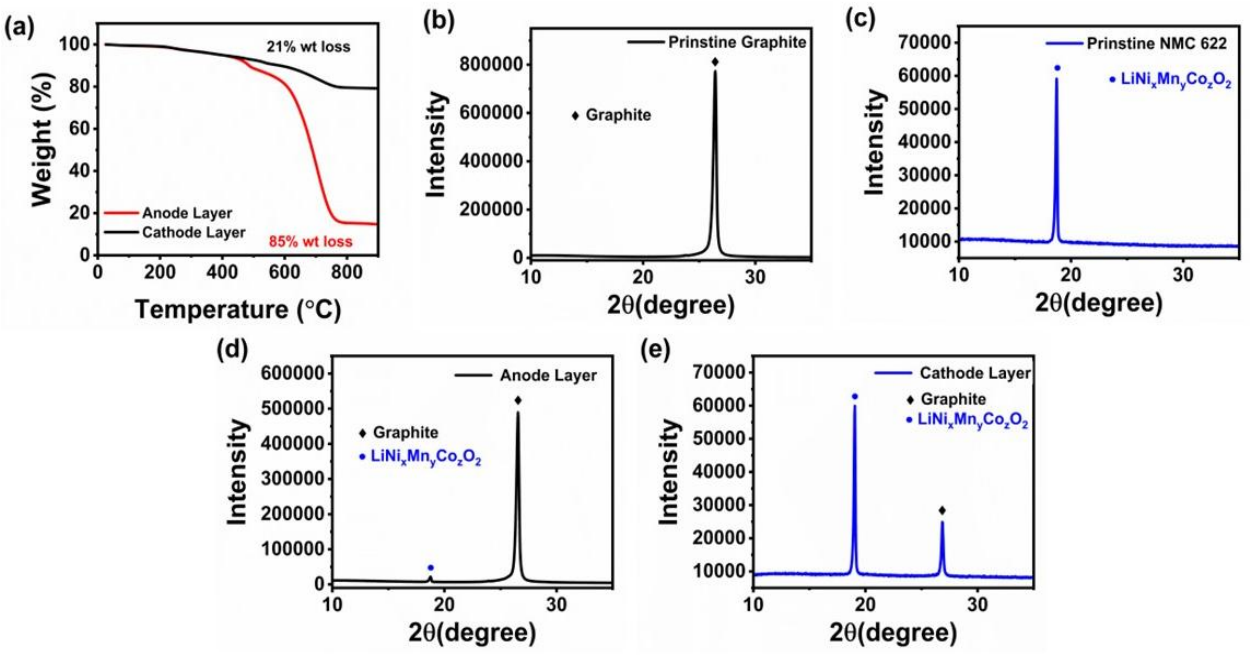

Figure S.6 TGA curves of the separated bottom and upper layers, XRD peaks of (b) pristine graphite (c) pristine NMC (d) anode layer and (e) cathode layer after separation.

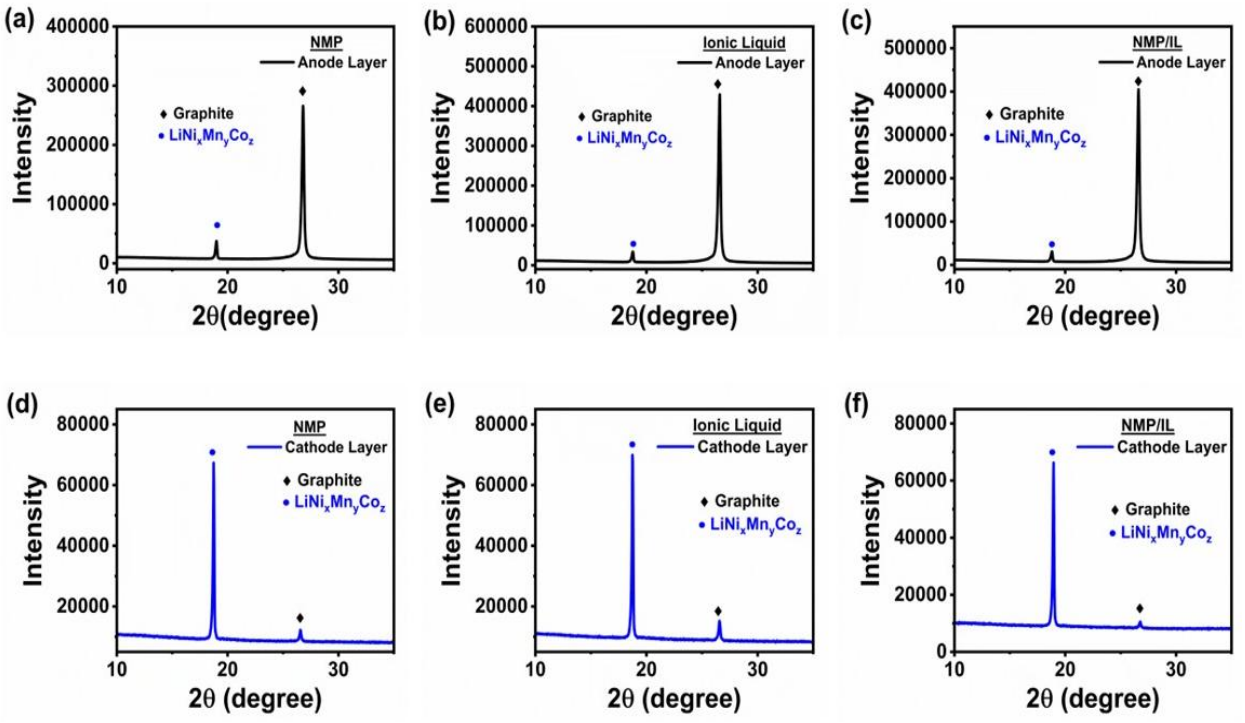

Figure S.7 XRD pattern for different additives added to bromoform (a) NMP (b) Ionic Liquid (c) NMP/Ionic Liquid of the anode layer (d) NMP (e) Ionic Liquid (f) NMP/Ionic Liquid of the cathode layer.

VITA

Babafemi Adigun was born and raised in Lagos, Nigeria. He completed his secondary education at Government College Lagos. He received his Bachelor of Science degree in Chemistry with First Class Honors from the University of Lagos, Nigeria. During his undergraduate studies, he developed a strong foundation in physical, analytical, and inorganic chemistry, which laid the groundwork for his graduate research career. After his undergraduate studies, Babafemi worked in KPMG Nigeria for 3 years as an audit associate before pursuing his doctoral studies at The University of Tennessee, Knoxville, where he conducted research in polymer inclusion membranes for selective separation and recovery of lithium, cobalt, nickel, and manganese from complex aqueous systems. His work focused on mechanistic transport analysis, ionic liquid integration, membrane stability, and structural optimization strategies, including Layer-by-Layer surface reinforcement. His research contributes to advancing solvent-reduced, sustainable separation technologies for critical metal recovery. Throughout his doctoral training, he has authored and co-authored peer-reviewed publications and presented his work at national and international scientific conferences. Babafemi has served as a Teaching Assistant, mentoring undergraduate students in laboratory and classroom settings. He is a member of the American Chemical Society (ACS) and the National Organization for the Professional Advancement of Black Chemists and Chemical Engineers (NOBCChE).